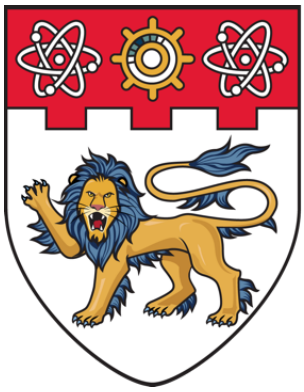

NANYANG TECHNOLOGICAL UNIVERSITY
SINGAPORE

Confined and active liquids: a computational investigation

Jing Yang

SCHOOL OF PHYSICAL AND MATHEMATICAL SCIENCES

A thesis submitted to the Nanyang Technological University
in partial fulfillment of the requirements for the degree of
Doctor of Philosophy

2023

Confined and active liquids: a computational investigation

Jing Yang

SCHOOL OF PHYSICAL AND MATHEMATICAL SCIENCES

A thesis submitted to the Nanyang Technological University
in partial fulfillment of the requirements for the degree of
Doctor of Philosophy

2023

Statement of Originality

I hereby certify that the work embodied in this thesis is the result of original research done by me except where otherwise stated in this thesis. The thesis work has not been submitted for a degree or professional qualification to any other university or institution. I declare that this thesis is written by myself and is free of plagiarism and of sufficient grammatical clarity to be examined. I confirm that the investigations were conducted in accord with the ethics policies and integrity standards of Nanyang Technological University and that the research data are presented honestly and without prejudice.

24/02/2023

.....

Date

.....

Jing Yang

Supervisor Declaration Statement

I have reviewed the content and presentation style of this thesis and declare it of sufficient grammatical clarity to be examined. To the best of my knowledge, the thesis is free of plagiarism and the research and writing are those of the candidate's except as acknowledged in the Author Attribution Statement. I confirm that the investigations were conducted in accord with the ethics policies and integrity standards of Nanyang Technological University and that the research data are presented honestly and without prejudice.

24/02/2023

.....

Date

.....

Prof. Massimo Pica Ciamarra

Authorship Attribution Statement

This thesis contains material from 2 paper published in the following peer-reviewed journal(s) in which I am listed as an author.

Chapter 3 is published as Jing, Y., Y.W, Li, and Ciamarra, M.P., 2021. Long-wavelength fluctuations and dimensionality crossover in confined liquids. Physical Review Research, 3(3), p.033172. DOI: 10.1103/PhysRevResearch.3.033172

The contributions of the co-authors are as follows:

- Prof. Massimo Pica Ciamarra conceived the initial direction of this project and helped to modify this manuscript draft.
- I prepared the manuscript drafts, and revised it with the help of Dr. Yanwei Li and Prof. Massimo Pica Ciamarra.
- I completed theoretical work through the assistance of Prof. Massimo Pica Ciamarra and performed all the simulation model, numerical experiments, data analysis and visualization with the assistance of Dr. Yanwei Li and Prof. Massimo Pica Ciamarra.

Chapter 4 is published as a letter by Physical Review E as Jing, Y., Ran, N., Ciamarra, M.P. Interplay between jamming and MIPS in persistent self-propelling particles, Physical Review E, 106(1), p.L012601. DOI: 10.1103/PhysRevE.106.L012601

The contributions of the co-authors are as follows:

- Prof. Massimo Pica Ciamarra conceived the initial direction of this project and helped to edit this manuscript draft.
- I prepared the manuscript drafts and revised it with Prof. Massimo Pica Ciamarra and Prof. Ran Ni.
- I conducted all molecular dynamics simulations and data analysis through the help of Prof. Massimo Pica Ciamarra.

24/02/2023

Jing

. . . . . .

Date

. . . . . .

Jing Yang

Abstract

Disordered many-particle systems have remarkable mechanical and transport properties, whose theoretical description is made difficult by the absence of crystalline-like periodicity. In this thesis, I investigate two aspects of the physics of these systems.

In the first part of the thesis, I consider how confinement influences the physical properties of many-particle systems to rationalise the crossover from a two- to three-dimensional physics. Previous works have shown that confinement may induce layering, a slowdown of the dynamics and a series of ordering transition. These confinement induced effects made difficult to rationalize how a three-dimensional system becomes effectively two-dimensional as the confinement increases. I demonstrated that the confinement dependence of the dynamical properties clearly reveals the dimensionality crossover. This result builds on recent works that have shown that Mermin-Wagner long-wavelength fluctuations influences the dynamical properties of two-dimensional solids and liquids and make them distinct from those of three-dimensional systems. I developed a theoretical model to rationalise the confinement dependence of the long-wavelength fluctuations, and used it to predict the confinement dependence of the dynamics. This model allowed me to make predictions on the dimensionality crossover, which I have verified via detailed numerical simulations.

In the second part of the thesis, I consider disordered many-particle systems of repulsive particles that move as able to self-propel rather than because of thermal effects. Self-propelling particles are attracting much interest in the literature as model biological systems and as a playground to explore the physics of driven non-equilibrium systems. The prototypical motility induced out-of-equilibrium effect is a phase coexistence of a liquid- and a gas-like phase (MIPS), which occurs at high enough density and motile forces dominating over other stochastic forces possibly acting on the particles and promoting an homogeneous phase. Besides MIPS, on increasing the density systems of active particles also present a phase

transition from a flowing to an arrested state, or jamming transitions. In my thesis, I considered the interplay between these two out-of-equilibrium transitions, MIPS and jamming. Via extensive numerical simulations I have shown that these two transitions, believed to be unrelated in the literature, do actually occur together in the limit of small self-propelled forces in systems of persistent active particles, each self-propelling in a fixed direction.

Acknowledgements

Recall the past four years PhD study in my life, I have enjoyed laughter and tears and I feel grateful for all ups and downs in this journey. At this moment, no words are amazing enough to express my appreciation, to my respectful supervisor, my dear senior colleagues, my lovely friends and my beloved families. First and foremost, I particularly express the utmost gratitude to my doctoral research supervisor, Prof. Massimo Pica Ciamarra, for his continuous patience and inspiration, and for encouraging me all along with my PhD life. He expertly provided me with perfect guidance in the fundamental knowledge of numerical simulations and how to solve complicated physics problems via these powerful tools. My PhD research would not have been achievable without his unwavering encouragement and support. He has taught me many things, but nothing was more valuable than his passion and enthusiasm for pushing the boundaries of human knowledge.

My deepest appreciation also goes to all advisory committee members of my thesis, Prof. Ran Ni, Prof. Pinaki Sengupta, and Prof. Bingsui Lu, for their support and encouragement of my doctoral research. I genuinely thank the research fellows in our research lab, Dr. Yanwei Li, Dr. Sudhir N. Pathak, and Dr. Joyjit Chattoraj, for their motivation and valuable advice on technical problems. A big thank you to my wonderful friends in Singapore, Anshuman, Yuanjian, Shivam, Arpit, and Pin. The parties we had, the happiness and sentiments we shared, and the memories we made together keep me away from upset and homesick.

I dedicate my thesis with humble words to my beloved family. I would love to thank my husband, future Dr. Junxiang Jia. Your love keeps me strong and makes me a better myself. Thank you for sharing your life with me and being a part of my life, for being my husband, soulmate, and my best friend. The best thing that ever happened to me is I've been surrounded by the love of my parents. I am greatly indebted to my mom and dad for their unconditional love, trust, and care, and for supporting me on every decision I made. Thanks for always having my back.

Table of Contents

List of Figures

Symbols and Acronyms

Acronyms

1D	One Dimensional
2D	Two Dimensional
3D	Three Dimensional
ABPs	Active Brownian Particles
CR	Cage-relative Coordinates
DOS	Density of States
ISF	Self-intermediate Scattering Function
KA	Kob-Andersen
LJ	Lennard-Jones
LW	Long-wavelength
MD	Molecular Dynamics
MIPS	Motility-induced Phase Separation
MSD	Mean Squared Displacement
MW	Mermin-Wagner
SPPs	Self-propelled Particles

Chapter 1

Introduction

1.1 Motivation and background

Disordered systems comprising many particles are ubiquitous around us and are found in various natural and engineered materials. These systems exhibit a range of physical and chemical properties that give rise to unique behaviors and functions. Examples of such disordered systems include foams, which are formed by a network of gas bubbles within a liquid matrix, granular assemblies, which consist of a collection of macroscopic particles, glasses, which are amorphous materials with no long-range structural order, and active systems, which comprise self-propelling particles that exhibit non-equilibrium behavior.

In addition to these, disordered systems may also include liquid crystals, which are materials with intermediate structural order between liquids and solids, colloids, which consist of small particles suspended in a fluid, polymers, which are large molecules made up of repeating subunits, and cell tissues, which are biological structures composed of cells and extracellular matrix.

These disordered systems exist on varying length scales and exhibit remarkable mechanical and transport properties, which are not understood with the assistance of traditional approaches. On the one side, it is because these systems do not have ordered arrangement of atoms i.e. they lack crystalline-like periodicity in their structure. Additionally, some disordered systems, e.g., biological systems with

self-driven force, are out-of-equilibrium so that their properties defy traditional statistical mechanics and depend on their preparation protocol.

Confined liquids and active liquids are two types of disordered systems, which can be further categorized into non-active and active systems. Specifically, active systems are considered to be out-of-equilibrium due to the presence of self-propelling forces that act on individual particles, enabling them to move by consuming their internal energy.

In this thesis, we focus our attention on two broad classes of disordered systems: 1. Confined liquids 2. Active liquids. In the following, I briefly discuss the interesting physical properties of these systems that motivated my study.

1.1.1 Confined liquids

Liquids confined between two plates exhibit a variety of properties depending on the confining width, the roughness of the confining boundaries, and the interaction between liquids molecules and the boundaries. From a structural perspective, confinement induces particles' layering [1], and crystallization due to stacking [2, 3]. Confinement might also influence the dynamical properties by slowing-down or speeding-up the dynamics [4, 5]. Further, confinement may lead to the emergence of novel phases, e.g., a quasi-crystalline phase with 20-fold bond order [6], and affect the glass transition from liquids to disordered solids [1, 7]. A proper description of these complex phenomena requires a fundamental understanding on the behavior of liquids. Furthermore, this understanding is precious in all applications involving the flow of confining liquids, including material manufacturing lubrication, and many biological instances where the flow of liquids occurs in spatially restricted regions.

Confined liquids also offer the unique opportunity to investigate the crossover from a three- to a two-dimensional physics. This crossover occurs as the confining width decreases until a liquid is confined to a monolayer and is de-facto a two-dimensional system. The melting transition of strongly confined liquid have been found to involve the hexatic phase [8, 9], which demonstrates how confinement induces a unique two-dimensional feature. However, it has also been clarified that confinement strongly affects the phase behavior inducing novel phases [6] that are

not observed in 2D and 3D bulk systems. As such, the study of the dependence of the phase behavior on the confining width did not result useful to characterize the dimensionality crossover. It is still unclear how a liquid crossovers from a three to a two-dimensional behavior as it is increasingly confined.

Recent works have demonstrated that two dimensional systems differ from their three-dimensional counterpart in the dependence of their dynamical properties on the system size. Specifically, while the relaxation dynamics of three dimensional systems has a negligible size dependence, long-wavelength Mermin-Wagner fluctuations make the dynamics of two-dimensional solids and liquids dependent on their lateral size [10]. In my work, I have thus explored the possibility of resolving the crossover from a two- to a three-dimensional physics by investigating how the later size dependence of the relaxation dynamical properties varies with the degree of confining.

1.1.2 Active liquids

Fish schools, bird flocks and herd of animals are examples of systems comprising many "particles" that self-propel by consuming their stored energy [11]. We behave similarly. In the synthetic world, colloidal particles with a similar self-propelling ability can be fabricated [12]. All these so-called active systems exhibit collective properties that cannot be described using the traditional tools of statistical mechanics.

To assess how self-propulsion influence the behavior of these systems, in the last few years researcher have been focused on a model system in which each particle self-propel along its own polar direction. This polar direction may evolve in time, usually via rotational diffusion. The correlation time of the self-propelling direction defines the persistent time, which equals to the inverse rotational diffusion coefficient [13]. This so-called Active Brownian Particle model allows us to identify what features of the complex phenomenology exhibited by systems of active particles can be ascribed to their ability to self-propel.

These model systems have been shown to exhibit two non-equilibrium phase transitions. One is a so-called motility-induced phase transition, whereby the system phase separates into a lower density gas-like phase and a higher density liquid-like phase [14]. The occurrence of this transition depends on the magnitude of self-propelled velocity and on the rotational diffusivity of the polarity, and possibly, on other parameters characterizing the dynamics. The other out-of-equilibrium transition is a jamming transition [15] from a liquid to a dynamically arrested state. The jammed phase occurs at high density and low self-propelling forces.

Previous works have investigated experimentally and numerically these two transitions. When the persistence time of the polarity (inverse rotational diffusion) is small, motility-induced phase separation and active jamming occur in different regions of the activity-density plane [16]. On increasing the persistence time, these two transitions appear to approach [17]. This suggest a possible interplay between these two non-equilibrium transitions, which is however controversial.

As a second aim of my thesis, I address the possible connection between MIPS and jamming in active systems in the limit of infinite persistent time. My results clarified that these two transitions occur together in the limit of infinite persistent time, and unveiled the rich dynamics that characterize this limit.

1.2 Thesis organization

In this thesis, we undertake a comprehensive investigation of the dynamics and the phase behavior of confined and active systems. To facilitate these work, Chapter 2 provides a review of the theoretical concepts and previous research findings that are relevant to our work.

In Chapter 3, we focus on the dynamics of confined systems and investigate the dependence of the dynamics on the confinement gap width. Our numerical simulations reveal a crossover from a two-dimensional to a three-dimensional physics, in addition, we develop a theoretical model for the density of vibrational states in confined systems, based on the Debye model. We validate this model by performing large molecular dynamics simulations, further considering both schematic and realistic conditions for confining a liquid in slab geometry.

Moving on to Chapter 4, we explore the phase behavior of out-of-equilibrium active systems and investigate the possible connection between the motility-induced phase separation (MIPS) and the active jamming. Our numerical findings shed light on the complex interplay between jamming and phase separation in these active systems.

Finally, in Chapter 5, we discuss our main research findings and propose relevant future research directions. Overall, this thesis might make a contribution to our understanding of the phase behavior and dynamics of confined and active systems and provides important insights into the physics of disordered systems. The findings from this work have the potential to impact a range of disciplines, from materials science to biology and beyond.

References

[1] Carolyn R Nugent, Kazem V Edmond, Hetal N Patel, and Eric R Weeks. Colloidal glass transition observed in confinement. *Physical Review Letters*, 99(2):025702, 2007.

[2] Matthias Schmidt and Hartmut Löwen. Phase diagram of hard spheres confined between two parallel plates. *Physical Review E*, 55(6):7228, 1997.

[3] Matthias Schmidt and Hartmut Löwen. Freezing between Two and Three Dimensions. *Phys. Rev. Lett.*, 76:4552, 1996.

[4] Hartmut Löwen. Colloidal soft matter under external control. *Journal of Physics: Condensed Matter*, 13(24):R415, 2001.

[5] C Alba-Simionesco, Benoit Coasne, G Dosseh, G Dudziak, KE Gubbins, R Radhakrishnan, and MJPCM Sliwinska-Bartkowiak. Effects of confinement on freezing and melting. *Journal of Physics: Condensed Matter*, 18(6):R15, 2006.

[6] H Löwen. Twenty years of confined colloids: from confinement-induced freezing to giant breathing. *Journal of Physics: Condensed Matter*, 21(47):474203, 2009. doi: 10.1088/0953-8984/21/47/474203.

[7] HB Eral, Dirk van den Ende, F Mugele, and MHG Duits. Influence of confinement by smooth and rough walls on particle dynamics in dense hard-sphere suspensions. *Physical Review E*, 80(6):061403, 2009.

[8] John Michael Kosterlitz and David James Thouless. Ordering, metastability and phase transitions in two-dimensional systems. *Journal of Physics C: Solid State Physics*, 6(7):1181, 1973.

[9] BI Halperin and David R Nelson. Theory of two-dimensional melting. *Physical Review Letters*, 41(2):121, 1978.

[10] Hayato Shiba, Takeshi Kawasaki, and Kang Kim. Local density fluctuation governs the divergence of viscosity underlying elastic and hydrodynamic anomalies in a 2d glass-forming liquid. *Physical Review Letters*, 123(26): 265501, 2019. doi: 10.1103/PhysRevLett.123.265501.

[11] Gerhard Gompper, Roland G Winkler, Thomas Speck, Alexandre Solon, Cesare Nardini, Fernando Peruani, Hartmut Löwen, Ramin Golestanian, U Benjamin Kaupp, Luis Alvarez, et al. The 2020 motile active matter roadmap. *Journal of Physics: Condensed Matter*, 32(19):193001, 2020.

[12] Jeremie Palacci, Stefano Sacanna, Asher Preska Steinberg, David J Pine, and Paul M Chaikin. Living crystals of light-activated colloidal surfers. *Science*, 339(6122):936–940, 2013.

[13] Suvendu Mandal, Benno Liebchen, and Hartmut Löwen. Motility-induced temperature difference in coexisting phases. *Physical review letters*, 123(22): 228001, 2019.

[14] Yaouen Fily and M Cristina Marchetti. Athermal phase separation of self-propelled particles with no alignment. *Physical review letters*, 108(23):235702, 2012.

[15] Silke Henkes, Yaouen Fily, and M Cristina Marchetti. Active jamming: Self-propelled soft particles at high density. *Physical Review E*, 84(4):040301, 2011.

[16] Yaouen Fily, Silke Henkes, and M Cristina Marchetti. Freezing and phase separation of self-propelled disks. *Soft Matter*, 10(13):2132–2140, 2014.

[17] Yann-Edwin Keta, Robert L Jack, and Ludovic Berthier. Disordered collective motion in dense assemblies of persistent particles. *arXiv preprint arXiv:2201.04902*, 2022.

Chapter 2

State of the art

This chapter aims to provide a comprehensive overview of the previous studies that have reported and motivated my investigations, as well as to introduce the theoretical concepts and models that I have adopted in this thesis. It also serves as an important foundation for the subsequent analysis and discussion in my work, providing the necessary context and theoretical framework for the reader to fully understand the research question and the methods used to address it.

Previous studies investigated the dimensionality crossover considering how confinement influences the phase behavior. I take a different approach by investigating how confinement influences the dynamical properties. My original approach is motivated by recent results demonstrating that long-wavelength Mermin-Wagner fluctuations influence the dynamical properties of two-dimensional systems. In Section 2.2 I introduce these long-wavelength fluctuations and review the previous works [1–3] that have demonstrated their influence on the dynamical properties of two-dimensional solids and liquids.

The chapter is structured as follows. In Section 2.1, I review recent experimental and numerical studies on the behaviour of liquids confined in a gap geometry. Confinement means that the particle motion is restricted in one of the spatial directions, and unconstrained in the other transverse directions. When the gap width H is larger than all other relevant length scales, e.g. particle size and structural correlation length, confinement is expected to play a minor role, and the liquid to behave as a bulk 3D system, if not very close to the confining walls. Conversely, when the gap width becomes of the order of the particle size the liquid is confined

to a monolayer, and behaves as a two-dimensional system. As such, tuning the gap width offers us the opportunity to investigate the crossover from a two- to a three-dimensional system.

In this chapter, I also review physical properties of model systems of particles able to self-propel (SPPs). These models schematically describe the behavior of biological and colloidal systems and exhibit two out-of-equilibrium transitions. One is a jamming transition from a flowing to an arrested state, discussed in Section 2.3. The other is the transition from a homogeneous to a phase-separated state, known as motility-induced phase separation, which I review in Section 2.4. These sections serve as an introduction to my results of Chapter 4, where I investigate the interplay between motility-induced phase separation (MIPS) and jamming.

2.1 Confined liquid

Confined liquids are common in real-life applications [4, 5], like microfabricated integrated circuits, early embryogenesis, and nano-flow technology, to name a few. The simplest confined liquid one can think of, is a liquid confined between two plates. Confinement has been reported to influence liquid's properties [6, 7]. For example, confining a liquid makes the dynamics different from that observed in the bulk [8], renders the local structure inhomogeneous [9, 10], and may also induce a series of ordering transitions [11, 12].

I am interested in unveiling the crossover from a 3D to a 2D physics in a liquid confined in a gap geometry as the distance H between the confining plates decreases. Previous works [13, 14] considered that the melting transition may be strongly dimensionality dependent due to the possible existence of an hexatic phase intermediate between a solid and a liquid one, in two dimensional systems. Henceforth, they studied the confinement dependence of the phase behavior to unveil the dimensionality crossover. The interpretation of the obtained results are difficult, because, on increasing confinement, one does not simply observe a crossover from a 3D to a 2D melting scenario. Rather, confinement induces a variety of ordering transitions as a consequence of the competition between the confining length H, the structural correlation length of 3D systems, and the particle size.

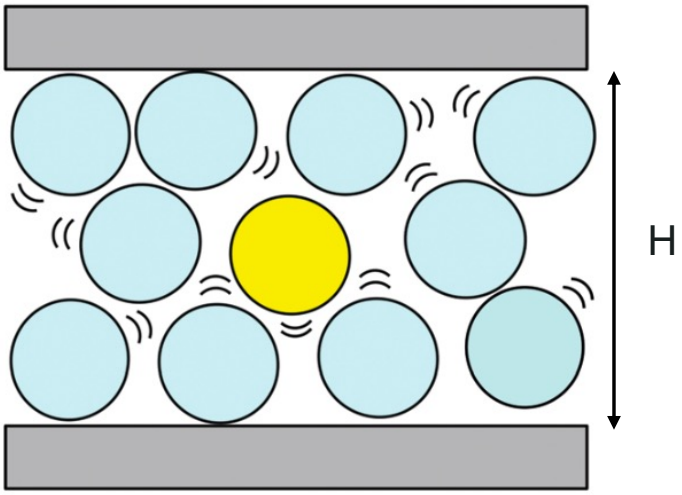

FIGURE 2.1: The schematic diagram of confined liquid with gap width H. This figure is reproduced from Ref. [15].

The issue is intricate as confinement introduces not only a length scale H measuring the distance between the confining boundaries, but also a length scale related to their roughness, and an energy scale related to an interaction between the confining boundaries and the confined molecules. It is currently unclear what is the underlying mechanism through which a three dimensional systems transforms into a two-dimensional one as particle motion in a spatial direction becomes increasingly confined. In the following, I briefly review the differences observed in terms of structural and dynamical properties in these previous works.

2.1.1 Experimental studies on confined systems

A variety of experimental studies have been performed on confined molecular and colloidal systems. The fundamental distinction between these two systems is in terms of the typical particle size and the interaction potential. In the colloidal models and experiments considered in the literature, particles only interact via repulsive forces. Conversely, in molecular systems, the interparticle interaction potential also has an attractive tail. In the following, I highlight the major differences observed between these two systems in terms of their dynamics, structure and phase transition.

In Ref. [16], Weeks et. al. studied the influence of tuning the gap width H on dynamical properties, the mean square displacements of a bi-disperse colloidal

mixture confined between rough walls and observed the dynamics to slow down with decreasing H. They also observed that the motion in the direction perpendicular to the confining walls is markedly slower than that in the parallel direction [17]. This decoupled dynamics of a confined liquid are due to the restriction of particle motion perpendicular to the confining walls. The presence of walls impedes particles close to them from moving toward the walls, whereas the motion parallel to the walls remains relatively less restricted.

Similar experimental studies have also been made for molecular systems. In confined molecular liquids, tuning the gap width H might slow-down or accelerate the dynamics of molecular system depending on the wall-particle interaction potential [18]. The experiment investigated the dynamics of polymer PMMA molecules confined between plates of different kinds. When this liquid is confined in silica plates, there is a strong attractive interaction between the confined molecules and the confining plates. This is because PMMA make hydrogen bonds with the hydroxyl groups naturally occurring on the silica. In this instance, the dynamics has been observed to slow down on increasing the confinement. Conversely, when a PMMA layer is confined by gold plates, molecules are not strongly attracted to the walls, because there is no hydroxyl groups on the gold. In this instance, confinement accelerate the dynamics [18].

That confinement may slow down or speed up the dynamics has also been suggested by other works [19–21]. The study conducted by Schuller et al. [19] presents a novel finding regarding the dynamics of confined liquid. The researchers observed that the liquid, which was confined within the pore-shaped glass with a strong attraction caused by hydrogen bonding, exhibited a slow-down in dynamics. This slow-down can be attributed to the attractive potential of the wall-particle interaction. On the other hand, a study of organic liquids under pore-shaped confinement [20] has suggested that the dynamics can be enhanced with increased confinement. In addition, an experimental study of dense hard-sphere suspensions under confinement [21] observed that the mean square displacements were notably different at the smooth and rough walls. This suggests that the dynamics of confined liquids of hard-sphere suspensions are sensitive to the interparticle and particle-wall interactions.

Confinement have also been observed to influence the glass transition of colloidal and molecular systems. Weeks et al. [16] introduced a bi-disperse mixture

to prevent crystallization in a confined colloidal liquid. They confined the colloidal system in a wedge geometry and fix the volume fraction to 0.42, a value which is far below the volume fraction $\phi = 0.6$, at which the glass transition occurs in a 3D bulk system. By investigating the mean square displacement at different values of H, they found the particle motion starts to slow down at a thickness of $H \simeq 10$ particle diameters, and that the glass transition happens at $H \simeq 5$ particle diameters.

In Ref. [22], Zanten et al. investigated a liquid of poly-(2)-vinylpyridine molecules confined by silicon oxide plates. In this configuration, there is an attractive molecule-plate interaction. They observed the glass transition temperature to increase by $\sim 50\ ^{\circ}C$ over the value of 3D bulk systems. This is because the attractive wall-particle interaction lead to an increase in the number of contacts between the particles and confining walls, and thus shifts the glass transition temperatures to higher values [23, 24]. On the contrary, polystyrene molecules confined by the polystyrene plates, the glass transition temperature is reduced [18].

Besides affecting the dynamics and glass transition, confinement have also been observed to influence the structure of colloidal and molecular systems.

To probe the effect of confinement on the structure of colloidal systems, Edmond et al. and Nugent et al. [16, 17] resorted to a wedge geometry, where the confinement gap vary along the transverse direction. A wedge-shaped confinement is frequently adopted in experimental studies [16, 17] to realise a continuous range of confining gap sizes. The reduction of the gap distance induced layering close to the wall suggesting that stronger interaction with the boundary induces structural changes. It is worth noting that this layering observed close to the wall is not responsible for the slow down of the dynamics observed in Ref. [16]. Rather, it was observed that some of the particles in their system stick to the confining glass walls, making them rough on the particle length scale. It is this roughness that possibly induces the slowing down of the dynamics. Numerical studies (see Section 2.1.2) do indeed suggest that rough walls slow down the relaxation dynamics of confined liquids, as I will discuss in Section 2.1.2.

In molecular systems with silica as a confining boundary, weak attractive forces have been found to induce liquid-like layers closer to the wall, which co-exist along with the crystalline layers in the bulk. However, as the attractive interactions

become stronger, as in a system of particles confined by mica surfaces, crystalline layers adjacent to the confining walls could coexist with a liquid in the bulk [25].

The above results suggest that the presence of confinement is responsible for the structural inhomogeneities in confined systems. Moreover, confinement induced crystallization and layering depends on interaction from walls and wall textures. These complex behaviors of confined liquids makes it challenging to unveil the dimensionality crossover from 3D to 2D with decreasing confined gap width.

2.1.2 Numerical studies

In addition to experimental research, numerical studies have been conducted to understand the dimensionality crossover in confined systems by modifying the width of the confinement gap. The findings suggest that as the confinement gap width decreases, a crossover occurs in the melting behavior. For large gap widths, a solid-liquid first-order transition occurs, while for small gap widths, such as in a monolayer system, a continuous transition with an intermediate hexatic phase is expected.

Previous works have addressed the dimensionality crossover focusing on the gap-width dependence of the phase behaviour, which may differ in two and three spatial dimensions. For example, a numerical work on an assembly of hard spheres by Lowen et al. [12], modified the degree of confinement by tuning the separation gap width between two parallel walls forcing the system to transition from a multi- to a mono-layer structure and investigated the phases of the system as its density and confinement width are varied. As a function of these two control parameters, they found a variety of equilibrium structures, including a liquid one and several different crystalline phases, with bucked, layered and rhombic symmetry.

As an alternative method to modify separation gap width, a numerical study by Gerhard et al. [26] tilted one of the parallel walls by a small angle α, keeping it fixed, to create a wedge-shaped confinement, following an approach also used in experiments (see Section 2.1.1). They observed different crystalline structures in their wedge-shaped system, demonstrating that these structures are dictated by the separation between the walls. Jabbarzadeh et al. [27] studied a standard

Lennard-Jones (LJ) model of a dodecane molecular liquid and found that confining walls with different roughness influence differently its dynamics. With rough confining walls, the dynamics continuously slows down with decreasing gap width. Conversely, smooth confining walls speed-up the dynamics.

Scheidler et al. [28] also investigated the role of the roughness of the confining walls via molecular dynamics simulations of a bi-disperse mixture of LJ particles. Smooth and rough confining walls result in different liquid dynamics. Below figure represents the relaxation dynamics as a function of the distance z from the confining walls, as illustrated in Figure 2.2.

They investigate the relaxation dynamical property as a function of a distance z from the confining walls via the introduction of a z-conditioned intermediate self-scattering function,

$$F_s(\boldsymbol{q}, z, t) = \frac{1}{N_p} \sum_{k=1}^{N_p} \langle \exp\left[i\boldsymbol{q} \cdot \left(\boldsymbol{r}_k(t) - \boldsymbol{r}_k(0)\right)\right] \delta\left(z_k(0) - z\right) \rangle \,, \tag{2.1}$$

where N_p is the number of particles in the particular layer with a distance z from the confining wall, $\boldsymbol{q}$ is the wave vector of the first peak of the structure factor, and $\boldsymbol{r}_k(t)$ indicates the particle displacement at t. The relaxation behavior at a specific distance z from the confinement wall of a system can be characterized by the decay of the above self-scattering function. From the decay of this function, they extracted a z-dependent relaxation time.

Figure 2.2 (left panel) considers the case of rough walls. In this case, the relaxation time decreases on increasing z, until it reaches the typical value of bulk systems. Henceforth, confinement slows down the dynamics of particles located close to the wall. In contrast, in the presence of flat walls (right panel), the relaxation time decreases from the bulk value as z decreases. Henceforth, flat walls speed-up the relaxation dynamics [28, 29] as evaluated from the decay of the self-intermediate scattering function. For both rough and flat walls, the effect of confinement on the dynamics weakens on increasing the temperature (from top to bottom in Figure 2.2).

They also estimated the temperature dependence of the typical distance $\xi_0(T)$

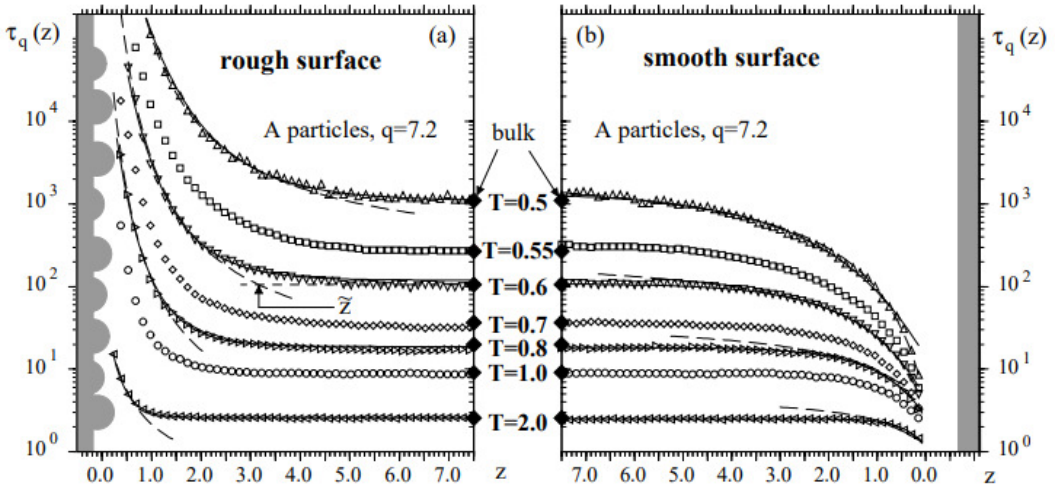

FIGURE 2.2: Structural relaxation time $\tau_q(z)$ as a function of a distance z in the unit of particle size from confining walls. In panel (a), the confining wall is rough, while in panel (b) it is smooth. This figure is reproduced from Ref. [28].

above which the effect of the confinement disappears by approximating the z-dependence of the relaxation time with [28]

$$\ln\left[\tau_q(z)\right] = B\exp\left(-\frac{z}{\xi_0(T)}\right) + \ln\left(\tau_{q,\infty}\right), \tag{2.2}$$

with B a constant, and $\tau_{q,\infty}$ the structural relaxation time of a bulk system. The typical distance $\xi_0(T)$ grows as $e^{E_a/T}$ for both rough and flat wall cases. The activation energy E_a is independent on the types of confining walls which implies this activation energy is an intrinsic properties of the considered liquid. The length $\xi_0(T)$ decreases on increasing the temperature.

Hocky et al. [30] prepared a system with confining rough walls by first bringing to equilibrium a large system, and then freezing the positions of the particles not included in a rectangular slab, placed in the bulk. They considered a bi-disperse system of particles interacting via the Kob-Andersen potential (a Lennard-Jones potential truncated in its minimum), harmonic potential, and WCA potential. They revealed a decoupling between the dynamics in the directions parallel and transverse to the confining walls.

Via decomposing the motion of each particle in components parallel and perpendicular to the walls, they extracted a parallel $\tau^{\parallel}(z)$ and a perpendicular $\tau^{\perp}(z)$ relaxation time. They found these two relaxation times to decouple.

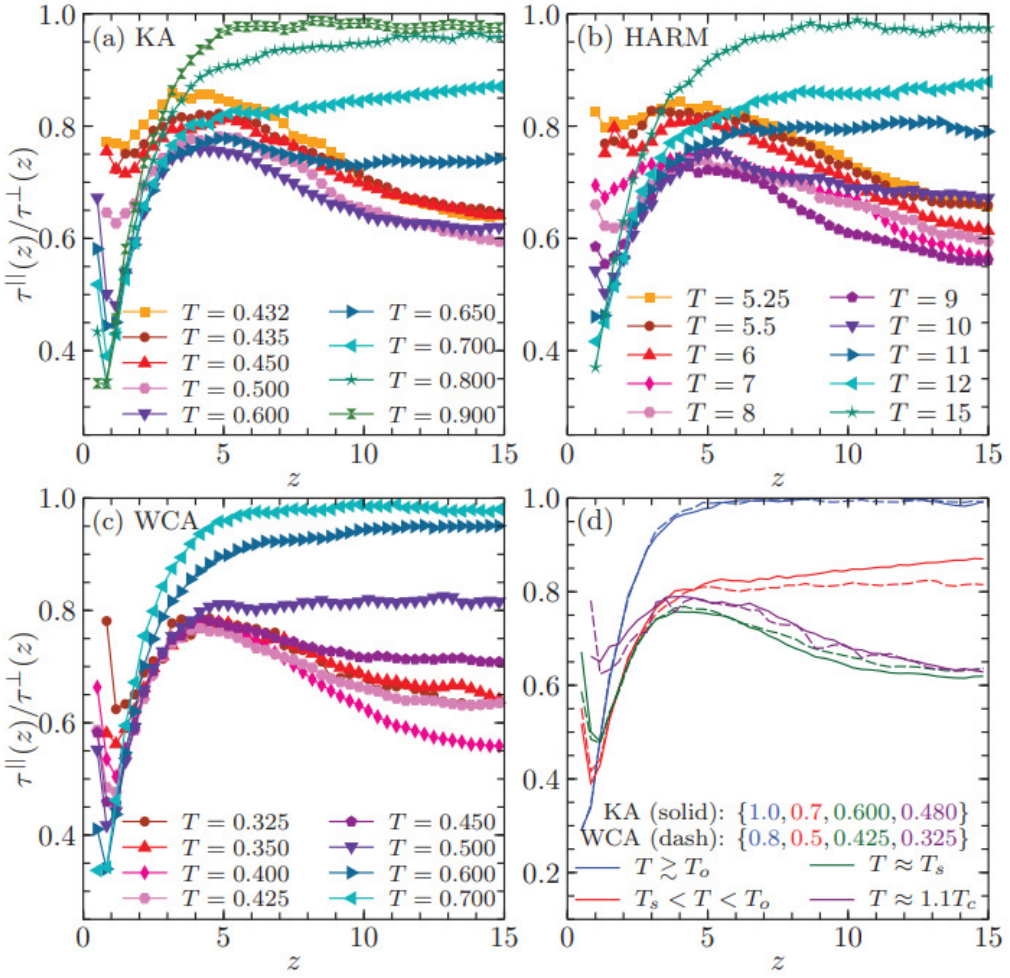

FIGURE 2.3: (a-c) Dependence of the ratio between the relaxation time in direction parallel and perpendicular to a confining wall, on the distance from the wall, for different interaction potential. (d) The identified profiles of the curves to highlight the maximum ratio at z in the different regimes. This figure is reproduced from Ref. [30].

One would expect these two times to be equal in bulk i.e., far away from the walls, which is indeed observed at high temperature. At lower temperature, they found the transverse and perpendicular dynamics to differ up to the largest wall-distance separation they investigated. The perpendicular dynamics is suppressed (larger relaxation time), and the z dependence of the ratio between the two time scales does not depend monotonically on z.

These results concern the relaxation time as evaluated from the decay of the self-scattering function. In the following paragraph, I discuss recent works that have shown that in two-dimensional systems this relaxation time is affected by long-wavelength fluctuations. In other words, the decay of the relaxation time

does not imply that particles are changing their neighbors. This suggests the need of focusing on diverse measures of structural relaxation, which is what I will do in my study.

2.2 Long-wavelength fluctuations

Long wavelength fluctuations (LWs) are the low frequency extended (plane waves) excitations occurring in solids. According to the Debye's model for the vibrational spectrum, the distribution in frequency ω of these excitations scale as ω^{D-1}, with D the dimensionality. As such, the influence of these excitations on a system's physical properties depends on its dimensionality. LWs have no influence on the amplitude of the vibrational motion of the particles in $D = 3$. Conversely, they make this amplitude to diverge with the system size both in $D = 1$ and $D = 2$. They are known as Peierls instability [31] ($D = 1$) and Mermin-Wagner (MW) theorem [1, 32] ($D = 2$). In particular, the MW theorem states that in 2D solids with short-range interactions, LWs prevent the presence of long-range translational order, at finite temperatures, at variance with their three dimensional counterparts [13, 33].

Recent results have demonstrated that LWs not only influence the phase behaviour of two-dimensional systems, but also the dynamical one. This influence occurs in amorphous solids [2], supercooled liquids [3, 34, 35] as well as high-temperature liquids [36]. In this section, I briefly introduce LWs and highlight their important influence on the physics of 2D crystals, glasses and liquids.

2.2.1 Mermin-Wagner theorem

The early arguments for the non-existence of long-range order in 1D and 2D go back to as far as the 1930s, notably the works by Bloch [37], Peierls [38], and Landau [39]. In 1966, D. Mermin and H.Wagner [1], and P. Hohenberg [40] independently gave a rigorous proof that in $D \leq 2$, spontaneous symmetry breaking does not occur at finite temperature in systems with continuous symmetry and short-range interactions. The impossibility of reaching ordered states has so far been verified in various two dimensional systems, including xy and Heisenberg models for spin

systems [1], 2D Bose or Fermi liquids [40], and 2D glass systems [2, 3, 34, 41]. In this section, I describe the effect of LW fluctuations in solids.

Let's consider a 2D solid as described within the framework of linear continuum elasticity. If a material point is in position $\boldsymbol{R}$ at zero temperature, then it will be in position $\boldsymbol{r}(t) = \boldsymbol{R} + \boldsymbol{u}(\boldsymbol{R}, t)$, at time t and at finite temperature. Here $\boldsymbol{u}(\boldsymbol{R}, t)$ is the displacement caused by thermal fluctuations, which is the superpositions of the contribution of the plane waves of wavevector $\boldsymbol{k}$. The displacement field is defined as

$$\boldsymbol{u}(\boldsymbol{R}, t) = \left(\frac{L}{2\pi}\right)^D \int \boldsymbol{u}_k(t) \exp(i\boldsymbol{k} \cdot \boldsymbol{R}) \mathrm{d}^D k. \tag{2.3}$$

Here, D is the dimensionality and L is the system size.

Plane waves follow the linear dispersion relation $\omega_k = c_s k$ where c_s is the sound velocity. Making use of the equipartition theorem, we can thus evaluate the mean square displacement as an integral over the frequencies,

$$\langle |\boldsymbol{u}|^2 \rangle = \frac{D k_B T}{m} \int \frac{D(\omega)}{\omega^2} \mathrm{d}\omega. \tag{2.4}$$

Here, m is the mass of a particle, k_B is the Boltzmann constant, and $D(\omega)$ represents the vibrational density of states (VDOS). In Debye's model, $D(\omega)$ is proportional to ω^{D-1} for acoustic plane waves. For 2D systems,

$$D(\omega) = c_1 \omega, \quad \omega > \omega_{\min} = \frac{2\pi c_s}{L}, \tag{2.5}$$

where $c_1 \simeq 2/\omega_D^2$ depends on the Debye frequency $\omega_D = 2\pi c_s / \lambda_D$, and $\omega_{\min}$ is the minimum phonon frequency compatible with the linear size L of system. One can thus estimate mean square thermal displacement,

$$\langle |\boldsymbol{u}|^2 \rangle \simeq \frac{\lambda_D k_B T}{\pi^2 c_s^2} \ln\left(\frac{L}{\lambda_D}\right). \tag{2.6}$$

This result demonstrates that, in 2D, fluctuations diverge with logarithm of L. As a consequence, LWs prevent the presence of long-range translational order in $D = 2$.

2.2.2 Long-wavelength fluctuations: dynamical effects

At very low temperature, liquids exhibit a glassy dynamics whose main feature is an extended solid-like transient, whose duration increases as the temperature decreases. Common measure of the relaxation dynamics are the self scattering function,

$$F_s(\mathbf{k},t) = \frac{1}{n_i}\sum_{i=1}^{n_i} \langle \exp\left[-i\mathbf{k}\cdot\left(\boldsymbol{r}_i(t)-\boldsymbol{r}_i(0)\right)\right]\rangle \,. \tag{2.7}$$

where $\mathbf{k}$ denotes the wave vector of the first peak in static structure factor, and the mean square displacement,

$$\left\langle \Delta\boldsymbol{r}^2(t)\right\rangle = \left\langle \frac{1}{n_i}\sum_{i=1}^{n_i} \left|\boldsymbol{r}_i(t)-\boldsymbol{r}_i(0)\right|^2 \right\rangle = 2dDt, \quad t\to\infty, \tag{2.8}$$

where d denotes the system dimensionality and D represents the diffusion coefficient.

I illustrate the emergence of a glassy dynamics in Figure 2.4, by showing how the self-scattering function and the mean square displacement evolves on cooling, for a 3D system.

At low temperature, $F_s(\mathbf{k},t)$ develops a plateau as particles spend a large fraction of their time confined by their neighbors. $F_s(\mathbf{k},t)$ decreases at longer time as particles change neighbors, moving over a distance larger that $1/k$, inducing structural relaxation. Similarly, Figure 2.4 (b) shows that the MSD saturates to a Debye-Waller factor, as in solids, before eventually growing as the system enters a diffusive regime. This phenomenology was long tough to be dimensionality independent [42].

By studying the size dependence of the relaxation dynamics of two dimensional systems, Flenner and Szamenl [35] recently showed that this glass transition phenomenology is dimensionality dependent. In particular, they showed that the transient solid-like response characterizing the dynamics of supercooled liquids disappears in two dimensional systems as the linear size L increases.

Subsequent works by Illing et al. [2], and Vivek et al. [34], clarified that this difference is an influence of LWs. Indeed, the linear size L of a system sets a lower

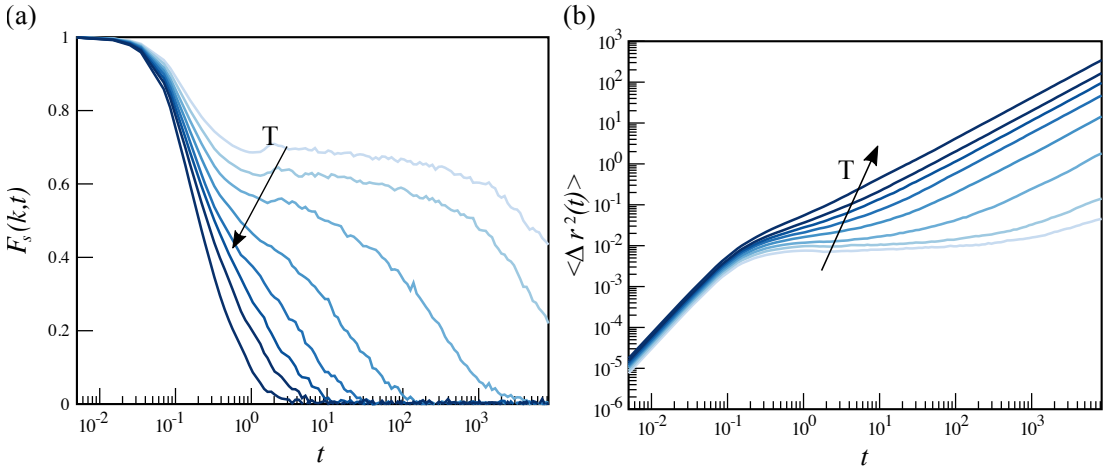

FIGURE 2.4: Plot of (a) self scattering function and (b) mean square displacement at different temperatures for a bidisperse LJ system in 3D. For lower temperatures, the system exhibits the solid-like transient behavior, illustrated as plateaus in $F_s(\mathbf{k}, t)$ and $\langle \Delta \boldsymbol{r}^2(t) \rangle$.

bound for the frequency ω of its LWs, which scales as c_s/L whit c_s the sound velocity (see Equation 2.5). This lower-bound and the dimensionality dependence of the low-frequency excitation distribution in frequency, which scales as ω^{D-1} according to Debye's model, makes the amplitude of particle's vibrational motion dimensionality dependent. In solids, this amplitude saturates to a constant value, known as Debey-Waller factor, which in 2D systems LWs make to grow as $\log(L)$. As we have shown in the prevision section (see Equation 2.6), it is this size dependence that wash out the typical glassy dynamics in two-dimensional systems.

To prove that the dimensionality dependence of the relaxation dynamics is an effect of the LWs, Ref. [43] and Ref. [2] probed the relaxation dynamics using a measure that filters out the effect of the LWs. In a extended plane wave, the displacement of a particle and that of its neighbor are similar. Instead, these displacements are different when one of the particle changes neighbors through an activated event. Henceforth, to filter out the effect on the LWs it is convenient to introduce a cage-relative measure that compares the displacement of a particle i with that of its immediate n_j neighbors.

If $\boldsymbol{r}_i(t)$ indicates the position of particle i at time t, its displacement is defined as

$$\Delta \boldsymbol{r}_i(t) = \boldsymbol{r}_i(t) - \boldsymbol{r}_i(0). \tag{2.9}$$

The cage-relative displacement of particle i equals to its displacement minus the average displacement of its n_j neighbors:

$$\Delta \boldsymbol{r}_i^{CR}(t) = \Delta \boldsymbol{r}_i(t) - \frac{1}{n_i} \sum_{j=1}^{n_i} \Delta \boldsymbol{r}_j(t). \tag{2.10}$$

Recall that the MSD is defined as,

$$\left\langle \Delta \boldsymbol{r}^2(t) \right\rangle = \left\langle \frac{1}{N} \sum_{i=1}^{N} \left| \boldsymbol{r}_i(t) - \boldsymbol{r}_i(0) \right|^2 \right\rangle. \tag{2.11}$$

The cage-relative displacements allow us to introduce a cage relative mean square displacement,

$$\left\langle \Delta_{CR} \boldsymbol{r}^2(t) \right\rangle = \left\langle \frac{1}{N} \sum_{i=1}^{N} \left| \Delta \boldsymbol{r}_i^{CR}(t) \right|^2 \right\rangle, \tag{2.12}$$

and, in a similar way, a cage-relative intermediate scattering function.

Via numerical simulations, Illing et al. [2] studied the size dependence of the dynamics of a 2D system of hard disks. Figure 2.5 demonstrates that the plateau value of the mean square displacement grows with the number of particles N in the systems. As predicted for a solid in Equation 2.6, the MSD in the plateau grows as $\log(L) = \log(\sqrt{N})$ as demonstrated in the inset. Conversely, the cage-relative MSD is size independent. This finding connects the reported anomalous dynamics of 2D supercooled liquids [35] to MW fluctuations. The CR method unmasks the local relaxation events and makes the relaxation dynamics of 2D liquids analogous to that of 3D systems.

Analogous results were also found by Shiba et al. [43], that unmasked the 2D structural relaxation covered by LW fluctuations via cage-relative MSD. Their study also suggested that cage-relative MSD is an effective method to separate LW from 2D glassy dynamics.

By combining numerical and experimental results, Li et al. [36] clarified that LWs also influence the relaxation dynamics of 2D system in the liquids regime. As in the supercooled regime, also in the liquid one LWs induce a speed-up of the dynamics.

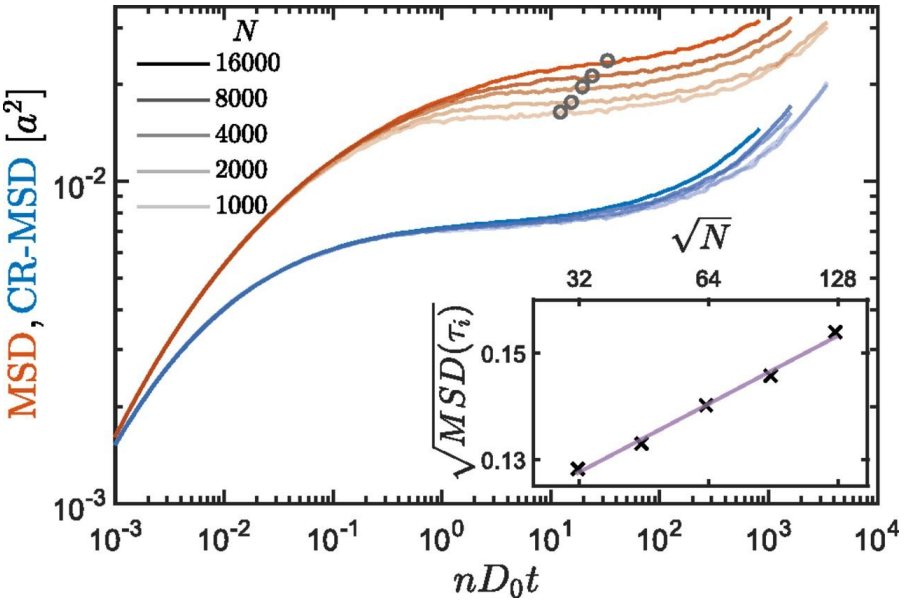

FIGURE 2.5: MSD and cage-relative MSD of 2D hard disk. Normal MSD illustrate a divergence with increasing system size. The inset reveals a logarithmic enhancement of asymptotic MSD with the growth of system lateral size L or alternatively $\sqrt{N}$. After introducing cage-relative into the system, the MSD shows no finite size effect. The figure is reproduced from Ref. [2]

These previous works suggest that the LW fluctuations influence the relaxation dynamics of 2D systems. In particular, in 2D Mermin-Wagner LW fluctuations make the relaxation dynamics size dependent. Overall, these works suggests that the dimensionality crossover could be revealed by studying how the lateral (L) size dependence of the relaxation dynamics vary with the confining width (H).

It is on the basis on these previous results that in my thesis I study the size-dependent dynamics of confined systems varies with the degree of confinement and temperature.

2.3 Jamming

2.3.1 Jamming phase diagram

The relaxation dynamics of liquids slows down as the temperature decreases, as we have seen in Figure 2.4. This slows down can be tracked by investigating the temperature dependence of the viscosity or relaxation time, which is the time at

which the self-scattering function (Equation 2.7) acquires a small value. Conceptually, at the relaxation time a large fraction of the molecules has moved a distance comparable to the typical interparticle spacing. The relaxation time sharply grows as the temperature decreases.

The temperature dependence of the relaxation time and its divergence at a finite or zero temperature are longstanding questions in the glass transition literature [44]. They are difficult to address as experiments have a maximum duration of the order of days. Regardless, the viscosity increases so dramatically as the temperature decreases that at some point liquids become so viscous that they cannot be equilibrated on experimental timescales and can be considered as disordered solid. This loosely defined liquid to disordered solid crossover temperature defines the glass transition.

Density is an alternative control parameter that influences the dynamics of liquids. The role of density is best elucidated by referring to systems of particles interacting via purely repulsive forces where inhomogeneities due to the formations of attractive clusters are absent. The same way the relaxation time decreases on cooling, so it does on increasing the density. Henceforth, in the temperature-density plane a line separates a liquid and an arrested or jammed state, the former occurring at low densities and high temperatures. The transition from the liquid to the jammed state has been investigated extensively in the limit of zero temperature [45, 46].

Thermal motion can be seen as one of the many factors promoting an unjamming transition from a solid to a flowing state. Another relevant control parameter is the shear stress applied to the system. Solid to fluid transitions driven by an increase in the shear stress are common in the geophysical world, as they drive the occurrence of earthquakes and avalanches [48]. Liu and Nagel [47] proposed a unifying description of the effect of temperature and density via the introduction of a jamming phase diagram, reproduced in Figure 2.6, with axis inverse density, temperature and shear stress, so that the jammed phase occurs close to the origin. A number of variants of this original phase diagram have been introduced in the literature, e.g. to account for the effect of friction [49], of the attraction [50] between the particles, and so on.

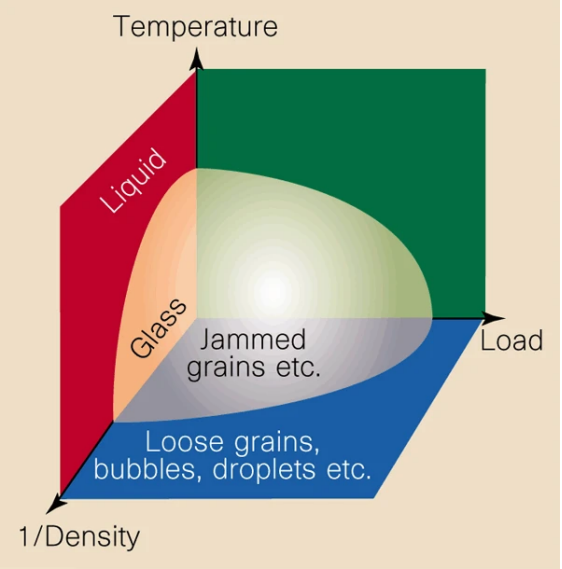

FIGURE 2.6: Jamming transition phase diagram, reproduced from Ref. [47].

In my thesis, I consider the jamming transition of systems of particles that self-propel, I introduce in the next section. Henceforth, rather that temperature or shear stress, the magnitude of the self-propelling forces is the control parameter driving the jammed to fluid transition [51–53].

2.4 Self-propelled particles

Nature is full of examples of living objects that move, such as ourselves. By consuming energy internally stored, living objects exert forces on their surroundings to self-propel. They could walk, fly, swim or propel via diverse actions [54, 55]. Such self-propelling objects can even be manufactured in a laboratory [56].

In the natural world, self-propelling animals could be extremely complex as we are, and perform movement according to their internal states and the sensing of the environment [57]. Examples could be biological systems [58], cell tissues [59, 60], fish flock [61], bird aggregation [62], and ants [63]. Engineering self-propelling

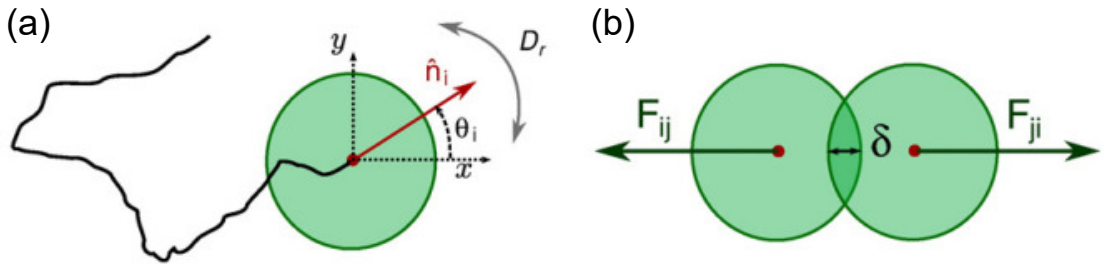

FIGURE 2.7: Diagram of the minimal model for active Brownian particles. (a) The particle i is self-propelled at velocity v_0 in the direction $\boldsymbol{n}_i$ (also noted as the unit vector $\boldsymbol{e}_i = (\cos\theta_i, \sin\theta_i)$). (b) The repulsive force $F_{ij} = F_{ji}$ between particle i and j is proportional to the overlap δ. The figure is reproduced from Ref. [69].

particles may require to mimic this complexity, e.g. in autonomous vehicles and robots, or might implement simpler propelling forces [64–67].

From a fundamental perspective it is of interest to consider the limiting case of "dull" self-propelling particles, that are not able to sense the environment and whose movement (motility) is guided by simple rules. The study of these simple models clarify what features of the complex phenomenology exhibited by active particles could be ascribed to their motility.

The rest of this section is organized as follows. In Section 2.4.1, I introduce the typical models used to investigate these phenomenologies. In Section 2.4.2 and Section 2.4.3, I first review the main feature of Active Brownian Particles (ABPs), which is their motility induced phase separation in a gas-like and a liquid-like phase, and then describe recent results on the relation between jamming and self-propulsion.

2.4.1 Numerical models

Several models have been introduced to describe biological and synthetic systems of self-propelled (active) particles. Here, I consider the simplest one, the ABPs model [68, 69].

ABPs describe spherical active Brownian particles. Each particle has a polarity $\hat{\mathbf{e}}_i = (\cos\theta_i, \sin\theta_i)$ that diffuses with rotational diffusion coefficient D_r.

Consider a system with N ABPs. In its most general formulation, three forces act on the translational degrees of freedom of a particle i. One force is the resultant of the interaction forces f_{ij} of particle i with other particles j. A second force is an active force, F_A, that acts in the direction of the polarity of the particle. The last force is a stochastic one, which would induce a Brownian dynamics with translational diffusion coefficient D_t. In the absence of any other forces and in the overdamped limit (where inertia effects are negligible), the equation of motion is

$$\begin{cases} \dot{\mathbf{r}}_i(t) = \frac{1}{\gamma}\sum_{j=1,j\neq i}^{N} \boldsymbol{f}_{ij} + v_A\hat{\mathbf{e}}_i + \sqrt{2D_t}\eta_i, \\ \dot{\theta}_i = \sqrt{2D_r}\eta_i, \end{cases} \tag{2.13}$$

with translational diffusion coefficient $D_t = k_BT/6\pi\eta r$, rotational diffusion coefficient $D_r = k_BT/8\pi\eta r^3$, constant γ a damping parameter, variable $v_A = F_A/\gamma$ the self-propelling velocity, and η a Gaussian white noise with zero mean. In general, Boltzmann's constant k_B is set to 1 in the simulations.

The rotational diffusion coefficient fixes the persistent time τ_p, which is the decay time of the time-autocorrelation function of the polarities, $C(t) = \langle\hat{\mathbf{e}}(t)\hat{\mathbf{e}}(0)\rangle$. In the zero rotational diffusion limit, where $D_r \to 0$, the orientation of active force remains fixed over time.

2.4.2 Motility induced phase separation

The most surprising phenomenon occurring in the systems of active particles is a phase separation between a gas-like and a liquid-like phase, known as motility induced phase separation (MIPS) [70–73]. Importantly, MIPS occurs in ABPs model in which particles interact via purely repulsive forces. Henceforth, this phase separation is not driven by interparticle attraction as for the standard gas-liquid coexistence.

MIPS has been observed both in simulations and experiments. Here I review a few numerical and theoretical results, which qualitatively reproduce the experimental observations. Before comparing numerical and experimental results, it needs to be highlighted that numerical simulations generally neglects hydrodynamic effects that could be experimentally relevant. Secondly, simulations most frequently use

periodic boundary conditions, while experiments do not. Finally, a detailed experimental investigation of MIPS as a function of the main control parameters, density and strength of the active forces, has not yet been carried out. It is noteworthy to mention that a recent study employed a machine learning model to effectively extract active and two-body forces from experiments of electrophoretic Janus particles. This development represents a significant step forward in comprehending the underlying physics of MIPS [74].

Fily et al. [71] first numerically investigated MIPS in ABPs systems. They considered a 2D systems of repulsive disks in the presence of active forces. At constant values of the noise and magnitude of the active forces, they observed the coexistence of a gas and a fluid phase on increasing the density, as illustrated in Figure 2.8.

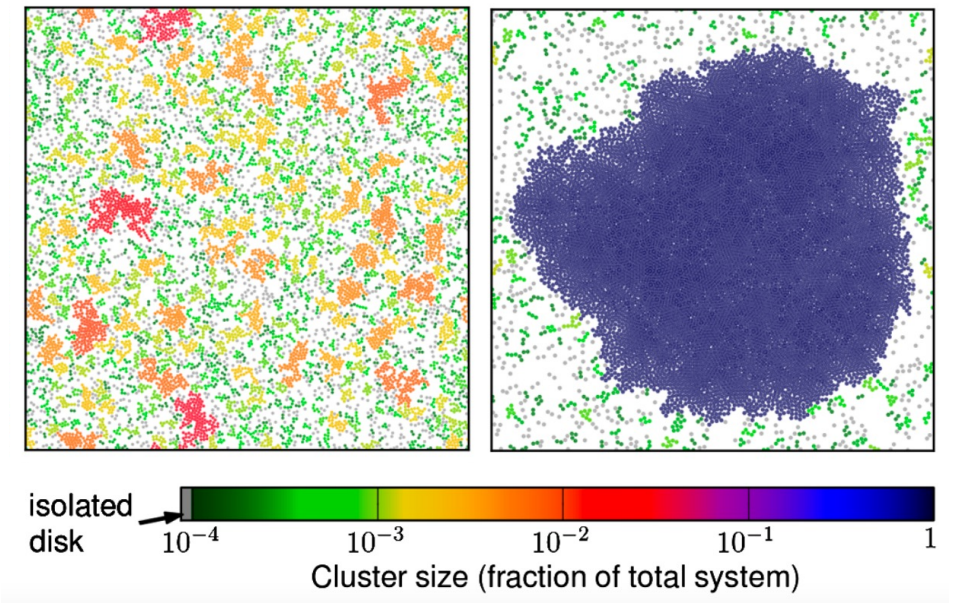

FIGURE 2.8: Snapshots of MIPS phase in active systems. With a constant active force, MIPS occurs at an active system with higher density. The densities of active systems are (a) $\phi = 0.39$ and (b) $\phi = 0.7$, respectively. This figure is reproduced from Ref. [71].

Moving towards a more dense active suspension, Marchetti et al. developed a model of active colloids for spherical Brownian active particles interacting via isotropic purely repulsive interactions [69, 75]. In their work, they numerically varied both the density ϕ and the active velocity $\tilde{v}$ and observed a MIPS and jamming transition. They obtained the phase diagram I reproduce in Figure 2.9, where the red region represents the separated liquid and gas phases, and occurs at

large volume fraction and active velocity. A homogeneous glassy phase is observed at very high volume fraction and small velocities, represented by blue region in the diagram. The MIPS region is indeed enclosed by a liquid one suggesting that MIPS and jamming are disconnected.

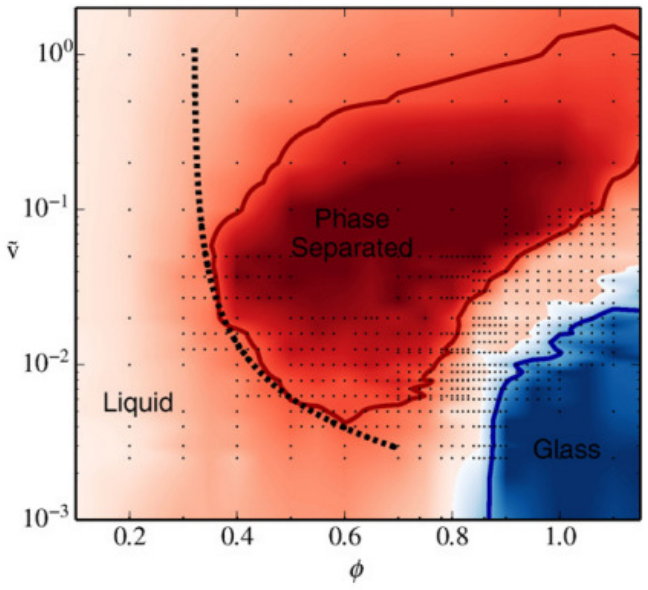

FIGURE 2.9: The phase diagram for system of polydisperse active particles. In a dense active suspension, the MIPS and active jammed phase are observed in distinct regions of a $\phi - \tilde{v}$ phase plane. The figure is reproduced from Ref. [75].

Redner et al. [72] numerically studied the phase diagram of ABPs and proposed a kinetic theory to describe the low-density MIPS coexistence line. They studied how an homogeneous state becomes unstable as clusters of particles form and break apart. They considered that the size of a cluster varies as there is a flux of gas particles that join the cluster, and an opposite flux of particles that leave the cluster and join the gas phase. The system phase separates when the former flux dominate. In their work, they suggested that the flux of particles joining a cluster from the gas phase is $K_{in} = \rho_{Gas} v_a / \pi$, where ρ_{Gas} denotes the gas density and v_a is active velocity. Once a particle join a cluster, the typical time it needs to leave depends on the rotation of its self-propelling direction: the particle will leave the cluster when its direction of self-propulsion points away from the cluster. As such, they approximated the flux of particles leaving a cluster with $K_{out} = kD_r/\sigma$.

In the steady state, $K_{in} = K_{out}$. This balance allows predicting the density of the gas on the phase separating boundary,

$$\rho_{Gas} = \pi k D_r / \sigma v_a, \tag{2.14}$$

with a fitting constant k representing the probability of several particles escaping the cluster at the same time.

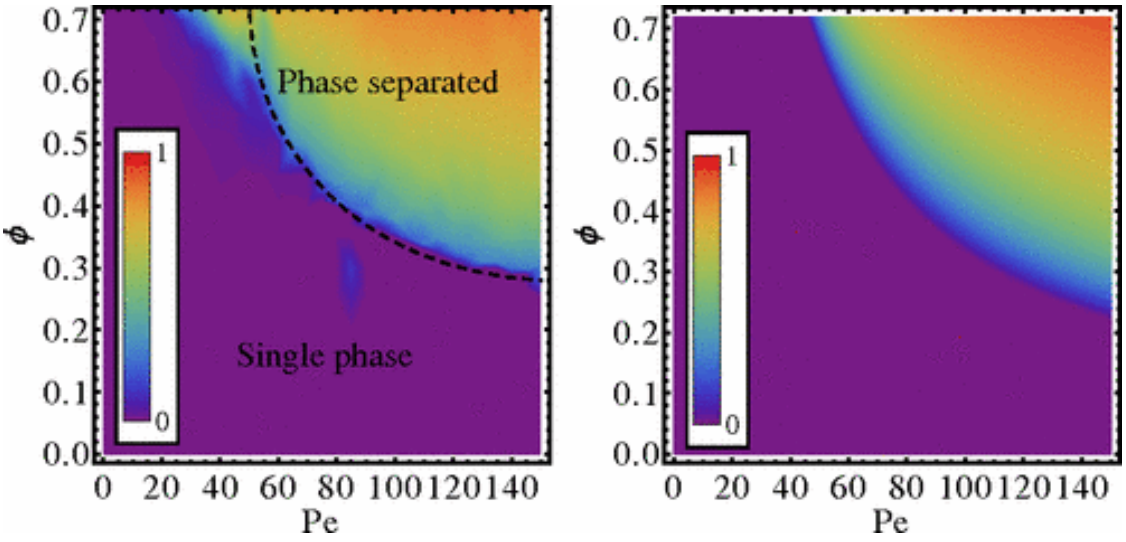

FIGURE 2.10: Phase diagram of homogeneous phase and MIPS in 2D ABPs. Left panel shows the predicted separated phase boundary in dashed curve and right panel shows the predicted cluster by the kinetic theory. This figure is reproduced from Ref. [72]

Based on their theory, the successfully predicted the low-density boundary of the MIPS in the Peclet number density phase diagram, as illustrated in Figure 2.10.

While certainly able to make some correct predictions, this theory fails in describing other features of the phase diagram. For instance, the theory predicts MIPS to occur in the large τ_p limit regardless of the density. Numerical simulations show that this is not the case. Furthermore, this theory does not predict a critical point. To address this point, Nie et al. [76] extended this model to incorporate a novel mechanism allowing particles to escape a cluster.

Besides the kinetic models, other continuous approaches have been introduced to try to rationalize the physics driving MIPS, as reviewed in Ref. [77]. I do not discuss them here as the study of the mechanism inducing MIPS is beyond the scope of this thesis.

2.4.3 Active jamming

In systems of self-propelling particles, the magnitude of the active forces and density control the jamming and glass transition. The system flows at low density and large motile forces, while it is in an arrested state in the opposite limit of high density and small active forces.

The jamming transition of active systems has received considerable interest due to its occurrence in biological systems. For instance, cells in tissue [78, 79] transition from a solid to a flowing state, e.g., during morphogenesis or wound healing.

Besides undergoing a jamming transitions, ABPs may also undergo a crystallization transition. This occurs if particles are monodisperse, or if their size polydispersity is small. Recent works have investigated the interplay between MIPS and crystallization [80]. In three dimensions, Omar et al. [80] suggested that MIPS is a metastable state enroute crystallization. That is, the MIPS coexistence curve occurs within the liquid-crystal coexistence curve. In two dimensions the situation is more complex, as in the absence of activity the melting transition follows a so-called mixed scenario [81].

In Ref. [13, 14, 82], disks were reported to first undergo a discontinuous liquid-hexatic transition, and then a continuous hexatic/triangular lattice transitions, with increasing density. Ref. [83] investigated how this scenario varies on changing the activity, and clarified the presence of motility shifted the hexatic order towards higher packing fractions. Meanwhile, the phase coexistence region is expanded by increasing motility and eventually passes the phase boundary of solid and hexatic phase.

Henceforth, in line with the focus of my thesis, we will limit our discussion to ABPs, in which size polydispersity suppresses crystallization.

Marchetti et al. [84] studied ABPs as a function of volume fraction and active velocity in a system of 2D repulsive disks and observed a jammed phase at high density and small active velocity. Their work do not consider MIPS, but clearly in their system jamming does not interfere with any phase-separated region even in this system (analogous to Figure 2.9).

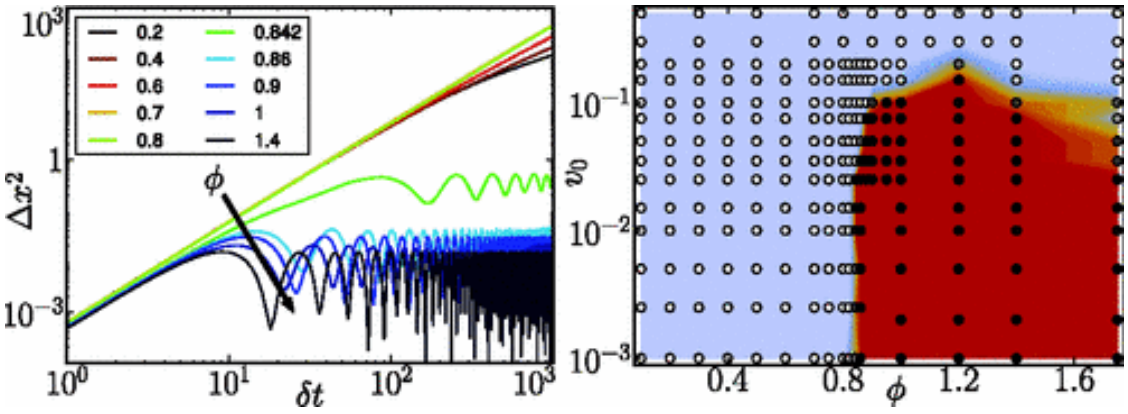

FIGURE 2.11: Active jamming in self-propelled dense system. The left panel shows mean square displacement for systems at different densities for fixed active velocity. The right panel shows a resulting density-motility phase plane. This figure is reproduced from Ref. [84]

In the presence of motility, Ran et al. [85] noticed a speed-up in the relaxation dynamics of an active system of hard particles. They also found that in the limit of low rotational diffusion, the self-propelled force has a more noticeable effect on dynamics. On the other hand, in the limit of infinite high rotational diffusion, the dynamical properties of active hard particles become Brownian. The influence of self-propulsion on the zero-temperature jamming transition, however, is not the major focus of their research.

Indeed, Liao et al. [52] numerically investigated a self-propelled dense repulsive system of ABPs focusing on the influence of mobility on zero-temperature jamming transition. They found self-propulsion to increase the volume fraction of the jamming transition. A similar observation is reported in Ref. [85], but the latter focuses on finite persistence time scale.

Recent works have also studied how the persistence time (inverse rotational diffusion) influences the transition from a fluid to a jammed/glassy phase [86–88]. Mandal et. al [89] investigated the dependence of the phase behavior of ABPs on the persistent time, at constant density. At short persistent times, a transition from a liquid to a disordered jammed phase occurs with decreasing active forces, as displayed in Figure 2.12. At intermediate persistent times, the liquid and a disordered jammed phase can be separated by a new intermittent phase. However, in the limit of infinite persistent time, the active system undergoes transition to a jammed configuration at small active forces.

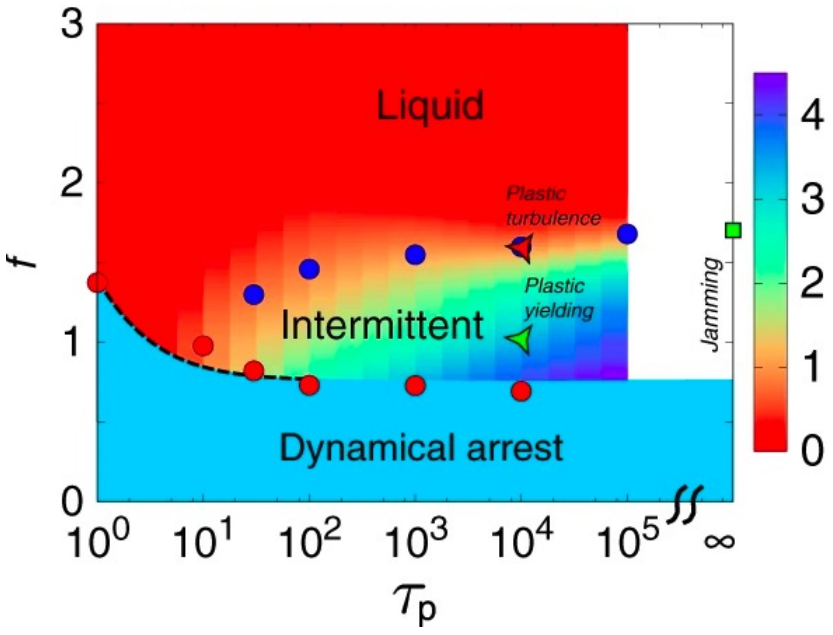

FIGURE 2.12: Motility-persistence phase plane for fixed dense active glassy system. The liquid, intermittent, and disordered solid phases are colored. The red circles are indicating the liquid-solid phase boundary, blue circles indicates the phase transition from liquid to for dynamically arrested phase. This figure is reproduced from Ref. [89]

These findings suggest that dense active amorphous systems with different values of persistent times have qualitatively distinct behavior [87]. In the limit of infinite persistence, a fluid and a jammed phase are observed. However, at finite persistence the dynamics could also be intermittent. Indeed, recent research [75, 90] explored ABPs models with different ranges of persistent time and came up with contradictory conclusions: at small persistent times, the MIPS and disordered solid phases appear in well distinct regions [75]. Conversely, Ref. [90] suggests these two transitions approach one another with increasing persistent times. This results clarify that the connection between MIPS and jamming is still elusive. In second part focus of my thesis, I investigate MIPS and jamming, in systems of self-propelled particles and clarify their relation in the limit of infinite persistent time.

References

[1] N David Mermin and Herbert Wagner. Absence of ferromagnetism or antiferromagnetism in one-or two-dimensional isotropic heisenberg models. *Physical Review Letters*, 17(22):1133, 1966.

[2] Bernd Illing, Sebastian Fritschi, Herbert Kaiser, Christian L Klix, Georg Maret, and Peter Keim. Mermin–wagner fluctuations in 2d amorphous solids. *Proceedings of the National Academy of Sciences*, 114(8):1856–1861, 2017.

[3] Hayato Shiba, Yasunori Yamada, Takeshi Kawasaki, and Kang Kim. Unveiling dimensionality dependence of glassy dynamics: 2d infinite fluctuation eclipses inherent structural relaxation. *Physical Review Letters*, 117(24):245701, 2016.

[4] Todd M Squires and Stephen R Quake. Microfluidics: Fluid physics at the nanoliter scale. *Reviews of modern physics*, 77(3):977, 2005.

[5] James Giammona and Otger Campàs. Physical constraints on early blastomere packings. *PLoS Computational Biology*, 17(1):e1007994, 2021.

[6] Hartmut Löwen. Colloidal soft matter under external control. *Journal of Physics: Condensed Matter*, 13(24):R415, 2001.

[7] C Alba-Simionesco, Benoit Coasne, G Dosseh, G Dudziak, KE Gubbins, R Radhakrishnan, and MJPCM Sliwinska-Bartkowiak. Effects of confinement on freezing and melting. *Journal of Physics: Condensed Matter*, 18(6):R15, 2006.

[8] Joseph Klafter and J Michael Drake. *Molecular dynamics in restricted geometries*, volume 154. Wiley-Interscience, 1989.

[9] AO Parry, Carlos Rascón, and Robert Evans. The local structure factor near an interface; beyond extended capillary-wave models. *Journal of Physics: Condensed Matter*, 28(24):244013, 2016.

[10] Felix Höfling and Siegfried Dietrich. Finite-size corrections for the static structure factor of a liquid slab with open boundaries. *arXiv preprint arXiv:2006.06083*, 2020.

[11] Matthias Schmidt and Hartmut Löwen. Phase diagram of hard spheres confined between two parallel plates. *Physical Review E*, 55(6):7228, 1997.

[12] Matthias Schmidt and Hartmut Löwen. Freezing between Two and Three Dimensions. *Phys. Rev. Lett.*, 76:4552, 1996.

[13] BI Halperin and David R Nelson. Theory of two-dimensional melting. *Physical Review Letters*, 41(2):121, 1978.

[14] AP Young. Melting and the vector coulomb gas in two dimensions. *Physical Review B*, 19(4):1855, 1979.

[15] Kim Nygård. Colloidal diffusion in confined geometries. *Physical Chemistry Chemical Physics*, 19(35):23632–23641, 2017.

[16] Carolyn R Nugent, Kazem V Edmond, Hetal N Patel, and Eric R Weeks. Colloidal Glass Transition Observed in Confinement. *Phys. Rev. Lett.*, 99: 025702, 2007.

[17] Kazem V Edmond, Carolyn R Nugent, and Eric R Weeks. Influence of confinement on dynamical heterogeneities in dense colloidal samples. *Phys. Rev. E*, 85:41401, 2012.

[18] Connie B Roth, Katie L McNerny, Wolter F Jager, and John M Torkelson. Eliminating the enhanced mobility at the free surface of polystyrene: fluorescence studies of the glass transition temperature in thin bilayer films of immiscible polymers. *Macromolecules*, 40(7):2568–2574, 2007.

[19] J Schüller, Yu B Mel'Nichenko, Ranko Richert, and Erhard W Fischer. Dielectric studies of the glass transition in porous media. *Physical review letters*, 73(16):2224, 1994.

[20] Catheryn L Jackson and Gregory B McKenna. Vitrification and crystallization of organic liquids confined to nanoscale pores. *Chemistry of Materials*, 8(8): 2128–2137, 1996.

[21] H. B. Eral, D. Van Den Ende, F. Mugele, and M. H.G. Duits. Influence of confinement by smooth and rough walls on particle dynamics in dense hard-sphere suspensions. *Physical Review E - Statistical, Nonlinear, and Soft Matter Physics*, 80(6):061403, dec 2009.

[22] John H van Zanten, William E Wallace, and Wen-li Wu. Effect of strongly favorable substrate interactions on the thermal properties of ultrathin polymer films. *Physical Review E*, 53(3):R2053, 1996.

[23] KL Ngai. Relaxation in nanometre-size polymers and glass formers: application of the coupling model to some current problems. *Philosophical Magazine B*, 82(3):291–303, 2002.

[24] J. A. Forrest, K. Dalnoki-Veress, and J. R. Dutcher. Interface and chain confinement effects on the glass transition temperature of thin polymer films. *Phys. Rev. E*, 56:5705–5716, Nov 1997.

[25] C Alba-Simionesco, B Coasne, G Dosseh, G Dudziak, K E Gubbins, R Radhakrishnan, and M Sliwinska-Bartkowiak. Effects of confinement on freezing and melting. *J. Phys.: Condens. Matter*, 18:15–68, 2006. doi: 10.1088/0953-8984/18/6/R01.

[26] Gerhard Jung and Charlotte F Petersen. Confinement-induced demixing and crystallization. *Physical Review Research*, 2(3):033207, 2020.

[27] A Jabbarzadeh, Peter Harrowell, and RI Tanner. Low friction lubrication between amorphous walls: Unraveling the contributions of surface roughness and in-plane disorder. *The Journal of chemical physics*, 125(3):034703, 2006. doi: 10.1063/1.2216695.

[28] Peter Scheidler, Walter Kob, and Kurt Binder. Cooperative motion and growing length scales in supercooled confined liquids. *EPL (Europhysics Letters)*, 59(5):701, 2002.

[29] Cong Cao, Xinru Huang, Connie B Roth, and Eric R Weeks. Aging near rough and smooth boundaries in colloidal glasses. *The Journal of Chemical Physics*, 147(22):224505, 2017.

[30] Glen M Hocky, Ludovic Berthier, Walter Kob, and David R Reichman. Crossovers in the dynamics of supercooled liquids probed by an amorphous wall. *Physical Review E*, 89(5):052311, 2014.

[31] Rudolf Peierls. Quelques propriétés typiques des corps solides. In *Annales de l'institut Henri Poincaré*, volume 5, pages 177–222, 1935.

[32] N David Mermin. Crystalline order in two dimensions. *Physical Review*, 176 (1):250, 1968.

[33] J. M. Kosterlitz and D. J. Thouless. Ordering, metastability and phase transitions in two-dimensional systems. *Journal of Physics C*, 6(7):1181, 1973.

[34] Skanda Vivek, Colm P Kelleher, Paul M Chaikin, and Eric R Weeks. Long-wavelength fluctuations and the glass transition in two dimensions and three dimensions. *Proceedings of the National Academy of Sciences*, 114(8):1850–1855, 2017.

[35] Elijah Flenner and Grzegorz Szamel. Fundamental differences between glassy dynamics in two and three dimensions. *Nature Communications*, 6:7392, 2015.

[36] Yan-Wei Li, Chandan K Mishra, Zhao-Yan Sun, Kun Zhao, Thomas G Mason, Rajesh Ganapathy, and Massimo Pica Ciamarra. Long-wavelength fluctuations and anomalous dynamics in 2-dimensional liquids. *Proceedings of the National Academy of Sciences*, 116(46):22977–22982, 2019.

[37] Felix Bloch. Zur theorie des ferromagnetismus. *Zeitschrift für Physik*, 61(3): 206–219, 1930.

[38] Rudolf Peierls. Quelques propriétés typiques des corps solides. In *Annales de l'institut Henri Poincaré*, volume 5, pages 177–222, 1935.

[39] Lev Davidovich Landau. On the theory of phase transitions. i. *Zh. Eksp. Teor. Fiz.*, 11:19, 1937.

[40] Pierre C Hohenberg. Existence of long-range order in one and two dimensions. *Physical Review*, 158(2):383, 1967.

[41] John M Kosterlitz and DJ Thouless. Long range order and metastability in two dimensional solids and superfluids.(application of dislocation theory). *Journal of Physics C: Solid State Physics*, 5(11):L124, 1972.

[42] Peter Harrowell. Glass transitions in plane view. *Nature Physics*, 2(3):157–158, 2006. ISSN 1745-2481.

[43] Hayato Shiba, Peter Keim, and Takeshi Kawasaki. Isolating long-wavelength fluctuation from structural relaxation in two-dimensional glass: Cage-relative displacement. *Journal of Physics: Condensed Matter*, 30(9):094004, 2018.

[44] Pablo G Debenedetti and Frank H Stillinger. Supercooled liquids and the glass transition. *Nature*, 410(6825):259, 2001.

[45] Ludovic Berthier, Daniele Coslovich, Andrea Ninarello, and Misaki Ozawa. Equilibrium sampling of hard spheres up to the jamming density and beyond. *Physical Review Letters*, 116(23):238002, 2016.

[46] Zexin Zhang, Ning Xu, Daniel TN Chen, Peter Yunker, Ahmed M Alsayed, Kevin B Aptowicz, Piotr Habdas, Andrea J Liu, Sidney R Nagel, and Arjun G Yodh. Thermal vestige of the zero-temperature jamming transition. *Nature*, 459(7244):230–233, 2009.

[47] Andrea J Liu and Sidney R Nagel. Jamming is not just cool any more. *Nature*, 396(6706):21–22, 1998.

[48] Massimo Pica Ciamarra and Antonio Coniglio. Jamming at zero temperature, zero friction, and finite applied shear stress. *Physical Review Letters*, 103(23): 235701, 2009.

[49] Massimo Pica Ciamarra, Raffaele Pastore, Mario Nicodemi, and Antonio Coniglio. Jamming phase diagram for frictional particles. *Phys. Rev. E*, 84: 041308, Oct 2011.

[50] A. B. Slowman, M. R. Evans, and R. A. Blythe. Jamming and attraction of interacting run-and-tumble random walkers. *Phys. Rev. Lett.*, 116:218101, May 2016.

[51] Silke Henkes, Yaouen Fily, and M. Cristina Marchetti. Active jamming: Self-propelled soft particles at high density. *Physical Review E*, 84(4):040301, oct 2011.

[52] Qinyi Liao and Ning Xu. Criticality of the zero-temperature jamming transition probed by self-propelled particles. *Soft Matter*, 14(5):853–860, 2018.

[53] Ran Ni, Martien A Cohen Stuart, and Marjolein Dijkstra. Pushing the glass transition towards random close packing using self-propelled hard spheres. *Nature Communications*, 4(1):1–7, 2013.

[54] Craig W Reynolds. Flocks, herds and schools: A distributed behavioral model. In *Proceedings of the 14th annual conference on Computer graphics and interactive techniques*, pages 25–34, 1987.

[55] Tamás Vicsek, András Czirók, Eshel Ben-Jacob, Inon Cohen, and Ofer Shochet. Novel type of phase transition in a system of self-driven particles. *Physical Review Letters*, 75(6):1226, 1995.

[56] Clemens Bechinger, R. Di Leonardo, Hartmut Lowen, C. J. O. Reichhardt, Giorgio Volpe, and Giovanni Volpe. Active particles in complex and crowded environments. *Reviews of Modern Physics*, 88:045006, 2016.

[57] Jerome Buhl, David JT Sumpter, Iain D Couzin, Joe J Hale, Emma Despland, Edgar R Miller, and Steve J Simpson. From disorder to order in marching locusts. *Science*, 312(5778):1402–1406, 2006.

[58] Saroj Kumar Nandi. Activity-dependent self-regulation of viscous length scales in biological systems. *Phys. Rev. E*, 97:052404, May 2018.

[59] Thomas E. Angelini, Edouard Hannezo, Xavier Trepat, Manuel Marquez, Jeffrey J. Fredberg, and David A. Weitz. Glass-like dynamics of collective cell migration. *Proceedings of the National Academy of Sciences*, 108(12):4714–4719, 2011. ISSN 0027-8424.

[60] Kenji Nishizawa, Kei Fujiwara, Masahiro Ikenaga, Nobushige Nakajo, Miho Yanagisawa, and Daisuke Mizuno. Universal glass-forming behavior of in vitro and living cytoplasm. *Scientific reports*, 7(1):1–12, 2017.

[61] Tamás Vicsek and Anna Zafeiris. Collective motion. *Physics reports*, 517(3-4): 71–140, 2012.

[62] David Sloan Wilson and Edward O Wilson. Rethinking the theoretical foundation of sociobiology. *The Quarterly review of biology*, 82(4):327–348, 2007.

[63] Nick Gravish, Gregory Gold, Andrew Zangwill, Michael AD Goodisman, and Daniel I Goldman. Glass-like dynamics in confined and congested ant traffic. *Soft matter*, 11(33):6552–6561, 2015.

[64] Manuele Brambilla, Eliseo Ferrante, Mauro Birattari, and Marco Dorigo. Swarm robotics: a review from the swarm engineering perspective. *Swarm Intelligence*, 7(1):1–41, 2013.

[65] Natsuda Klongvessa, Félix Ginot, Christophe Ybert, Cécile Cottin-Bizonne, and Mathieu Leocmach. Nonmonotonic behavior in dense assemblies of active colloids. *Phys. Rev. E*, 100:062603, Dec 2019. doi: 10.1103/PhysRevE.100.062603. URL `https://link.aps.org/doi/10.1103/PhysRevE.100.062603`.

[66] Natsuda Klongvessa, Félix Ginot, Christophe Ybert, Cécile Cottin-Bizonne, and Mathieu Leocmach. Active glass: Ergodicity breaking dramatically affects response to self-propulsion. *Physical review letters*, 123(24):248004, 2019.

[67] Stephen J Ebbens and Jonathan R Howse. In pursuit of propulsion at the nanoscale. *Soft Matter*, 6(4):726–738, 2010.

[68] Andreas Zöttl and Holger Stark. Emergent behavior in active colloids. *Journal of Physics: Condensed Matter*, 28(25):253001, may 2016.

[69] M Cristina Marchetti, Yaouen Fily, Silke Henkes, Adam Patch, and David Yllanes. Minimal model of active colloids highlights the role of mechanical interactions in controlling the emergent behavior of active matter. *Current Opinion in Colloid & Interface Science*, 21:34–43, 2016.

[70] Gabriel S Redner, Caleb G Wagner, Aparna Baskaran, and Michael F Hagan. Classical nucleation theory description of active colloid assembly. *Physical review letters*, 117(14):148002, 2016.

[71] Yaouen Fily and M Cristina Marchetti. Athermal phase separation of self-propelled particles with no alignment. *Physical review letters*, 108(23):235702, 2012.

[72] Gabriel S Redner, Michael F Hagan, and Aparna Baskaran. Structure and dynamics of a phase-separating active colloidal fluid. *Physical Review Letters*, 110(5):055701, 2013.

[73] Adam Wysocki, Roland G. Winkler, and Gerhard Gompper. Cooperative motion of active Brownian spheres in three-dimensional dense suspensions. *EPL (Europhysics Letters)*, 105(4):48004, feb 2014. ISSN 0295-5075. doi: 10.1209/0295-5075/105/48004.

[74] Miguel Ruiz-Garcia, C Gutierrez, Lachlan C Alexander, Dirk GAL Aarts, Luca Ghiringhelli, and Chantal Valeriani. Discovering dynamic laws from observations: the case of self-propelled, interacting colloids. *arXiv preprint arXiv:2203.14846*, 2022.

[75] Yaouen Fily, Silke Henkes, and M Cristina Marchetti. Freezing and phase separation of self-propelled disks. *Soft Matter*, 10(13):2132–2140, 2014.

[76] Pin Nie, Joyjit Chattoraj, Antonio Piscitelli, Patrick Doyle, Ran Ni, and Massimo Pica Ciamarra. Stability phase diagram of active brownian particles. *Physical Review Research*, 2(2):023010, 2020.

[77] Michael E Cates and Julien Tailleur. Motility-induced phase separation. *Annu. Rev. Condens. Matter Phys.*, 6(1):219–244, 2015.

[78] Kenechukwu David Nnetu, Melanie Knorr, Josef Käs, and Mareike Zink. The impact of jamming on boundaries of collectively moving weak-interacting cells. *New Journal of Physics*, 14(11):115012, 2012.

[79] Melody A Swartz. Cell jam. *Nature Materials*, 14(10):970–971, 2015.

[80] Ahmad K Omar, Katherine Klymko, Trevor GrandPre, and Phillip L Geissler. Phase diagram of active brownian spheres: Crystallization and the metastability of motility-induced phase separation. *Physical Review Letters*, 126(18): 188002, 2021.

[81] Etienne P Bernard and Werner Krauth. Two-Step Melting in Two Dimensions: First-Order Liquid-Hexatic Transition. *Phys. Rev. Lett.*, 107(15):155704, 2011.

[82] John Michael Kosterlitz and David James Thouless. Ordering, metastability and phase transitions in two-dimensional systems. *Journal of Physics C: Solid State Physics*, 6(7):1181, 1973.

[83] Pasquale Digregorio, Demian Levis, Antonio Suma, Leticia F Cugliandolo, Giuseppe Gonnella, and Ignacio Pagonabarraga. Full phase diagram of active brownian disks: From melting to motility-induced phase separation. *Physical review letters*, 121(9):098003, 2018.

[84] Silke Henkes, Yaouen Fily, and M Cristina Marchetti. Active jamming: Self-propelled soft particles at high density. *Physical Review E*, 84(4):040301, 2011.

[85] Ran Ni, Martien A.Cohen Stuart, and Marjolein Dijkstra. Pushing the glass transition towards random close packing using self-propelled hard spheres. *Nature Communications*, 4(1):1–7, oct 2013. doi: 10.1038/ncomms3704.

[86] Matteo Paoluzzi, Demian Levis, and Ignacio Pagonabarraga. Are motility-induced phase-separation and glassiness compatible in dense active matter? *arXiv preprint arXiv:2109.14948*, 2021.

[87] Rituparno Mandal and Peter Sollich. Multiple types of aging in active glasses. *Physical Review Letters*, 125(21):218001, 2020.

[88] Ludovic Berthier. Nonequilibrium glassy dynamics of self-propelled hard disks. *Physical Review Letters*, 112(22):220602, 2014.

[89] Rituparno Mandal, Pranab Jyoti Bhuyan, Pinaki Chaudhuri, Chandan Dasgupta, and Madan Rao. Extreme active matter at high densities. *Nature communications*, 11(1):1–8, 2020.

[90] Yann-Edwin Keta, Robert L Jack, and Ludovic Berthier. Disordered collective motion in dense assemblies of persistent particles. *arXiv preprint arXiv:2201.04902*, 2022.

Chapter 3

Long-wavelength fluctuations and dimensionality crossover in confined liquids

In this chapter, we demonstrate that the dimensionality crossover is apparent in the lateral size dependence of the relaxation dynamics of confined liquids, developing a Debye model for the density of vibrational states of confined systems and performing extensive numerical simulations. In confined systems, Mermin-Wagner fluctuations enhance the amplitude of vibrational motion or Debye-Waller factor by a quantity scaling as the inverse gap width and proportional to the logarithm of the aspect ratio. This is a clear signature of a two-dimensional behaviour. As the temperature or lateral system size increases, the crossover to a size-independent relaxation dynamics occurs when structural relaxation takes place before the vibrational modes with the longest wavelength develop.

3.1 Introduction

The phase behaviour and dynamics of liquids confined in slit geometries are affected by the competition of several length scales.

The confined slab geometry introduces an additional length scale, denoted as H, into the system. H represents the distance between the two confining walls and

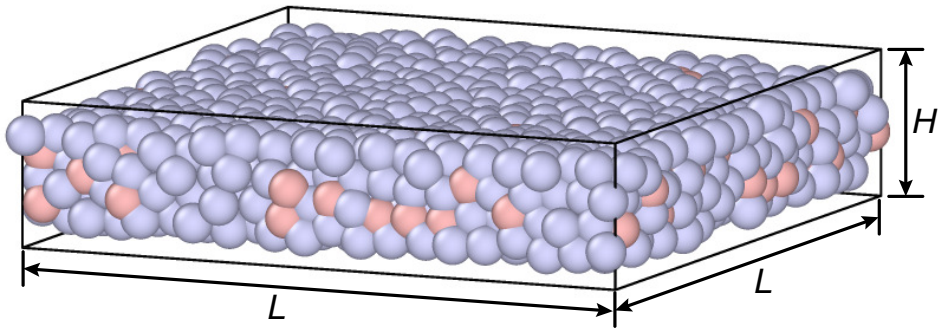

FIGURE 3.1: Schematic configuration of the system confined in slit of dimension $L \times L \times H$. Particles are colored based on their types in Kob-Andersen Lennard-Jones mixture [1].

determines the degree of confinement of the liquid in the gap between the walls. As a result, in a confined system, the lateral length of the gap L, and the gap width H are two control parameters that can govern the behavior of the system.

We illustrate in Figure 3.1 a liquid confined in a slab geometry. We recognize the presence of two confining length scales, the lateral length L and the width H. These length scale may interfere with bulk-liquid length scales, such as the typical distance between the particles, $a_0 = \rho^{-1/3}$, and the structural correlation length, $\xi_{\text{bulk}} \simeq 10$, e.g., as estimated from the decay of the radial distribution function [2–4]. The competition between H and ξ_{bulk} induces a cascade of confinement-induced ordering transitions [3, 5–7], and a solid like behaviour interpreted as a signal of a first-order transition [8, 9] or, more recently [10–12], as a continuous glass transition. For molecular liquids in very narrow confinements, length scales associated with the anisotropic molecular structure [2, 13–15] and the details of the interaction between the molecules and the confining walls also play a role.

The rich and system-dependent phase behaviour of confined systems makes difficult rationalizing the crossover from three to two dimensions focusing on its gap size dependence. Indeed the hexatic phase, which is a phase with short-ranged

translational order and long-ranged bond-orientational order only occurring in two-dimensional systems, has been only reported for $H \simeq a_0$ in Lennard-Jones systems [16]. In this extremely confined limit, the occurrence of a two-dimensional behaviour is in line with the observed decoupling of the lateral and transverse degrees of freedom [17, 18].

The size dependence of the relaxation dynamics of confined liquids offers an alternative and unexplored approach to investigate the dimensionality crossover. Indeed, two-dimensional systems differ from their three-dimensional counterpart because Mermin-Wagner [19] long-wavelength (LW) fluctuations make their relaxation dynamics size dependent [20–26]. This alternative approach is also convenient as Mermin-Wagner fluctuations are always present in two-dimensional systems; conversely, the two- and the three-dimensional phase behaviour do not qualitatively differ in all systems [27–29].

We demonstrate that confined systems have a relaxation dynamics depending on the lateral size L, as two-dimensional ones, and rationalize the dimensionality crossover clarifying how this L dependence varies with the gap width H and relaxation time. We find that, in the solid regime, confinement enhances the asymptotic value of the mean-square displacement, or Debye-Waller factor, by a factor scaling as $(1/H)\ln(L/H)$. A similar enhancement of the mean square displacement occurs in the liquid phase. Liquids, however, exhibit a dimensionality crossover as size-effects vanish above a characteristic H-independent system size fixed by sound velocity and relaxation time. We further clarify that our predictions apply to both molecular and colloidal liquids through the investigation of experimentally relevant confinement settings.

The rest of this chapter is build up as follows. In Section 3.2.1, we develop a theoretical model for the vibrational density of states of confined systems, extending Debye's model. In Section 3.3.1, we detail our numerical approach. In Section 3.3.2, we validate our theoretical model via numerical simulations of confined solids. The Section 3.3.3 provides a further discussion about the the LWs influence on liquids and a quantitative investigation about dimensionality crossover focusing on the mean square displacement. In addition, we broaden our study to different boundary conditions and discussed the effect of smooth and rough walls on the dynamics of confined liquids in Section 3.4. In the last section of this chapter, we summary and conclude our study in the Section 3.5.

3.2 Theoretical model and predictions

3.2.1 Debye's DOS model in confinement

We develop a Debye-like model for the vibrational density of states (DOS) of confined amorphous solids to rationalize the size dependence of their dynamical properties. In confinement, the length scales L and H and the transverse sound velocity c_s fix two characteristic frequencies, shown as,

$$\begin{cases} \omega_{\mathrm{L}} = 2\pi c_s/L \\ \omega_{\mathrm{H}} = 2\pi c_s/H, \end{cases} \tag{3.1}$$

where ω_{L} is the smallest possible phonon frequency. The physical role of ω_{H} is understood considering that phonons with $\omega < \omega_{\mathrm{H}}$, which have a wavelength larger than H, do not fit along the transverse direction. Hence ω_{H} separates the spectrum into a low-frequency region, $\omega_{\mathrm{L}} < \omega < \omega_{\mathrm{H}}$ where excitations are essentially two dimensional, and in a high frequency region, $\omega_{\mathrm{H}} < \omega < \omega_{\mathrm{D}}$, with ω_{D} the Debye' frequency, where excitations are three dimensional.

Debye's approximation is a theoretical model used to describe a solid as a collection of harmonic oscillators. According to this model, each vibrational mode of the solid has a specific frequency, denoted by ω.

The Debye density of states describes the distribution of vibrational modes within a solid. It is proportional to ω to the power of $d-1$, where d represents the dimensionality of the system.

In the Debye' approximation, the density of states of confined solid is

$$D(\omega) = \begin{cases} c\,\dfrac{\omega}{\omega_{\mathrm{D}}^2} & \omega_{\mathrm{L}} \le \omega \le \omega_{\mathrm{H}} \\ c\,\dfrac{\omega^2}{\omega_{\mathrm{H}}\omega_{\mathrm{D}}^2} & \omega_{\mathrm{H}} \le \omega \le \omega_{\mathrm{D}}, \end{cases} \tag{3.2}$$

with c non-dimensional normalization constant,

$$c^{-1} = \frac{1}{2}\left[\left(\frac{\omega_{\mathrm{H}}}{\omega_{\mathrm{D}}}\right)^2 - \left(\frac{\omega_{\mathrm{L}}}{\omega_{\mathrm{D}}}\right)^2\right] - \frac{1}{3}\left[\frac{\omega_{\mathrm{D}}}{\omega_{\mathrm{H}}} - \left(\frac{\omega_{\mathrm{H}}}{\omega_{\mathrm{D}}}\right)^3\right]. \tag{3.3}$$

We remark that we have restricted the above investigation to the transverse modes, which are of greater relevance to our purposes as having a smaller frequency. The longitudinal modes can be similarly described.

The vibrational density of states allows us to evaluate the asymptotic value of the mean square displacement, or the Debye-Waller factor, averaging the contributions $k_BT/m\omega^2$ of the different modes. To highlight the dependence on the different length scales involved, we write $\omega_{\rm D} = 2\pi c_s/\lambda_{\rm D}$, finding

$$\mathrm{DW} = \frac{k_BT}{m\omega_{\rm D}^2} \frac{\ln\left(\frac{L}{H}\right) + \frac{H}{\lambda_{\rm D}} - 1}{\frac{1}{2}\left[\left(\frac{\lambda_{\rm D}}{H}\right)^2 - \left(\frac{\lambda_{\rm D}}{L}\right)^2\right] + \frac{1}{3}\left[\frac{H}{\lambda_{\rm D}} - \left(\frac{\lambda_{\rm D}}{H}\right)^2\right]}. \tag{3.4}$$

The three dimensional limit, $\mathrm{DW_{3D}} \simeq \frac{3k_BT}{m\omega_{\rm D}^2}$, and the two-dimensional one, $\mathrm{DW_{2D}} = \frac{2k_BT}{m\omega_{\rm D}^2}\ln\left(\frac{L}{H}\right)$, are recovered for $H \to L \gg \lambda_{\rm D}$ and for $H \to \lambda_{\rm D} \ll L$, respectively.

In quasi-2D systems, $L \gg H \gg \lambda_D$, Eq. 3.4 is approximated by

$$\mathrm{DW} \simeq \mathrm{DW_{3D}}\left[1 + \frac{\lambda_{\rm D}}{H}\left(\ln\left(\frac{L}{H}\right) - 1\right)\right]. \tag{3.5}$$

Hence, we predict that in confined systems the DW grows logarithmically with L, as in 2D, with a slope decreasing as $1/H$. We remark here that, as long as $H \gg \lambda_{\rm D}$, the DW factor *grows* as H decreases at constant L, e.g., as the system becomes more confined. This occurs because, as H decreases, a larger fraction of the phonon spectrum becomes effectively two-dimensional.

3.2.2 Analytical details

There is a broad agreement on the existence of Debye approximation for low-frequency excitations. Unlike 3D bulk, the slab geometry expected to have different length scales in the lateral and transverse directions. To show a detailed analytical demonstration of Eq. 3.4, we proposed our theoretical model to describe confined vibrational density of state $D(\omega)$. It has three characteristic frequencies and follows $\omega_{\rm L} < \omega_{\rm H} < \omega_{\rm D}$ with a cutoff Debye frequency $\omega_{\rm D}$, detailed in the Figure 3.2. We model the $D(\omega)$ as a piecewise function, where $\omega_{\rm H}$ separates the spectrum into the low and high ranges of frequencies. The density of states for confined solid thus

can be defined as,

$$D(\omega) = \begin{cases} c_1\omega & \omega_L \leq \omega \leq \omega_H \\ c_2\omega^2 & \omega_H \leq \omega \leq \omega_D \end{cases} \tag{3.6}$$

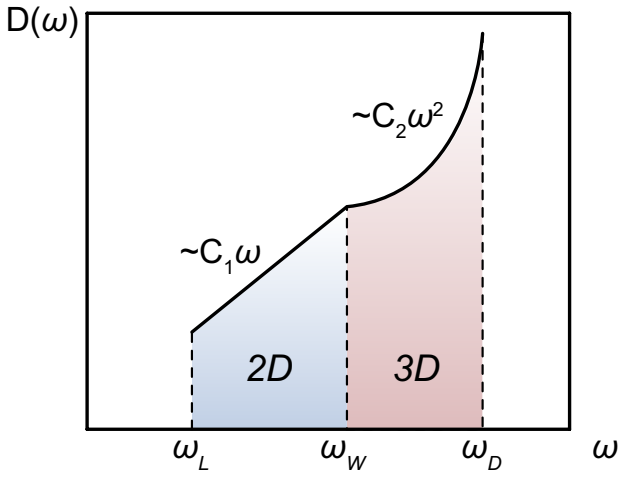

FIGURE 3.2: Schematic illustration of the Debye-like model of confined system.

The prefactor c_1 and c_2 of $D(\omega)$ can be evaluated as requiring the density of state to be continuous, and normalized to 1. For the continuity of density of states, at $\omega = \omega_{\mathrm{H}}$ we have,

$$c_1\omega_H = c_2\omega_H^2, \tag{3.7}$$

so that the constant $c_2 = c_1/\omega_{\mathrm{H}}$.

After the normalization,

$$\int_{\omega_L}^{\omega_D} D(\omega)d\omega = 1, \tag{3.8}$$

the density of states at the given range of frequencies is

$$c_1 \int_{\omega_L}^{\omega_H} \omega d\omega + \frac{c_1}{\omega_H} \int_{\omega_H}^{\omega_D} \omega^2 d\omega = \frac{c_1}{2}\left[\omega_H^2 - \omega_L^2\right] + \frac{c_1}{3\omega_H}\left[\omega_D^3 - \omega_H^3\right] = 1. \tag{3.9}$$

The frequencies dependent constant c_1 is therefore given by

$$c_1^{-1} = \frac{1}{2}\left[\omega_H^2 - \omega_L^2\right] + \frac{1}{3\omega_H}\left[\omega_D^3 - \omega_H^3\right]. \tag{3.10}$$

To non-dimensionalize, we define

$$\begin{cases} \omega_{\mathrm{H}} = a_H \omega_{\mathrm{D}} \\ \omega_{\mathrm{L}} = a_L \omega_{\mathrm{D}}, \end{cases} \tag{3.11}$$

at the given condition $\omega_{\mathrm{L}} \leq \omega_{\mathrm{H}} \leq 1$, the relevant range of parameters is $a_L \leq a_H \leq 1$.

Note that if $a_H = 1$ or equivalently $\omega_{\mathrm{H}} = \omega_{\mathrm{D}}$, the system is in the strictly confined geometry, in this scenario, the system is effective 2D-like. If $a_H = a_L$ or equivalently $\omega_{\mathrm{H}} = \omega_{\mathrm{L}}$, there is no confinement introduced to the system, the system is effective 3D-like. This allows us to introduce an increasing confinement by increasing a_H.

We thus have

$$\begin{aligned} c_1^{-1} &= \frac{\omega_D^2}{2}\left[a_H^2 - a_L^2\right] + \frac{\omega_D^3}{3\omega_H}\left[1 - a_H^3\right] \\ &= \omega_D^2 \left(\frac{1}{2}\left[a_H^2 - a_L^2\right] + \frac{1}{3a_H}\left[1 - a_H^3\right]\right) \end{aligned} \tag{3.12}$$

In general, a vibrational mode with eigenfrequency ω has an amplitude $A(\omega) = \frac{k_B T}{\omega^2}$ apart from a constant.

Hence, the mean square displacement for a confined solid can be described as

$$\begin{aligned} \boldsymbol{r}^2 &= \int_{\omega_L}^{\omega_D} \frac{k_B T}{\omega^2} D(\omega) d\omega \\ &= \int_{\omega_L}^{\omega_H} \frac{k_B T}{\omega^2} D(\omega) d\omega + \int_{\omega_H}^{\omega_D} \frac{k_B T}{\omega^2} D(\omega) d\omega. \end{aligned} \tag{3.13}$$

By considering averaged contributions of all vibrational modes,

$$\begin{aligned} \int_{\omega_L}^{\omega_H} \frac{k_B T}{\omega^2} D(\omega) d\omega &= \int_{\omega_L}^{\omega_H} \frac{k_B T}{\omega^2} c_1 \omega d\omega \\ &= k_B T c_1 \ln\left(\frac{\omega_H}{\omega_L}\right) \\ &= k_B T c_1 \ln\left(\frac{a_H}{a_L}\right), \end{aligned} \tag{3.14}$$

and

$$\begin{aligned}\int_{\omega_H}^{\omega_D} \frac{k_B T}{\omega^2} D(\omega) d\omega &= \int_{\omega_H}^{\omega_D} \frac{k_B T}{\omega^2} \frac{c_1}{\omega_H} \omega^2 d\omega \\ &= \frac{k_B T c_1}{\omega_H} (\omega_D - \omega_H) \\ &= \frac{k_B T c_1}{a_H} (1 - a_H),\end{aligned} \tag{3.15}$$

the overall mean square displacement is described as

$$\boldsymbol{r}^2(\omega_D, a_L, a_H) = \frac{k_B T}{\omega_D^2 \left(\frac{1}{2}[a_H^2 - a_L^2] + \frac{1}{3a_H}[1 - a_H^3]\right)} \left(\ln\left(\frac{a_H}{a_L}\right) + \frac{1}{a_H}(1 - a_H)\right). \tag{3.16}$$

The final expression of thermal mean square displacement thus can be evaluated in units of the contribution of the Debye mode,

$$\widetilde{\boldsymbol{r}^2}(a_L, a_H) = \frac{\boldsymbol{r}^2(\omega_D, a_L, a_H)\,\omega_D^2}{k_B T} = \frac{\ln\left(\frac{a_H}{a_L}\right) + \frac{1}{a_H}(1 - a_H)}{\frac{1}{2}[a_H^2 - a_L^2] + \frac{1}{3a_H}[1 - a_H^3]}, \tag{3.17}$$

where $\boldsymbol{r}^2(\omega_D, a_L, a_H)$ is demonstrated analytically to appear a monotonously increasing behavior with larger a_H or equivalently smaller H (the analytical plot shown in Figure 3.3). This suggests that more LW thermal modes have contribution to MSD in stronger confining geometries.

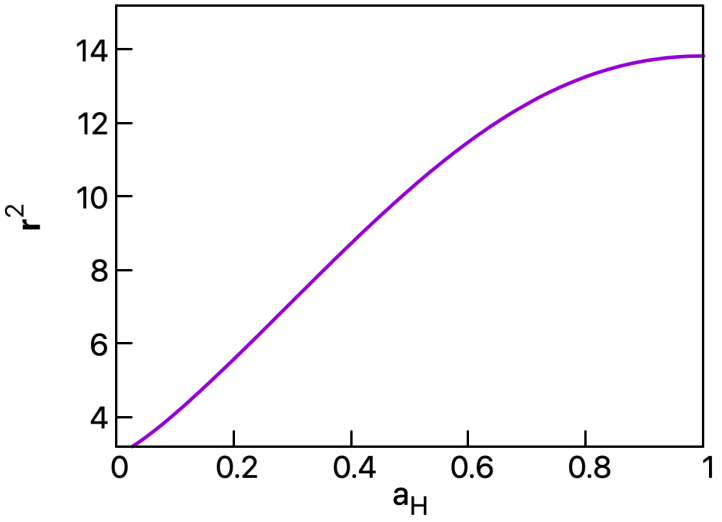

FIGURE 3.3: The plot of analytical function of $\boldsymbol{r}^2(\omega_D, a_L, a_H)$ as a function of a_H.

3.3 Numerical validations and simulation details

3.3.1 Numerical details

We validate our theoretical prediction, and explore the effect of confinement on the liquid phase, via extensive molecular dynamics simulations [30] of the standard A:B 80:20 Kob-Andersen (KA) Lennard-Jones (LJ) mixture [1] to avoid crystallization. The particles interact via the potential,

$$V_{\alpha\beta}(r) = 4\epsilon_{\alpha\beta}\left[\left(\frac{\sigma_{\alpha\beta}}{r}\right)^{12} - \left(\frac{\sigma_{\alpha\beta}}{r}\right)^{6} + C_{\alpha\beta}\right] \tag{3.18}$$

where $\epsilon_{AB} = 1.5\epsilon_{AA}$, $\epsilon_{BB} = 0.5\epsilon_{AA}$, $\sigma_{AB} = 0.8\sigma_{AA}$, $\sigma_{BB} = 0.88\sigma_{AA}$, $\alpha, \beta \in \{A, B\}$. The potential is truncated at $r_c = 2.5\sigma_{\alpha\beta}$, and $C_{\alpha\beta}$ enforces $V(r_c) = 0$. The mass of the particles m, ϵ_{AA}, and σ_{AA} are our unit of mass, energy and distance, respectively. We first thermalize the system in the NPT ensemble, at $P = 1.0$, allowing the box size to vary only in the lateral dimensions. Production runs are then performed in the NVE ensemble. The number of particles depends on L and H, and varies between 10^3 to 10^6 million. We average the dynamical data over at least four independent runs.

We monitor the relaxation dynamics studying the mean square displacement,

$$\langle \Delta \boldsymbol{r}^2(t) \rangle = \frac{1}{N} \sum \Delta \boldsymbol{r}_i^2(t), \tag{3.19}$$

where $\Delta \boldsymbol{r}_i$ is the displacement of particle i at time t, and the self-scattering function,

$$F_s(\boldsymbol{k}, t) = \frac{1}{N} \left\langle \sum_{j=1}^{N} e^{i\boldsymbol{k} \cdot \Delta \boldsymbol{r}_j(t)} \right\rangle, \tag{3.20}$$

where $\boldsymbol{k}$ the wavevector of the first peak of the static structure factor of bulk systems. The relaxation time τ is defined by $F_s(\boldsymbol{k}, \tau) = 1/e$.

We further investigate the dynamics using the cage-relative mean square displacement and self-scattering function [21–23, 31]. These are defined as above, with the displacement of particle i replaced by its cage-relative counterpart,

$$\Delta_{\mathrm{CR}} \boldsymbol{r}_i = \Delta \boldsymbol{r}_i - \frac{1}{n_i} \sum_j \Delta \boldsymbol{r}_j, \tag{3.21}$$

where the sum is over all neighbors of particle i at time $t = 0$. We identify the neighbors via the Voronoi construction.

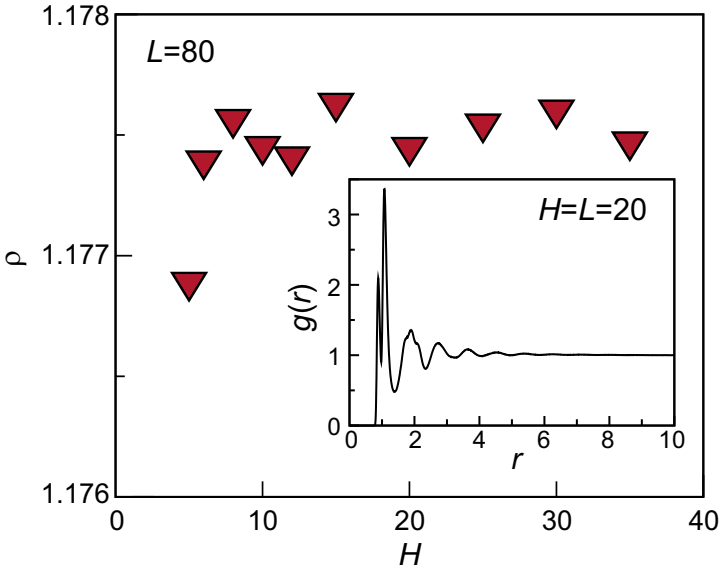

FIGURE 3.4: The dependence of the average density on the gap width, at $T = 0.35$, when periodic boundary conditions are used in the confining direction. Confinement does not strongly influence the average density, in the range of gap widths we have considered. The radial distribution function, shown in the inset for $H = 20$ and $L = 20$ at $T = 0.35$, approaches one at the correlation length $\xi_{\rm bulk}/2 \simeq 5$.

We consider three different confinement approaches. First, we use periodic boundary conditions in the confining direction, which is an approach that is useful to avoid layering as well as to compare with the theoretical predictions. When using this approach, the number density is essentially constant, $\rho = 1.1775(5)$, as we illustrate in the main panel of Figure 3.4. In the figure we also show that, for larger H values representative of the bulk limit, the radial distribution function becomes constant for $r \simeq \xi_{\rm bulk}/2 \simeq 5$.

Secondly, we confine the system between flat walls. In this case, the interaction between particles of type $i = A, B$ and the walls is given by a LJ potential with energy scale ϵ_{ii} and length scale σ_{ii}, truncated in its minimum. In the presence of flat walls, the density sensibly decreases with H, and layering occurs, as shown in the inset of Figure 3.5.

Finally, we perform simulations of systems confined between rough walls. In this case, we first thermalize at the desired state pressure large samples, using periodic boundary conditions in all directions, and then freeze the positions of all

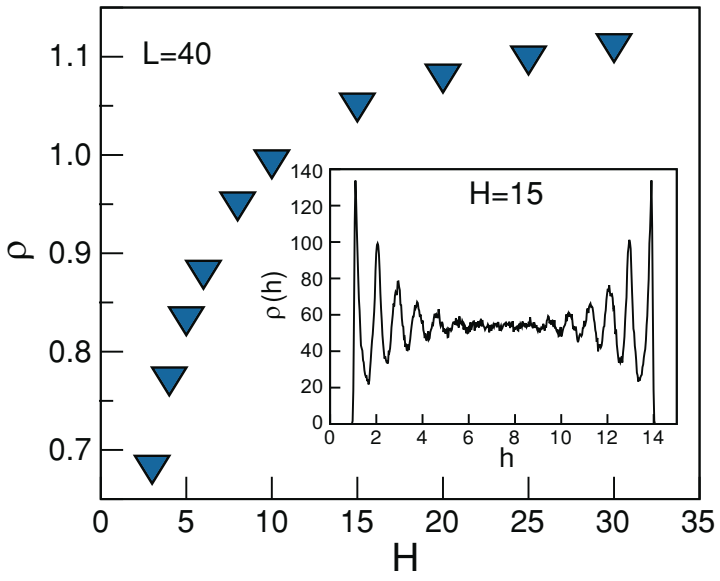

FIGURE 3.5: Dependence of the average density on the gap width, at $T = 0.35$, for a system confined in between flat walls at a separation H. The density decreases as the gap width decreases. Flat walls, furthermore, induce layering, as we illustrate in the inset by plotting the density at a distance h from a confining wall. The inset shows particle number density as a function of distance from confinement in the unit of particle size.

particles whose height is outside the interval $[0 : H]$ with confinement gap width H. When using rough walls, we work at fixed density rather than at fixed pressure.

3.3.2 Confined amorphous solids

We study the density of states of confined amorphous solid configurations generated by minimizing the energy of configurations equilibrated at low temperature. We fix the pressure of these low-temperature configurations to $P = 1.0$ by adjusting the lateral size, which slightly fluctuates around $L = 80$. We considered several H values, so that the number of particles ranges from 36000 to 150000. We further use periodic boundary conditions in all spatial directions to prevent structural inhomogeneities due to layering, hence allowing for a more transparent comparison with the theoretical predictions. The effect of walls is discussed in Section 3.4.

We evaluate the low-frequency end of the vibrational spectrum of the generated energy minima via the direct diagonalization of their Hessian matrix. To compare the numerical results with our theoretical prediction of Eq. 3.2, schematically illustrated in Figure 3.6(a), we focus on the frequency dependence of the

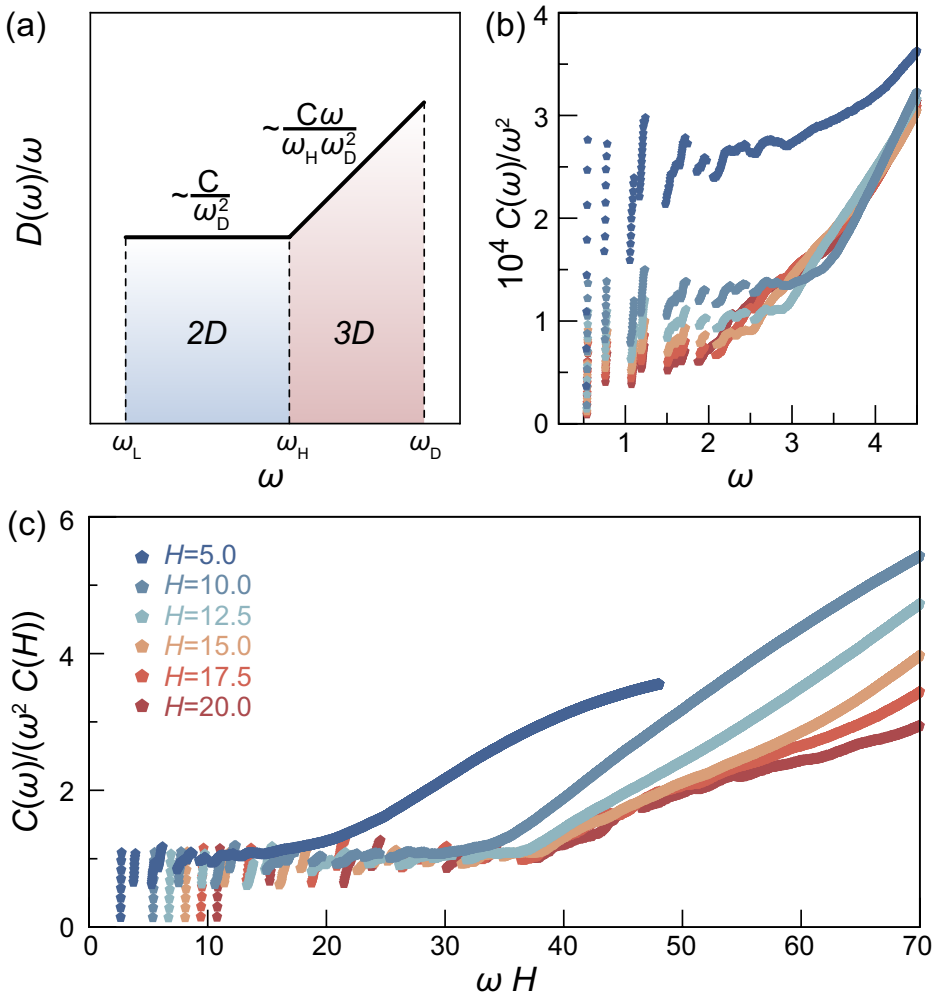

FIGURE 3.6: (a) Schematic illustration of the Debye's density of states of quasi-2D systems, Eq. 3.2. (b) Low-frequency cumulative density of states of confined solids with lateral length $L = 80$ and different gap sizes H. (c) The data in **a** collapses when plotted vs. ωH and vertically scaled, for $H > \xi_{\text{bulk}} \simeq 10$.

cumulative distribution $C(\omega) = \int D(\omega)d\omega$. Due to the large lateral size of our systems [32], we observe gaps at low frequency, as predicted by linear elasticity. We have verified that these gaps are not an artefact of the discontinuity of the force at the cutoff distance [33], as they persist when the interaction potential is appropriately smoothed. Figure 3.6(b) also demonstrates that $C(\omega)/\omega^2$ is constant at small frequencies, and increases above an H dependent crossover frequency which, according to Eq. 3.2, should scale as $\omega_H \propto c_s/H$. Indeed, when plotted versus ωH, and vertically scaled, the data collapse up to their crossover point, as we illustrate in Figure 3.6(c). The figure also supports the ω^2 to ω^3 crossover for the cumulative distribution suggested by the theoretical model.

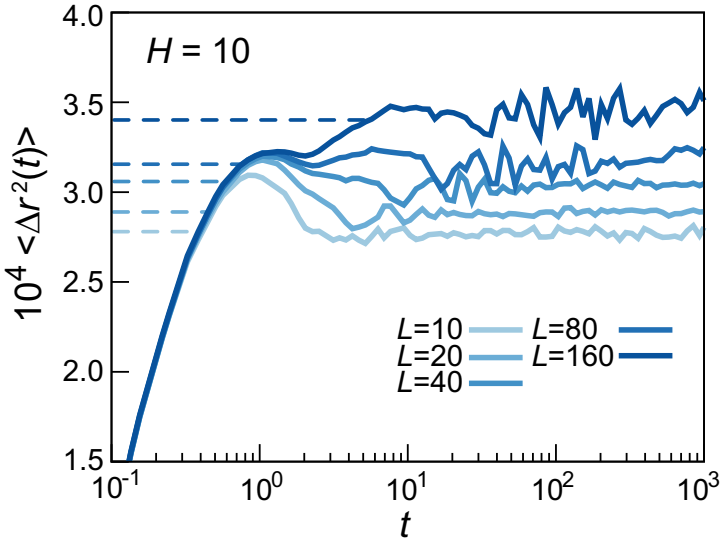

FIGURE 3.7: Mean square displacement of quasi-2D solids at $T = 0.005$ and $H = 10$, for different L values. Errors are smaller than the symbol size. The dash lines indicate the asymptotic DW values.

We remark that the data collapse of Figure 3.6(c) breaks for small H. To rationalize this observation, we investigate in Figure 3.4 the gap size dependence of the density and the radial correlation function of a low-temperature solid configuration. We observe that the density is almost H independent, for $H \geq 5$, and that the radial correlation function approaches the ideal gas limit at $r \simeq 5$. This allows us to estimate the structural correlation length of the bulk solid, $\xi_{\text{bulk}} \simeq 10$. We thus understand that, in Figure 3.6(c), no collapse occurs for small H as confinement interferes with the structural correlation length of the system.

We further validate our theoretical prediction for the dependence of the DW factor of amorphous solids on the relevant length scales L and H, Eq. 3.5, performing simulations at a low-temperature value at which structural relaxation is negligible. In this limit, the mean-square displacement approaches a constant DW value at long times, as illustrated in Figure 3.7 for $H = 10$. Figure 3.8(a) shows that this limiting DW factor grows as the logarithm of the lateral size L, with a slope scaling as $1/H$, in agreement with the predictions of Eq. 3.5.

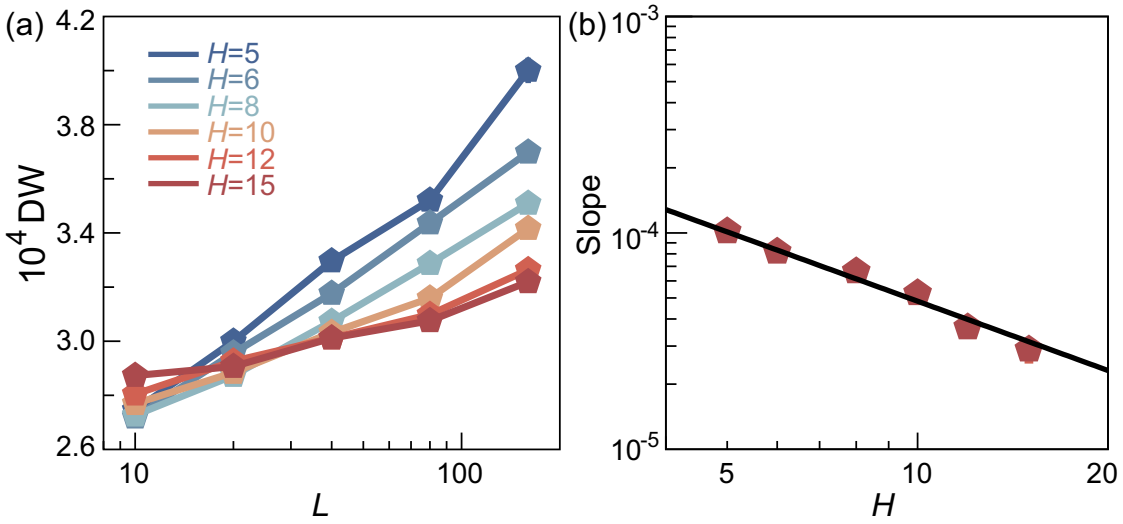

FIGURE 3.8: The asymptotic DW factor of quasi-2D systems with a slope. (a) The asymptotic DW factor grows logarithmically with the lateral size L. (b) The slope of asymptotic DW factor growth scaling as $1/H$. Errors are smaller than the symbol size.

3.3.3 Confined liquids

Having ascertained that LWs influence the behaviour of confined solids, we now demonstrate that they similarly affect the relaxation dynamics of quasi-2D supercooled-liquids. To this end, we investigate the size and temperature dependence of the mean square displacement and self-scattering function at the wave vector of the peak of the static structure factor of bulk systems. Figures 3.9(a) and (b) show that the transient solid-like response in which particles are temporary tracked in cages formed by their neighbors, revealed by the mean square displacement and the self-scattering function becomes less apparent as the system size decreases. This size dependence is more apparent at low temperature, where the transient solid like behaviour is manifest.

We prove that this observed size dependence originates from LW fluctuations by comparing the L dependence of the relaxation time τ and of the cage-relative (CR) relaxation time τ_{CR}. Cage-relative quantities, indeed, are insensitive to collective particle displacements and hence filter out the effect of LWs [21–23]. In Figure 3.11(a), we observe that, while the standard relaxation time decreases logarithmically with L, the CR one is L independent. These results closely parallel those observed in strictly two-dimensional systems [20–26] and demonstrate that

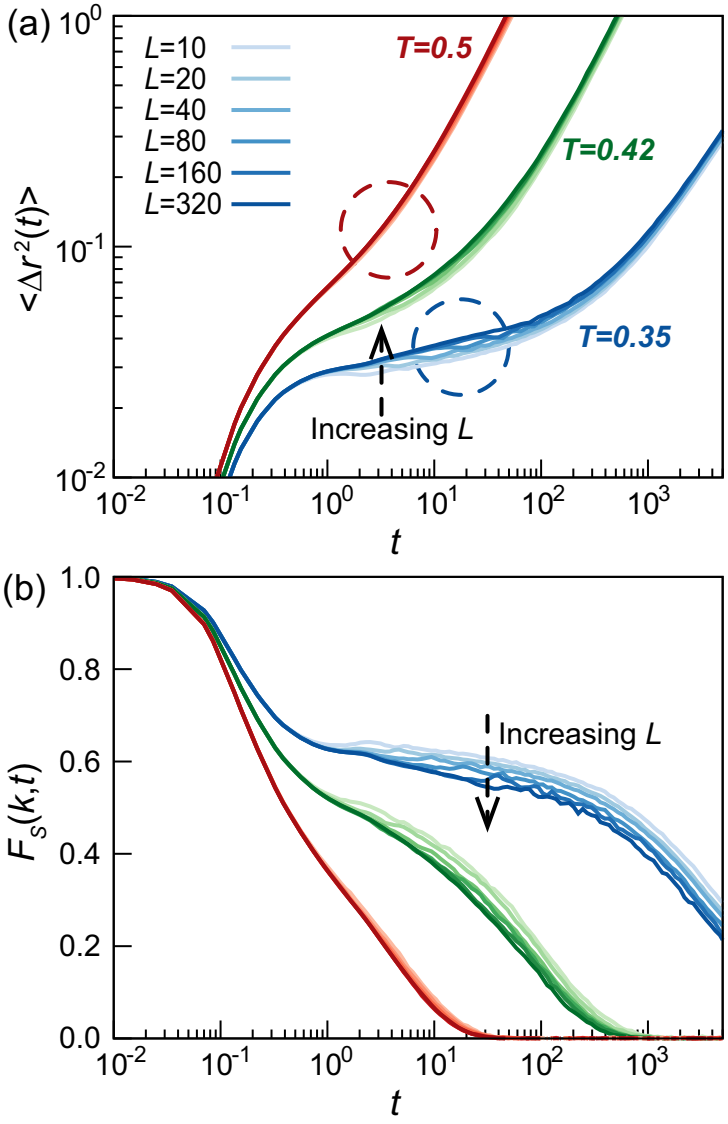

FIGURE 3.9: Long-wavelength fluctuations in confined amorphous supercooled liquids. (a) Mean square displacement, and (b), self-scattering function, at three different values of the temperature. We fix $H = 10$ and show, at each temperature, results for $10 \leq L \leq 320$. The dashed circles indicate the distinction of size effect at two different temperatures which are zoomed in as Figure 3.10.

LW fluctuations sensibly affect the structural relaxation dynamics of confined liquids. In Figure 3.11(b), we further show that the relaxation time τ decreases as the gap width is reduced and a larger fraction of the vibrational spectrum becomes effectively two-dimensional. This dynamical speed up is particularly relevant for $H < \xi_{\text{bulk}}$, indicating that the structural changes induced by such strong confinement promote LW fluctuations. This is consistent with the observation of a

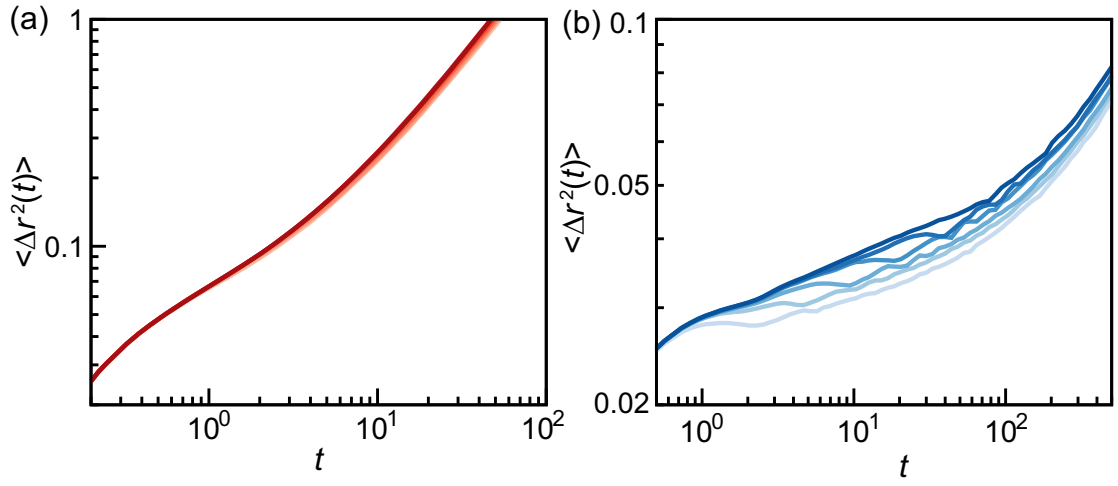

FIGURE 3.10: The distinction of size effect on mean squared displacement at two different temperatures, (a) higher temperature $T = 0.5$ and (b) lower temperature $T = 0.35$, We fix $H = 10$ and show, at each temperature, results for $10 \leq L \leq 320$.

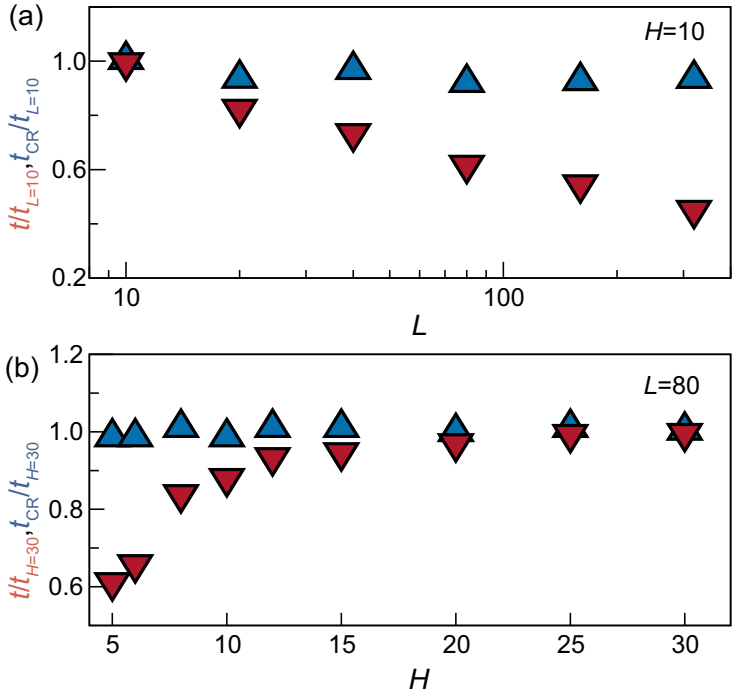

FIGURE 3.11: The L dependence of the relaxation time and cage-relative relaxation time. (a) The relaxation time decreases as the lateral size increases, while the cage-relative relaxation time is L-independent. (b) The relaxation time decreases as the gap-size decreases, particularly for $H \leq \xi_{\text{bulk}}$, while the cage-relative relaxation time is H-independent. The relaxation times in (a) and (b) are divided by their respective values at $L = 10$ and at $H = 30$, to facilitate their comparison. In (a) and (b), errors are smaller than the symbol size.

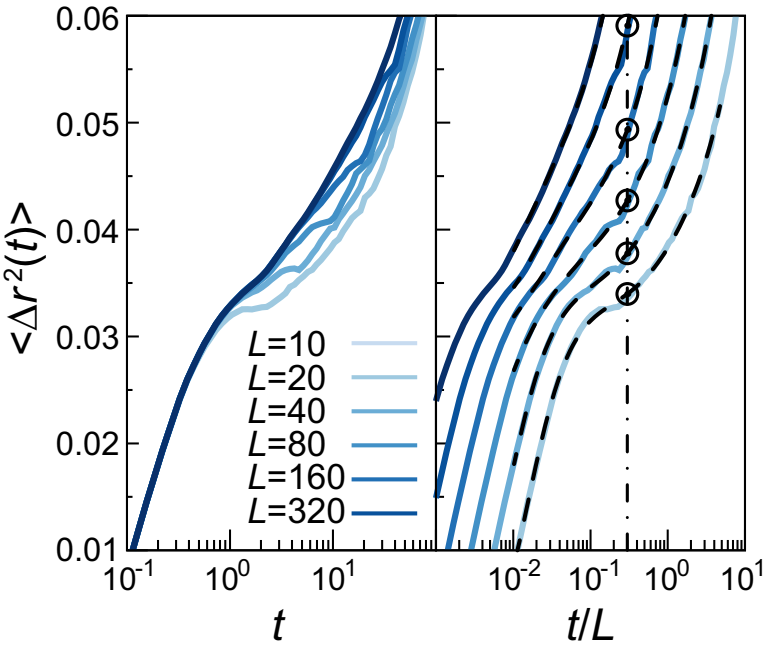

FIGURE 3.12: Dimensionality crossover in confined liquids. The mean square displacement exhibits a crossover between two different regimes at a time $t_{\rm LW} \simeq 0.3L$ (dash-dotted line). Dashed lines are polynomial fits used to estimate the mean square displacement at the crossover time (circles). Data are for $T = 0.35$, and different L values. The panel refers to $H = 10$.

significant increment in the density of low-frequency modes for $H = 5$, in Figure 3.6(b). The gap independence of the cage-relative relaxation time, also illustrated in Figure 3.11(b), confirms our interpretation, namely that the H-induced speed-up originates from LW fluctuations.

We quantitatively investigate the dimensionality crossover focusing on the mean square displacement, $\langle \Delta r^2(t) \rangle$. In the solid phase, $\langle \Delta r^2(t) \rangle$ approaches an asymptotic DW factor value on a time scale $t_{\rm LW} \propto \omega_L^{-1} \propto L$. The asymptotic value of the DW factor grows as $\ln L/f(L)$, with $f(L)$ a slowing increasing function of L, corresponding to the denominator of Eq. 3.4. In the liquid phase, therefore, we expect a crossover in the time dependence of the mean square displacement at a time $t_{\rm LW}$. Figures 3.12 and 3.13(a) demonstrate that such a crossover occurs at $t_{\rm LW} \simeq 0.3L$, for $T = 0.38$. At the same $t_{\rm LW}$ similar crossovers occur at all temperatures.

When LW fluctuations dominate the dynamics, as in the solid phase, $\frac{\langle \Delta r^2(t_{\rm LW}) \rangle}{\ln L} \propto 1/f(L)$ decreases with L. We therefore assume LW fluctuations to become negligible at L values at which $\langle \Delta r^2(t_{\rm LW}) \rangle$ grows faster than $\ln L$. When this occurs,

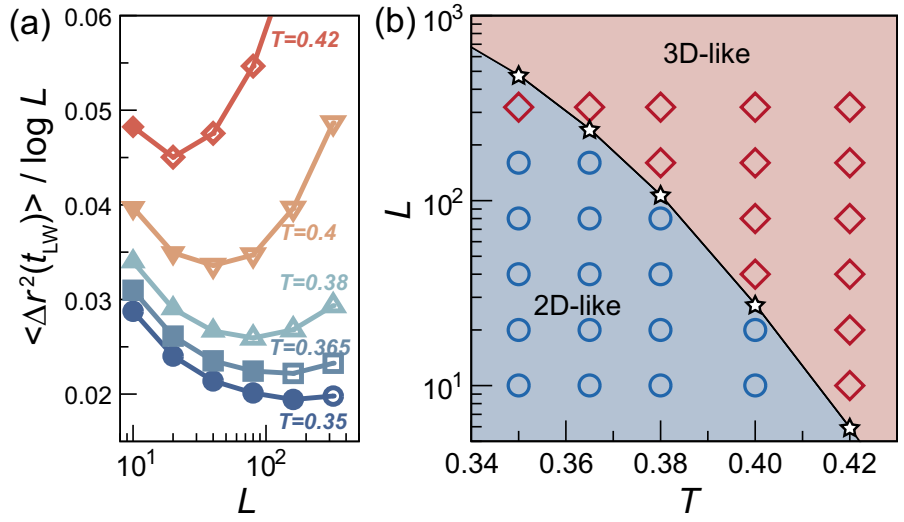

FIGURE 3.13: (a) The mean square displacement at the crossover time grows faster that $\ln L$ (open symbols), above a characteristic T dependent lateral system size. When this occurs, structural relaxation rather than LWs dominate the diffusivity, and hence the system has a 3D-like behaviour. (b) State points with an effective two-dimensional behaviour according to the analysis in (a), are illustrated as open circles. Diamonds, conversely, identify those having a three-dimensional behaviour. Stars correspond to the prediction of Eq. 3.22, $L = \alpha c_s \tau_{CR}(T)$, with $\alpha \simeq 0.018$. The interpolating solid line is a guide to the eye. Both panels refer to $H = 10$.

irreversible relaxation events rather than large-amplitude oscillations dominate the diffusivity. In Figure 3.13(a) we indeed observe that $\langle \Delta r^2(t_{\rm LW}) \rangle / \ln L$ is not monotonic in L, decreasing with L when LWs are relevant (solid symbols), and increasing when they are not (open symbols). This behavior allows us to identify crossover L values, which we have verified not to depend on the gap width. This study leads to the L-T diagram of Figure 3.13(b). The system-size dependent dynamics characteristic of two-dimensional behaviour occurs at low temperature and small lateral size and disappears as either the lateral length or the temperature increase. We remark that while this diagram does not depend on the confinement width H, size effects gradually fade away as $1/H$, as in the solid phase, and hence become not appreciable at large H.

We exploit the size independence of the cage-relative relaxation time to rationalize this observed dimensionality crossover. Indeed, vibrational excitations cannot last more than the cage-relative relaxation time, as on this time scale the structure of the system sensibly changes, as particles change neighbours. Since the vibrational modes influencing the structural relaxation dynamics are those

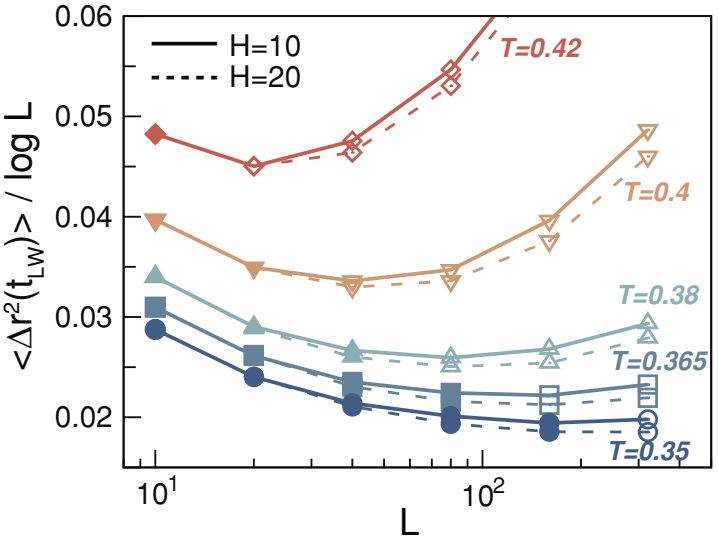

FIGURE 3.14: The dependence of $\langle r^2(t_{\mathrm{LW}})\rangle / \log L$ on L.

that have time to develop, we expect the crossover between a two-dimensional size-dependent relaxation dynamics and a three-dimensional size-independent relaxation dynamics to occur at

$$\frac{L}{\tau_{\mathrm{CR}}(T)} = \alpha c_s, \tag{3.22}$$

with c_s being the transverse sound velocity and α being a constant. In other words, size effects disappear for $L > \alpha c_s \tau_{\mathrm{CR}}(T)$, as the system relaxes before the lowest size-dependent mode develops. This theoretical prediction well describes the data of Figure 3.13(d). Figure 3.14 shows that the results are insensitive to changes in the gap width. We use to mark the crossover from a two-dimensional regime where LWs dominate the diffusivity, to a three-dimensional one where they do not, is qualitatively the same for different H values. The dimensionality crossover, therefore, does not depend on H.

We remark, however, that the quantitative effect of the LWs fluctuations on the relaxation dynamics fades away as H increases, suggesting that the crossover should become undetectable for large enough gap width. This large-gap regime is not accessible in our simulations; already for $H = 20$, indeed, we need to simulate systems with up 2M particles. But this trend can be seen at $T = 0.35$, the growths of the Debye-Waller factor due to the LW modes are visually revealed by different wall separations H.

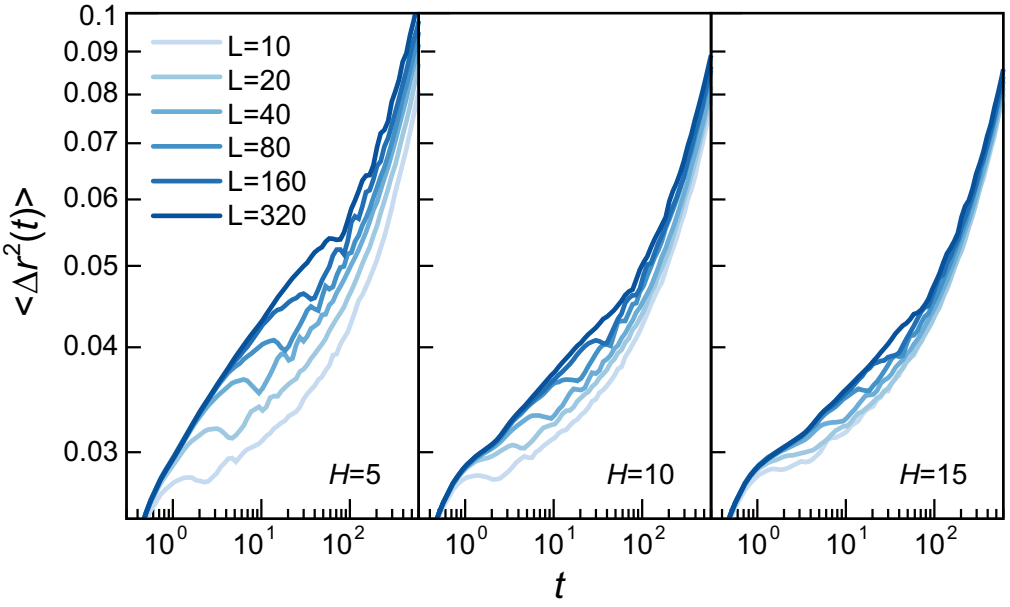

FIGURE 3.15: Dynamical quantities of time dependent MSD with different wall separations varying as $5 \leq H \leq 15$, at transverse system length scales $10 \leq L \leq 320$, for T = 0.35.

3.4 Effect of smooth and rough walls

3.4.1 Smooth walls confinement

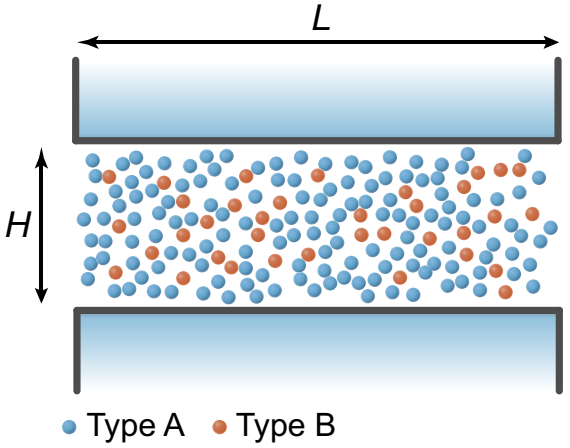

FIGURE 3.16: A schematic diagram of the confining smooth walls.

Our theoretical analysis and numerical simulations demonstrate that LW fluctuations affect the dynamics of confined liquids. However, so far we have described

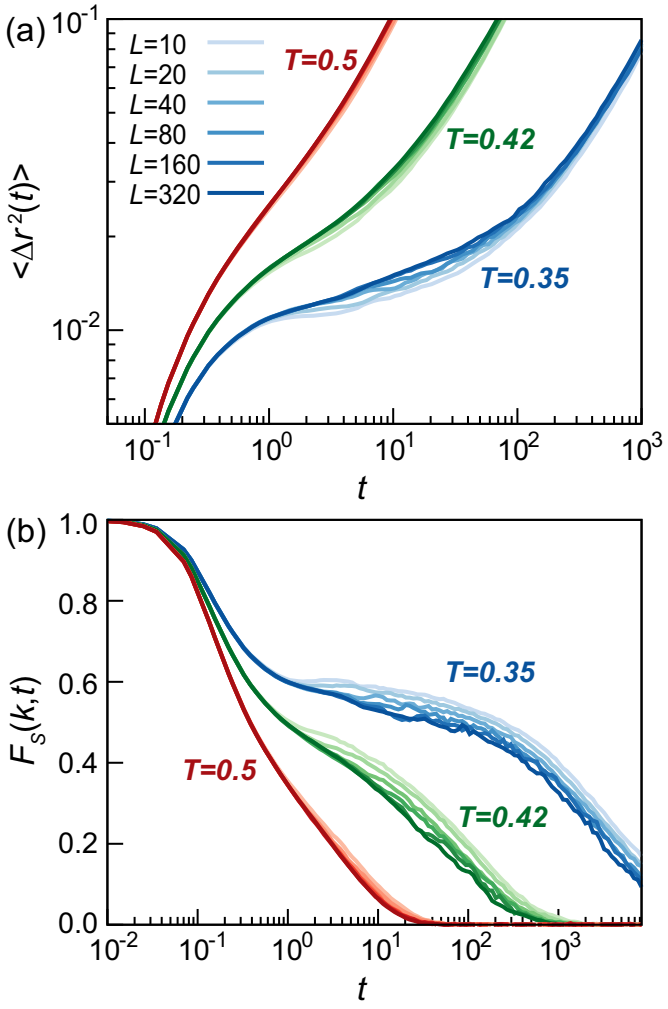

FIGURE 3.17: Long-wavelength fluctuations in flat slit geometries. (a) The transverse mean-square-displacement and (b) the self-intermediate scattering function for supercooled liquids with various transverse length scales $10 \leq L \leq 320$ at the same perpendicular length scale $H = 10$.

simulations obtained using periodic boundary conditions in all spatial directions; one might wonder, therefore, whether LWs also play a role in the experimentally relevant set up of liquids confined between two parallel walls at a separation H. To address this question, we investigate the relaxation dynamics of the KA LJ binary mixture confined between two atomically-smooth flat walls, as illustrated in Figure 3.16.

Since the walls prevent diffusion along the transverse direction, we focus on particle motion in the lateral directions, effectively defining two-dimensional mean-square displacement and self-scattering function. We find that, under wall confinement, the relaxation dynamics has the typical size dependence induced by LW

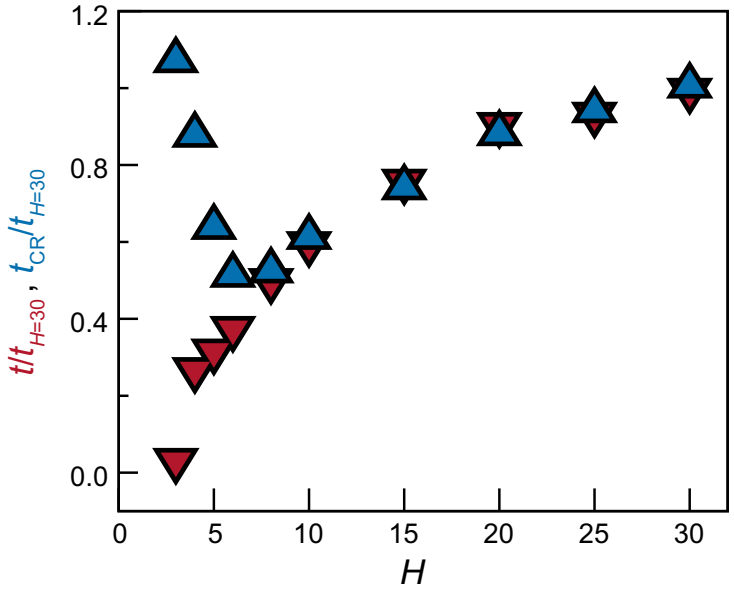

FIGURE 3.18: Width dependence of the relaxation time, and of the cage-relative relaxation time for a $L = 40$ system. Errors are smaller than the symbol size.

fluctuations, the caging regime becoming less apparent as L increases, as we illustrate in Figure 3.17(a) and Figure 3.17(b).

The structural changes induced by the walls, however, strongly affect the relaxation dynamics, as evidenced by the H dependence of the standard and CR relaxation times, which we illustrate in Figure 3.18. For $H \geq \xi_{\text{bulk}}$, both relaxation times decrease as the system becomes more confined; this is, we believe, the combined effect of layering and the reduction in the average density induced by the confinement.

Importantly, we observe in Fig. 3.17(c) that for $H \leq \xi_{\text{bulk}}$, while the relaxation time decreases as the gap width is reduced, the cage-relative relaxation sharply increases. This increase in the CR-relaxation time is in qualitative agreement with the many previous investigations reporting an increase in the viscosity of molecular liquids under confinement [2, 10, 12, 34, 35]. Indeed, we remind the reader that viscosity and cage-relative relaxation time are related [26, 36]. This observed decoupling demonstrates that smooth walls do not kill the LWs, but rather make their effect more apparent.

3.4.2 Rough walls confinement

While smooth walls do not kill LWs, rough walls strongly suppress them. Here we perform the numerical simulations to rationalize the liquids confined between two rough walls condition. The particles are first placed randomly in a 3D simulation box and then the system is equilibrated at different temperatures using periodic boundary conditions in all three directions. To construct the rough wall confined system, we pin particles placed at $z < -H/2$ and $z > H/2$, resulting in two symmetric rough walls at $z = \pm H/2$ and a region of free particles with the separation H (see Figure 3.19). This confined system is again equilibrated with periodic boundary conditions only in x and y directions, so that the free particles have time to relax. The free particles are therefore confined by rough walls. The thickness of the free particles region H set the strength of the spatial separation and thus the degree of confinement. By tuning this thickness, we investigate the system-size dependence of the dynamics at different degrees of confinement.

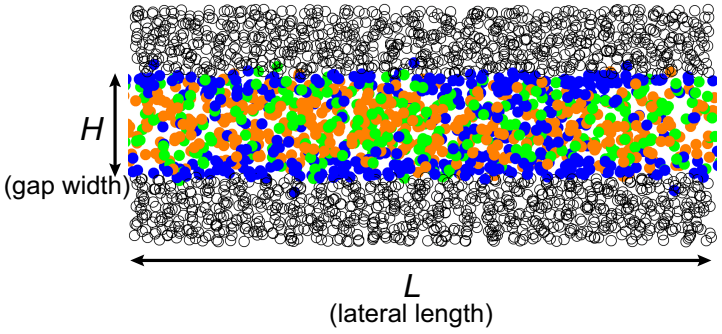

FIGURE 3.19: Schematic configuration of the rough-wall confined system with freely evolving particles (colored solid circles) sandwiched by two rough walls, which is composed of pinned particles (gray open circles).

Indeed, we show in Figure 3.20 that the relaxation dynamics of liquids confined between rough walls does not depend on the lateral system size.

For the studied range of the separation H, the system size dependence of the MSD and the ISF is very small, which is strikingly different from the observation in the case of smooth walls, as we illustrate in Figure 3.17. The above observations including the obvious plateau region in both MSD and ISF even at large system size as well as the absence of system size dependence of the dynamics implies that the effect the LW fluctuations is unobservable at given rough-wall separation condition.

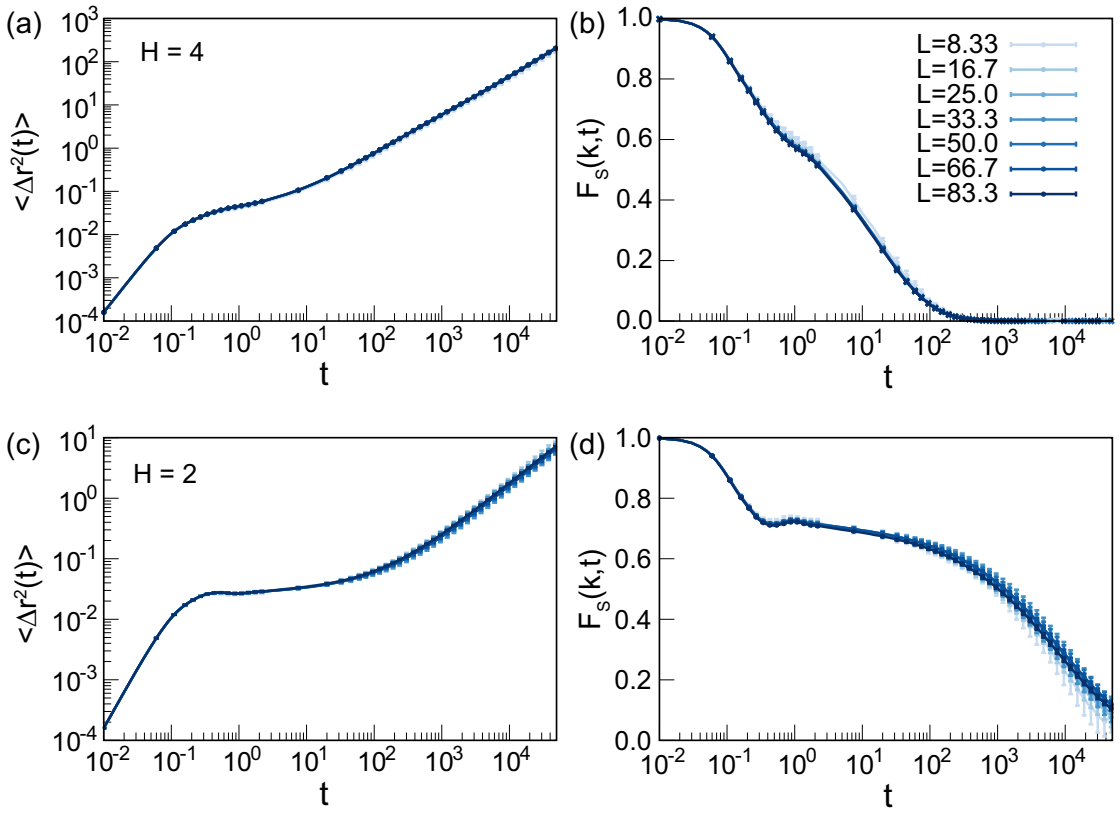

FIGURE 3.20: Mean-square displacement (a) and self-scattering function (b) of systems confined between rough walls, at $H = 2$ and $H = 4$. These quantities are evaluated focusing on the behavior of the central layer of particles. The relaxation dynamics does not depend on the lateral length, or system size N, indicating that the rough walls kill the LW fluctuations.

We remark that for very large gap widths the effect of the boundary should become negligible, and hence LW fluctuations should play a role. Since the influence of LWs on the dynamics scales as $1/H$, however, their effect in this large-H limit may be not easily appreciated. We expect variations [14] in the roughness of the confining walls and the wall-liquid interaction potential to only qualitatively affect the observed phenomenology.

3.5 Conclusions and discussions

3.5.1 Conclusions

The confinement-induced enhancement of the DW factor described Eq. 3.4 is an equilibrium property not affected by the underlying microscopic dynamics, equally

valid for molecular and colloidal solids. In the supercooled regime, the signatures of LW fluctuations conversely depend on how much the system moves along the phase-space directions of the low-frequency modes before particles rearrange. Since the size of this displacement depends on the microscopic dynamics and it is smaller if the system moves diffusively, rather than ballistically, we expect the influence of confinement to be more relevant at the molecular scale rather than at the colloidal scale. Nevertheless, we remind the reader that LWs are observed in experiments [23, 24, 26] and simulations [26] of two-dimensional colloidal systems; our predictions concerning the role of LW fluctuations in confined systems therefore apply to both molecular and colloidal systems.

3.5.2 Experimental relevance

For the effect of LW fluctuations to be experimentally visible, however, the roughness scale of the confining walls must be smaller than the size of the particles. Rough walls, indeed, affect the motion in the lateral dimensions and kill the LW fluctuations, as we have shown in Figure 3.20. The requirement of smooth confining walls is not a technical limitation. Walls that are *de facto* flat at the molecular scale exist [11], and it is undoubtedly possible to confine large colloidal particles between walls that are flat at the particle scale. In colloidal experiments, however, one should ascertain that no particles stick irreversibly to the walls, effectively making them rough, e.g., as observed in Refs. [37, 38]. Hence our predictions are experimentally testable both in confined molecular liquids, e.g., comparing the size dependence of the viscosity and of structural relaxation time, and in confined colloidal systems, comparing, e.g. the standard and cage-relative relaxation times.

Our results show that confined systems exhibit a gradual dimensionality crossover controlled by the gap width and the temperature, which is appreciable when investigating the lateral size dependence of the dynamics. The physics of confined liquids is thus richer than previously realised. These findings might be relevant to a variety of applications involving micro- and nanofluidics, e.g., lab-on-a-chip devices, where particles flow in confined geometries.

References

[1] Walter Kob and Hans C Andersen. Scaling behavior in the β-relaxation regime of a supercooled lennard-jones mixture. *Physical Review Letters*, 73(10):1376, 1994.

[2] Steve Granick. Motions and relaxations of confined liquids. *Science*, 253 (5026):1374, sep 1991. ISSN 00368075. doi: 10.1126/science.253.5026.1374.

[3] Suvendu Mandal, Simon Lang, Markus Gross, Martin Oettel, Dierk Raabe, Thomas Franosch, and Fathollah Varnik. Multiple reentrant glass transitions in confined hard-sphere glasses. *Nature Communications*, 5(1):1–8, 2014. doi: 10.1038/ncomms5435.

[4] Zhen Zhang and Walter Kob. Revealing the three-dimensional structure of liquids using four-point correlation functions. *Proceedings of the National Academy of Sciences*, 117:14032, 2020. doi: 10.1073/pnas.2005638117.

[5] Matthias Schmidt and Hartmut Löwen. Freezing between Two and Three Dimensions. *Phys. Rev. Lett.*, 76:4552, 1996.

[6] H Löwen. Twenty years of confined colloids: from confinement-induced freezing to giant breathing. *Journal of Physics: Condensed Matter*, 21(47):474203, 2009. doi: 10.1088/0953-8984/21/47/474203.

[7] Peter T. Cummings, Hugh Docherty, Christopher R. Iacovella, and Jayant K. Singh. Phase transitions in nanoconfined fluids: The evidence from simulation and theory. *AIChE Journal*, 56(4):842, apr 2010. ISSN 00011541. doi: 10.1002/aic.12226.

[8] Jacob Klein and Eugenia Kumacheva. Confinement-induced phase transitions in simple liquids. *Science*, 269(5225):816–819, 1995. doi: 10.1126/science.269.5225.816.

[9] Jacob Klein and Eugenia Kumacheva. Simple liquids confined to molecularly thin layers. i. confinement-induced liquid-to-solid phase transitions. *The Journal of chemical physics*, 108(16):6996–7009, 1998. doi: 10.1063/1.476114.

[10] A. Levent Demirel and Steve Granick. Origins of solidification when a simple molecular fluid is confined between two plates. *Journal of Chemical Physics*, 115(3):1498–1512, jul 2001. ISSN 00219606. doi: 10.1063/1.1380207.

[11] Yingxi Zhu and Steve Granick. Superlubricity: A paradox about confined fluids resolved. *Physical review letters*, 93(9):096101, 2004. doi: 10.1103/PhysRevLett.93.096101.

[12] Daniel F Kienle and Tonya L Kuhl. Density and Phase State of a Confined Nonpolar Fluid. *Phys.Rev. Lett.*, 117:036101, 2016. doi: 10.1103/PhysRevLett.117.036101.

[13] Ahmad Jabbarzadeh. Friction anisotropy in confined alkanes: linear and branched molecules. *Tribology International*, 97:108–115, 2016. doi: 10.1016/j.triboint.2016.01.004.

[14] A Jabbarzadeh, Peter Harrowell, and RI Tanner. Low friction lubrication between amorphous walls: Unraveling the contributions of surface roughness and in-plane disorder. *The Journal of chemical physics*, 125(3):034703, 2006. doi: 10.1063/1.2216695.

[15] A Jabbarzadeh, Peter Harrowell, and RI Tanner. Crystal bridges, tetratic order, and elusive equilibria: The role of structure in lubrication films, 2007.

[16] Nadezhda Gribova, Axel Arnold, Tanja Schilling, and Christian Holm. How close to two dimensions does a lennard-jones system need to be to produce a hexatic phase? *The Journal of chemical physics*, 135(5):054514, 2011. doi: 10.1063/1.3623783.

[17] Thomas Franosch, Simon Lang, and Rolf Schilling. Fluids in extreme confinement. *Physical Review Letters*, 109(24):240601, dec 2012. doi: 10.1103/PhysRevLett.109.240601.

[18] Suvendu Mandal and Thomas Franosch. Diverging time scale in the dimensional crossover for liquids in strong confinement. *Physical Review Letters*, 118 (6):065901, 2017. doi: 10.1103/PhysRevLett.118.065901.

[19] N David Mermin and Herbert Wagner. Absence of ferromagnetism or antiferromagnetism in one-or two-dimensional isotropic heisenberg models. *Physical Review Letters*, 17(22):1133, 1966.

[20] Elijah Flenner and Grzegorz Szamel. Fundamental differences between glassy dynamics in two and three dimensions. *Nature Communications*, 6:7392, 2015.

[21] Hayato Shiba, Yasunori Yamada, Takeshi Kawasaki, and Kang Kim. Unveiling dimensionality dependence of glassy dynamics: 2d infinite fluctuation eclipses inherent structural relaxation. *Physical Review Letters*, 117(24):245701, 2016.

[22] Bernd Illing, Sebastian Fritschi, Herbert Kaiser, Christian L Klix, Georg Maret, and Peter Keim. Mermin–wagner fluctuations in 2d amorphous solids. *Proceedings of the National Academy of Sciences*, 114(8):1856–1861, 2017.

[23] Skanda Vivek, Colm P Kelleher, Paul M Chaikin, and Eric R Weeks. Long-wavelength fluctuations and the glass transition in two dimensions and three dimensions. *Proceedings of the National Academy of Sciences*, 114(8):1850–1855, 2017.

[24] Bo Zhang and Xiang Cheng. Long-wavelength fluctuations and static correlations in quasi-2d colloidal suspensions. *Soft Matter*, 15(20):4087–4097, 2019.

[25] Hayato Shiba, Takeshi Kawasaki, and Kang Kim. Local density fluctuation governs the divergence of viscosity underlying elastic and hydrodynamic anomalies in a 2d glass-forming liquid. *Physical Review Letters*, 123(26): 265501, 2019. doi: 10.1103/PhysRevLett.123.265501.

[26] Yan-Wei Li, Chandan K Mishra, Zhao-Yan Sun, Kun Zhao, Thomas G Mason, Rajesh Ganapathy, and Massimo Pica Ciamarra. Long-wavelength fluctuations and anomalous dynamics in 2-dimensional liquids. *Proceedings of the National Academy of Sciences*, 116(46):22977–22982, 2019.

[27] Etienne P Bernard and Werner Krauth. Two-Step Melting in Two Dimensions: First-Order Liquid-Hexatic Transition. *Phys. Rev. Lett.*, 107(15):155704, 2011.

[28] Joshua A. Anderson, James Antonaglia, Jaime A. Millan, Michael Engel, and Sharon C. Glotzer. Shape and Symmetry Determine Two-Dimensional Melting Transitions of Hard Regular Polygons. *Physical Review X*, 7(2):021001, 2017. doi: 10.1103/PhysRevX.7.021001.

[29] Yan-Wei Li and Massimo Pica Ciamarra. Attraction tames two-dimensional melting: from continuous to discontinuous transitions. *Physical Review Letters*, 124(21):218002, 2020. doi: 10.1103/PhysRevLett.124.218002.

[30] Steve Plimpton. Fast parallel algorithms for short-range molecular dynamics. *Journal of computational physics*, 117(1):1–19, 1995. doi: 10.1006/jcph.1995.1039.

[31] Hua Tong and Hajime Tanaka. Revealing Hidden Structural Order Controlling Both Fast and Slow Glassy Dynamics in Supercooled Liquids. *Physical Review X*, 8:011041, 2018. doi: 10.1103/PhysRevX.8.011041.

[32] A Tanguy, JP Wittmer, F Leonforte, and J-L Barrat. Continuum limit of amorphous elastic bodies: A finite-size study of low-frequency harmonic vibrations. *Physical Review B*, 66(17):174205, 2002. doi: 10.1103/PhysRevB.66.174205.

[33] Masanari Shimada, Hideyuki Mizuno, and Atsushi Ikeda. Anomalous vibrational properties in the continuum limit of glasses. *Physical Review E*, 97:22609, 2018. doi: 10.1103/PhysRevE.97.022609.

[34] Hsuan-Wei Hu, George A Carson, and Steve Granick. Relaxation Time of Confined Liquids under Shear. *Phys. Rev. Lett.*, 66:2758, 1991. doi: 10.1103/PhysRevLett.66.2758.

[35] A Levent Demirel and Steve Granick. Glasslike Transition of a Confined Simple Fluid. *Phys. Rev. Lett.*, 77:2261, 1996. doi: 10.1103/PhysRevLett.77.2261.

[36] Elijah Flenner and Grzegorz Szamel. Viscoelastic shear stress relaxation in two-dimensional glass–forming liquids. *Proceedings of the National Academy of Sciences of the United States of America*, 116:2015–2020, 2019. doi: 10.1073/pnas.1815097116.

[37] Carolyn R Nugent, Kazem V Edmond, Hetal N Patel, and Eric R Weeks. Colloidal Glass Transition Observed in Confinement. *Phys. Rev. Lett.*, 99:025702, 2007.

[38] Kazem V Edmond, Carolyn R Nugent, and Eric R Weeks. Influence of confinement on dynamical heterogeneities in dense colloidal samples. *Phys. Rev. E*, 85:41401, 2012.

Chapter 4

Extreme mobility induced phase separation and jamming transition in self-propelling particles

In this chapter, we numerically study the phase behaviour and dynamics of two dimensional systems of persistent self-propelled particles, meaning that each particle self-propels in a fixed direction. The particles interact via short-ranged stiff repulsive forces. We demonstrate that, in this system, there is an interplay between the motility induced phase separation and jamming. The coexistence and jamming lines in the activity-density plane meet at the jamming transition point in the limit of hard particles or zero activity. This interplay induces an anomalous dynamic in the liquid phase and hysteresis at the active jamming transition.

4.1 Introduction

Giant density fluctuations and collective phenomena reminiscent of equilibrium phase transitions such as flocking [1], motility induced phase separation (MIPS) [2–5] and active crystallization [6] characterize living and engineered systems of particles able to self-propel. These phenomena emerge on increasing the strength of the self-propelling forces at the expense of other collective phenomena. For instance, in the prototypical hard-disk system, active forces affect equilibrium melting by first

suppressing liquid/hexatic coexistence and then inducing a MIPS between a low-density gas-like phase and a higher density liquid, hexatic or crystalline phase [7–9]. In three dimensions, the motility induced gas/liquid transition occurs within the gas/crystal MIPS coexistence region [10].

Active forces influence the glass and jamming transitions in systems that do not crystallize due to structural or energetic disorder, including cell aggregates [11–19], bacteria colonies [20–22] and polydisperse active Brownian particles [11, 23–25]. The interplay between MIPS and jamming depends on the persistence time of the active force, that influences MIPS [26]. In two dimensional systems of soft, bi-disperse active Brownian disks [11, 27] with a 'small' persistence time, jamming and MIPS appears unrelated as occurring in different regions of the density/activity plane. Recent works [25, 28] investigated the limit of high persistence in models differing in polydispersity, thermal noise and active velocity dynamics, reporting contrasting results. In [25], MIPS and jamming (glass) stay separate in the limit of high persistence, while in [28], they approach each other. The possible connection between MIPS and jamming thus remain elusive.

We demonstrate an interplay between MIPS and jamming in a two-dimensional system of active, purely repulsive particles via numerical simulation. We focus on the limit of persistent particles [29–31] and investigate MIPS and jamming as active forces, density, and stiffness of the particles vary. We find that the high-density gas/liquid MIPS coexistence curve and the jamming line are separated by a small volume fraction range of liquid phase that vanishes in the limits of small activities or hard particles. In these limits, MIPS and jamming occur together. In the liquid phase, particle motion is correlated over the whole system for a long, size-dependent transient, during which particles do not preferentially move along the direction of their self-propelling force. Correlations in the direction of the active forces that build up in the liquid phase induce hysteresis at the jamming transition.

The rest of this chapter is built up as follows. In Section 4.2, we introduce the detailed numerical model in this work. In the Section 4.3.1, we validate the numerical model by investigating and reproduce the jamming transition in the absence of motility. The Section 4.3.2 provides a thorough investigation of phase behavior in the presence self-propelled force and demonstrates the non-trivial interplay as jamming transition and MIPS converge. In Section 4.4.1, we unveil the anomalous dynamics in homogeneous liquid states. In the Section 4.4.2, we show different

transition thresholds at jamming/unjamming transition controlled by preparation protocols. In the last section of this chapter, we summary and conclude our study.

4.2 Numerical model

4.2.1 Model details

We simulate a 2D system with A:B 65 : 35 binary mixture [32] of $N = 16000$ particles of unit mass m and diameters d_{AA} and $d_{\mathrm{BB}} = d_{\mathrm{AA}}/1.4$, interacting via a LJ-like n-m potential with $m = n/2$,

$$V_{\mathrm{n,m}}(r) = \frac{\epsilon_{\alpha\beta}}{\mathrm{n}-\mathrm{m}}\left[\mathrm{m}\left(\frac{d_{\alpha\beta}}{r}\right)^{\mathrm{n}} - \mathrm{n}\left(\frac{d_{\alpha\beta}}{r}\right)^{\mathrm{m}}\right] \tag{4.1}$$

truncated in its minimum $d_{\alpha\beta}$. Hence, the interaction is purely repulsive. We fix the energy length scale $\epsilon_{\mathrm{AA}} = 1$, $\epsilon_{\mathrm{BB}} = 0.5\epsilon_{\mathrm{AA}}$ and $\epsilon_{\mathrm{AB}} = 1.5\epsilon_{\mathrm{AA}}$, and set $d_{AB} = 1/2(d_{\mathrm{AA}} + d_{\mathrm{BB}})$ and $\mathrm{n} = 12$ if not otherwise stated. The area fraction is $\phi = NL^{-2}\langle a\rangle$, with $\langle a\rangle$ the average particle area [1] and L the linear size of our square simulation domain.

The equation of motion for particle i is

$$m\ddot{\mathbf{r}}_i = \sum_j f_{ij} - \gamma\dot{\mathbf{r}}_i + \mathbf{F}_{A,i}, \tag{4.2}$$

where f_{ij} is the interaction force between particles i and j, $\gamma = 1$ is a damping parameter, and $\mathbf{F}_{A,i} = F_A\mathbf{e}_i$ the self-propelling force acting on the particle. In the range of parameters we consider, the damping parameter γ is large enough for inertial effect to be negligible, as we will explicitly demonstrate.

The active forces have magnitude F_A and fixed random orientations $\mathbf{e}_i$ which we chose with the constraint $\sum \mathbf{e}_i = 0$ to avoid the motion of the centre of mass. We indicate with $v_A = F_A/\gamma$ and $\tau_A = d_{\mathrm{AA}}/v_A$ the typical velocity and time scale set by the active force dynamics and particle size.

[1] $\langle a\rangle = \frac{\pi}{4}[0.64d_{\mathrm{AA}}^2 + 0.35d_{\mathrm{BB}}^2])$

4.3 MIPS and active jamming

4.3.1 Zero-activity jamming transition

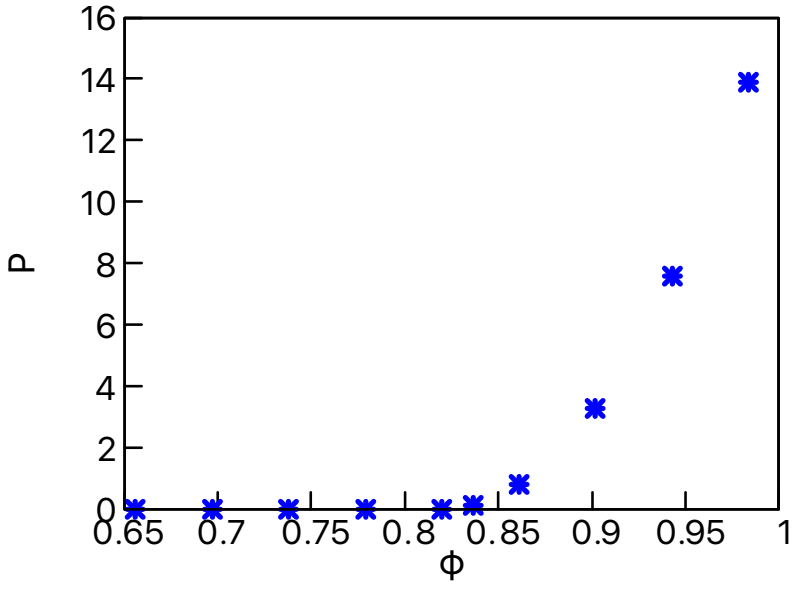

FIGURE 4.1: The zero-activity jamming transition. We assume the system to transition from a fluid to a jammed phase when the pressure of the system becomes non-zero as the packing fraction increases.

Our model reproduces the jamming phenomenology in the absence of active forces: energy minimal configurations acquire mechanical rigidity above a jamming area fraction that depends on their preparation protocol [33, 34]. We investigate the jamming transition by minimizing the energy of random configurations of area fraction ϕ via the conjugate-gradient method [35], using a protocol that is not affected by inertia in our active particle simulations. We estimate the jamming volume fraction to be $\phi_{\mathrm{J}} \simeq 0.828$, as illustrated in Figure 4.1.

4.3.2 Interplay between MIPS and jamming

In the presence of active forces, the system transitions from a flowing to a jammed regime as the density increases or the magnitude of the active forces decreases. We locate this transition by determining the state point $(\phi, F_A)_J$ at which the kinetic energy of the system vanishes as F_A slowly decreases at a constant ϕ, as illustrated

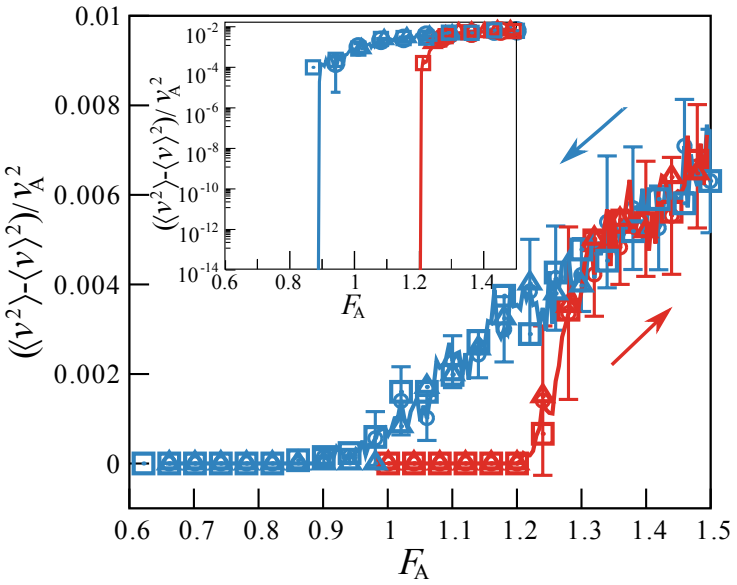

FIGURE 4.2: The velocity fluctuation as a function of a range of self-propelled force F_A at a fixed volume fraction $\phi = 0.98$. The blue arrow and the red arrow indicate the decreasing and increasing active force, respectively. The force rates are ranging from 10^{-6} (shown as circles), 5×10^{-7} (shown as triangles) to 2×10^{-6} (shown as squares). We assume the system to transition from a fluid to a jammed phase when the fluctuations vanish as the force decreases. Conversely, the system unjams as the fluctuations become non zero. The inset shown suddenly drop in kinetic energy indicates where the jamming/unjamming transition occurs.

in Figure 4.2. We repeat this study four times at each considered ϕ to estimate the average active force at jamming.

Besides controlling the jamming transition, active forces also induce MIPS between a gas and a liquid-like phase. As illustrated in Figure 4.3, an obvious MIPS occurs in a range of densities, where a dilute gas state and a fluid-like state coexistence.

Here, we cannot determine the MIPS phase boundary via the study of the equation of state as the pressure is not well defined for persistent self-propelling particles [36]. Henceforth, we assess phase separation by investigating the distribution of the local volume fraction ϕ_l obtained by coarse-graining the system on a square grid with edge length $4\sigma_{AA}$. We summarize the result of this standard investigation [8, 26, 37] in Figure 4.4. This figure indicates local volume distribution for given $\phi = 0.89$ at different active forces.

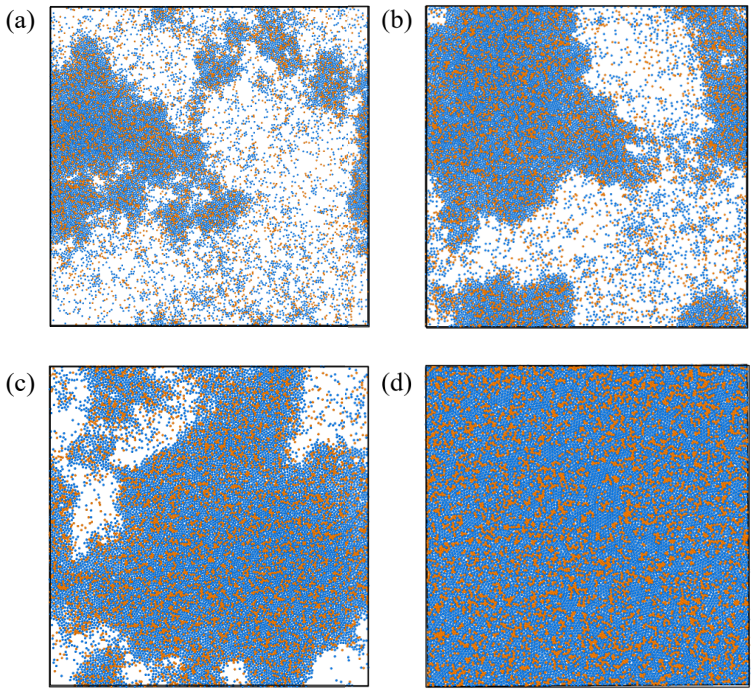

FIGURE 4.3: The MIPS occurs in the presence of active force where a dilute gas state and a fluid-like state coexistence. From panel (a) to (d), the system is prepared with a range of increasing densities at fixed active force. The bi-disperse mixture of particles is colored in red and blue.

We consider the system to be phase-separated when $P(\phi_l)$ has a bimodal distribution or has a long tail extending to low densities. Indeed, the direct visualization of the system clarifies that long tails occur in the presence of tiny 'gas bubbles' within the system, as in Figure 4.5.

In Figure 4.5, the phase separation starts to appear as the active force increased to 0.31 at fixed packing fraction $\phi = 0.89$. By considering the local volume fraction for each particle, a_i/s_i, we are allowed to get the clear visualization of the phase coexistence. a_i indicates the area of particle i and s_i indicates the Voronoi cell for the given particle i by a radical Voronoi tessellation. In large enough systems, one would observe many such cavities or bubbles at short times; these cavities or bubbles would then slowly converge via a slow coarsening process [8, 26, 37], making the volume fraction probability distribution bimodal shape.

Thus, we consider these bubbles a signal of phase separation as we expect them to merge and make the area fraction distribution bimodal via a coarsening process. At the considered high-density values, this coarsening dynamics is too slow to be numerically followed.

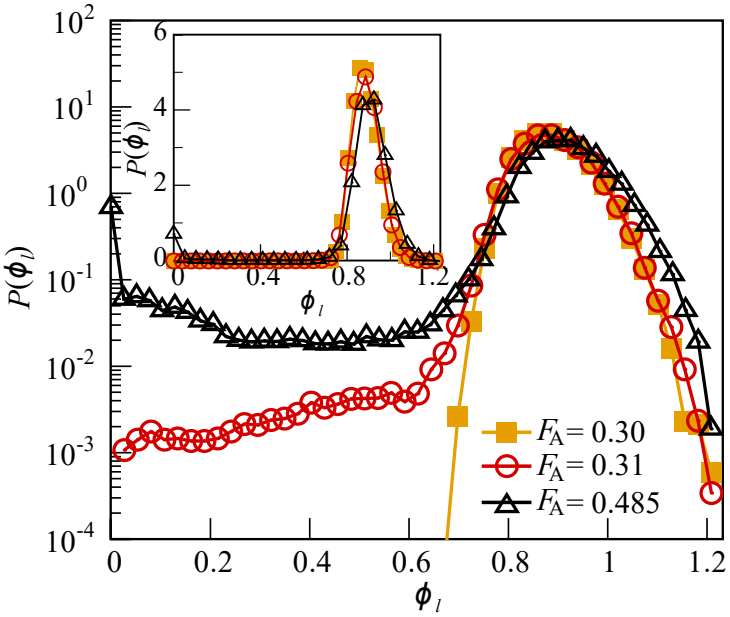

FIGURE 4.4: Probability distribution of the local volume fraction at $\phi = 0.89$ and different F_A values. We consider the system as phase separated when this distribution is bimodal, e.g., $F_A = 0.485$ or when it possesses an extended left tails, e.g., $F_A = 0.31$. Conversely, the system in in the homogeneous phase, e.g., $F_A = 0.30$.

The investigation of the jamming transition and the motility induced phase separation leads to the $F_A - \phi$ phase diagram of Figure 4.6. We use full and empty markers to indicate the state points in the homogeneous and coexistence phases, which are color-coded according to the value of a scaled kinetic energy. The black diamond marks the packing fraction at the zero-activity jamming, ϕ_J, and the white circles marks the phase states in jamming.

The jamming line $F_J(\phi)$ separating the fluid and the jammed phase and the high-density branch of the coexistence line $F_C(\phi) \geq F_J(\phi)$ are well described by power-law functional forms vanishing at the jamming volume fraction ϕ_{J},

$$\begin{cases} F_J = A_J(\phi - \phi_{\mathrm{J}})^{\beta_J} \\ F_C = A_C(\phi - \phi_{\mathrm{J}})^{\beta_C}. \end{cases} \tag{4.3}$$

We find $A_J < A_C$ and $\beta_J \simeq \beta_C \simeq 2$.

Within the coexistence region the system phase separates in a dilute and a dense phase. This phase diagram suggests that the coexisting phases are always of gas and a liquid type, rather than of gas and jam type [23]. In mono-disperse

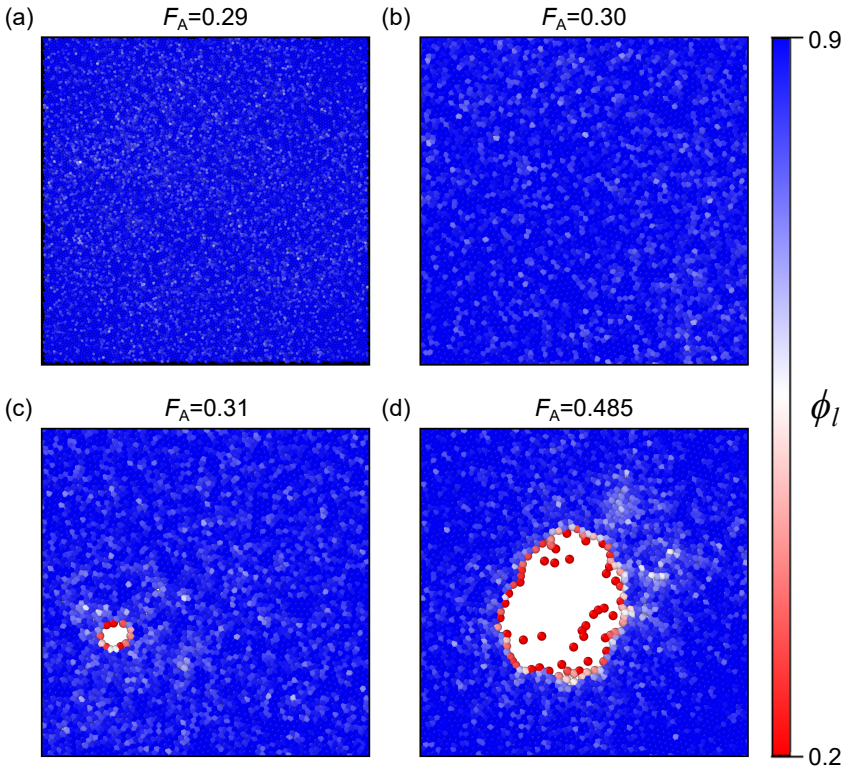

FIGURE 4.5: The visualization of phase separation in dense-active system at $\phi = 0.89$. The system starts to exhibit a phase coexistence at active force $F_A = 0.31$, where the long-tail expansion emerges in Figure 4.4. Particles are color coded according to their local volume fraction, a_i/s_i, where a_i is the particle area, and s_i the area of its Voronoi cell evaluated via a radical tessellation of the system. The peak in zero of $P(\phi_l)$ (Figure 4.4) and the system's illustrations clarify that the coexisting phases are a dense liquid and an empty gas with $\phi = 0$.

systems of active persistent particle, previous results showed the dense phase of coexistence region to be crystalline [31].

We have investigated the dynamics of the dense phase and found it to be of liquid type. To this end, we identify the particles of the dense phase via a threshold criterion on a particle-defined local density, at time $t = 0$. An example of this approach is in Figure 4.7, where particles are color coded if belonging to dense phase, and gray if belonging to the gas phase. The snapshots are at volume fraction $\phi = 0.41$, at different F_A values.

We have then investigated the cage-relative mean square displacement of the particles of the dense phase and observed that the high density clusters have a finite lifetime. The cage-relative mean square displacement is to filter out the collective

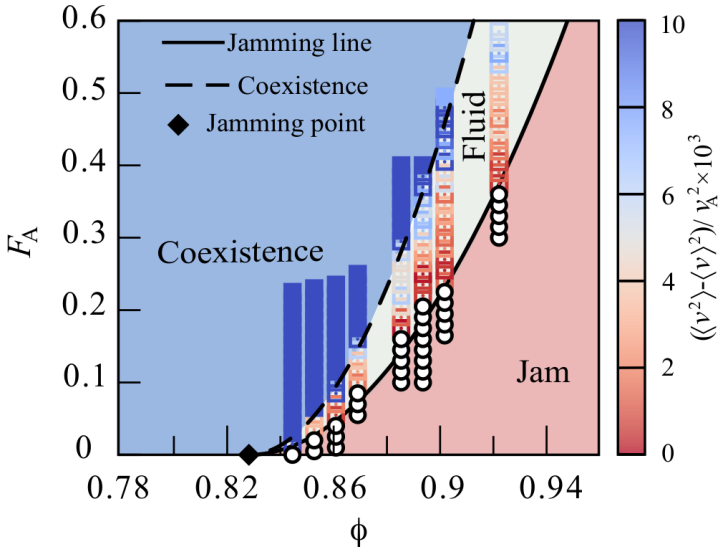

FIGURE 4.6: Phase diagram for stiffness exponent $n = 12$. Squares identifying phase separated (full) and homogeneous (empty) states are coloured according to the value of a scaled kinetic energy. White circles identify jammed configurations, and the black diamond marks the jamming volume fraction, ϕ_J. The jamming transition and the high-density branch of the coexistence line scales as $(\phi - \phi_J)^2$. The MIPS low-density branch (not shown) is at $\phi \simeq 0.2$ and depends weakly on F_A.

particle motions,

$$\begin{cases} \langle \Delta_{CR} \boldsymbol{r}_i^2(t) \rangle = \dfrac{1}{n_i} \sum \Delta_{CR} \boldsymbol{r}_i^2 \\ \Delta_{CR} \boldsymbol{r}_i = \Delta \boldsymbol{r}_i - \dfrac{1}{n_i} \sum_j \Delta \boldsymbol{r}_j. \end{cases} \tag{4.4}$$

Here, $\Delta \boldsymbol{r}_i$ is the displacement of particle i, and n_i is its neighbors at $t = 0$. We identify the neighbors via a Voronoi tessellation.

Figure 4.8 illustrates results at $\phi = 0.41$, for different values of the active force (see inset) in the coexistence region. Time is in unit of the characteristic time scale fixed by the active velocity, τ_A. The mean square displacement exhibits a crossover towards an asymptotic ballistic behavior, which is apparent at large enough F_A. This crossover signals the disruption of the dense cluster. The behavior of the mean square displacement proves that the dense phase is of liquid type.

Figure 4.8 further shows that the active force does not simply set the time scale of the system. Indeed, if F_A were only affecting the typical time scale τ_A, then data for different F_A values would collapse when plotted versus t/τ_{AA}. In Figure 4.8, we see that this occurs at large enough F_A. Conversely, as F_A decreases, the slowing

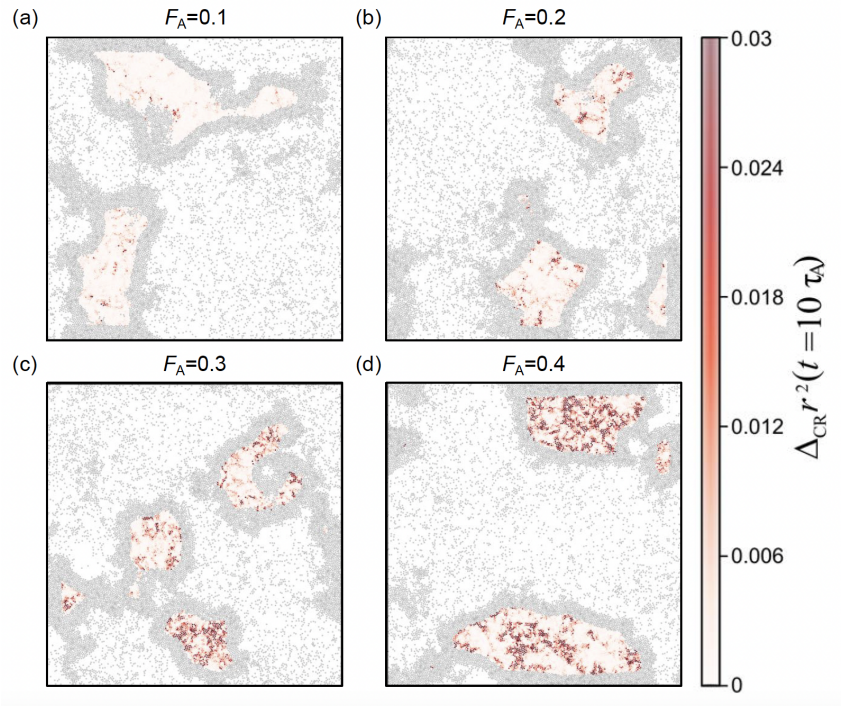

FIGURE 4.7: The snapshots of the system in the coexistence region, at $\phi = 0.41$ and increasing F_A values from panel (a) to (d). The particles belonging to the core of high density cluster at time t = 0 are identified by thresholding local density of individual particle, and then colour-mapped according to the cage-relative mean square displacement at time $t = 10\tau_A$. Particles are colored in gray represent the dilute phase.

down of the dynamics is faster than that of $1/\tau_A$. This result is apparent from the F_A dependence of the mean square displacement evaluated at $t = 10\tau_A$ illustrated in the inset. The direct visualization of the magnitude of the cage-relative square displacements at $t = 10\tau_A$ and different values of the active force in Figure 4.7 confirms this finding.

4.3.3 Role of potential stiffness

To assess the role of particles' stiffness we determine the activity/volume fraction phase diagram for interaction potentials differing in their stiffness exponent n. We identify the jamming density as that at which the kinetic energy drops to zero as the active force slowly decreases in magnitude, and the coexistence density as the highest density at which the local volume fraction distribution is unimodal, at the considered F_A value. To compare these potentials, we evaluate the relative particle deformation induced by the active forces, which in the harmonic approximation

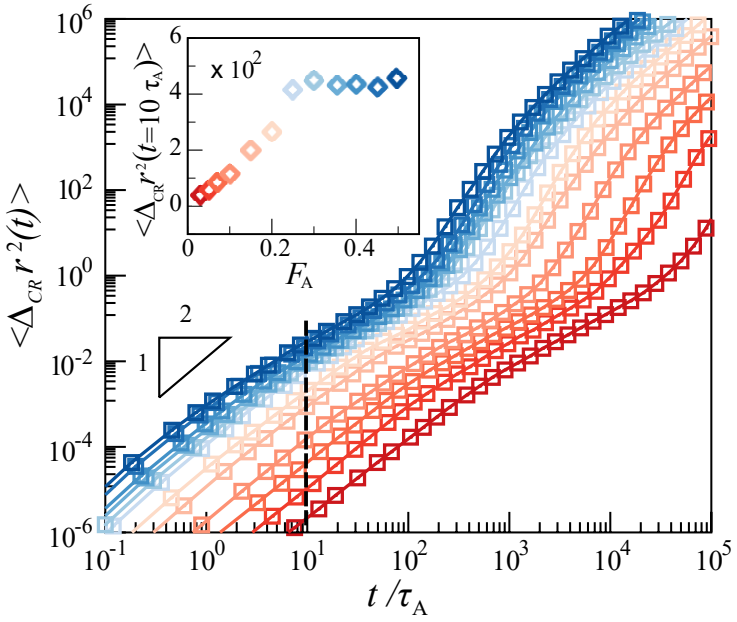

FIGURE 4.8: Cage-relative mean square displacement as a function of t/τ_A, for a range of active force values (see inset). Note the values of $\langle \Delta_{\mathrm{CR}} \boldsymbol{r}_i^2(t) \rangle$ are averaged among the particles within the high density region. The curve collapse at large F_A, as clarified by the active force dependence of their values at $t = 10\tau_A$, illustrated in the inset.

is $\Gamma \propto \frac{F_A d}{\epsilon n^2}$. In the limit of small Γ, the harmonic approximation holds, and the coexistence and jamming curve of potentials with different stiffness collapse in the Γ-ϕ plane, as shown in Figure 4.9. As Γ increases, the harmonic approximation breaks down, leading to an increase of the volume fraction range where the liquid phase occurs as the potential softens (n decreases).

Our investigation demonstrates that, for persistent particles, the fluid phase vanishes at the jamming point in the $F_A \to 0$ limit, or equivalently, in the limit of hard spheres, $n \to \infty$. In these limits, MIPS and jamming meet at the jamming transition point. To explain this result, we consider in the high-density coexistence region our system appears as a dense liquid punctuated by empty cavities, as in Figure 4.5. This is in agreement with previous observations reported in Ref. [38] and Ref. [39]. The shrinking of these cavities with the active force's magnitude drives the convergence of the high-density coexistence curve to the jamming point ϕ_J.

Another numerical evidence is illustrated as Figure 4.10. We clarify how a phase-separated system becomes unjammed or jammed as the magnitude of the active force decreases by illustrating the force dependence of the distribution of

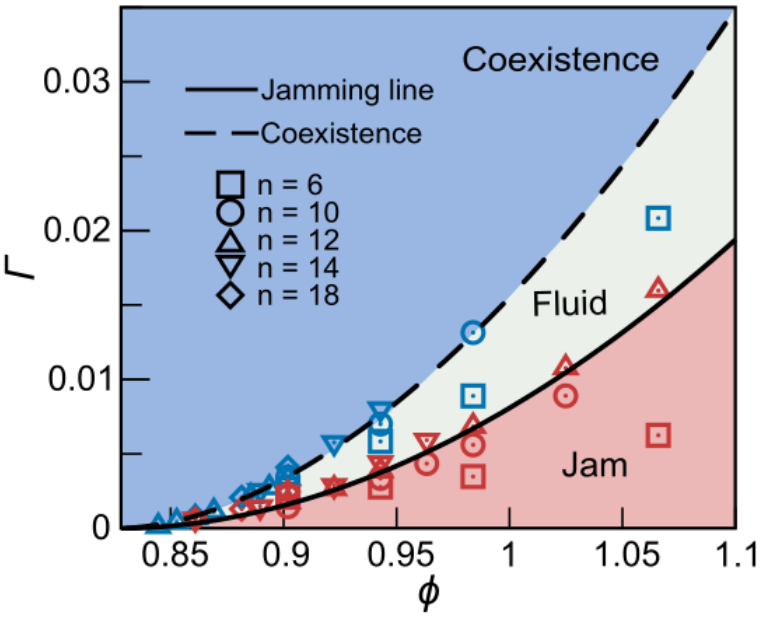

FIGURE 4.9: The $\Gamma - \phi$ phase diagram for different potentials with their exponents n. The plane demonstrates the jamming and MIPS phase as a function of the non-dimensional particle compression in the Harmonic approximation, Γ, and the area fraction ϕ, for potential differing in their stiffness exponent n. The red and blue symbols are state points on jamming and phase separation lines, respectively. The dashed and full lines are those estimated separated phase and jamming transition for $n = 12$, respectively. In the considered range of parameters, data for different potential collapse for large n and small forces.

the local volume fraction for densities below and above the jamming transition, respectively in Figure 4.10 (a) and (b).

Regardless of the density value, at high values of the active force in the MIPS region, the density distribution is bimodal and in the gas phase $\phi \simeq 0$. At the considered densities, the system appears as a liquid with cavities, e.g., like the one illustrated in Figure 4.5 for $F_A = 0.485$.

For $\phi < \phi_J$, the system reaches the hard-sphere limit as the magnitude of the active force decreases. Consistently, the density distributions of Figure 4.10 become active-force independent, and in the $F_A \to 0$ limit, the system converges to an unjammed inhomogeneous state.

For $\phi > \phi_J$, cavities shrink as the active force decreases. Indeed, we see a drop in the $\phi \simeq 0$ peak of the density distribution as F_A varies from 0.15 to 0.10.

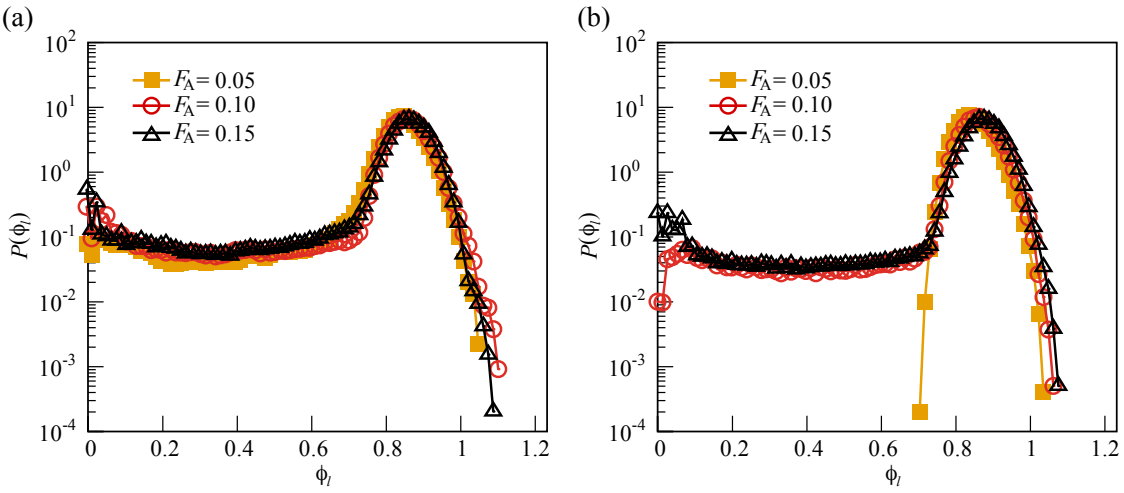

FIGURE 4.10: The evolution of the local density distribution with decreasing active force at densities slightly below jamming, panel (a) and slightly above it, panel (b).

Cavities disappear for small enough forces, and the system becomes jammed and homogeneous ($F_A = 0.05$).

The convergence of jamming and MIPS has significant consequences for the speculated analogy [30, 40, 41] between sheared amorphous solids and dense active matter. While both the increase of shear stress and activity induces an unjamming transition, the unjammed phase is homogeneous in the case of shear forces while it is phase-separated in the limit of small persistent active forces. Furthermore, in the case of shear [42] the jamming transition line scales linearly with the overcompression $\phi - \phi_J$, in the harmonic regime, while we find it here to scale quadratically.

4.4 Anomalous dynamics

4.4.1 Anomalous dynamics in homogeneous fluid state

The fluid phase enclosed between the coexistence and the jamming line exhibits anomalous dynamical features which we highlight by decomposing a particle's displacement in components parallel and orthogonal to its active force,

$$\mathbf{\Delta} r_i = \Delta r_i \mathbf{u}_i = \Delta r_{i,n} \mathbf{e}_i + \Delta r_{i,o} \mathbf{o}_i \tag{4.5}$$

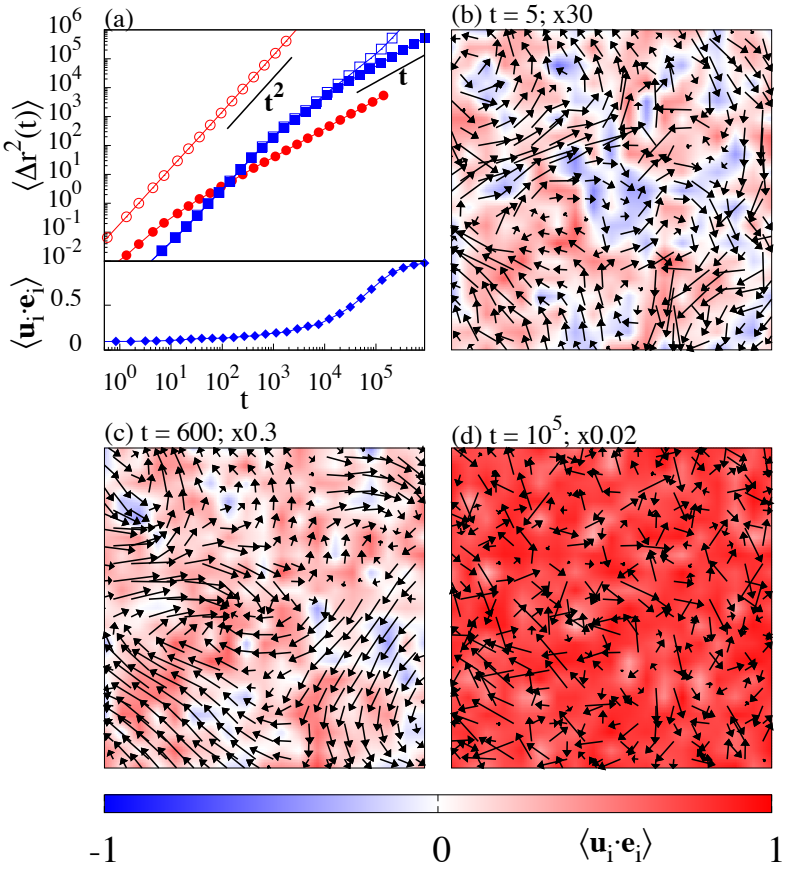

FIGURE 4.11: The dynamics in parallel and in orthogonal to the active force. The number of particles is $N = 4000$. (a, upper) The parallel and orthogonal MSD decomposed in the direction of active force, marked as open and full symbols, respectively. The dynamics is investigated in the dilute gas state (red markers) with $\phi = 0.08$ and in the fluid state (blue markers) $\phi = 0.9$ at active force $F_A = 0.5$. Panel (a, lower) indicates the alignment in displacements along the active force direction in fluid state after a long transient. Panels (b-d) demonstrate the scaled displacement field via a coarse-grain method, at increasing times.

where $\Delta r_{i,n}\mathbf{e}_i$ and $\Delta r_{i,o}\mathbf{o}_i$ are components parallel and orthogonal to active force on particle i, respectively.

This decomposition allows us to investigate the parallel $\langle \Delta r_{i,n}^2(t) \rangle$ and $\langle \Delta r_{i,o}^2(t) \rangle$ orthogonal mean square displacements (MSD). In the gas phase, the parallel MSD reflects ballistic dynamics with an effective volume fraction dependent velocity, while the orthogonal MSD reveals diffusive dynamics induced by the interparticle collisions [26], as we illustrate in Figure 4.11 (a).

Surprisingly, in the high-density liquid phase parallel and orthogonal dynamics are ballistic and identical for a long transient. During this transient, displacements

are not aligned to the self-propelling forces and $\langle \mathbf{u}_i \cdot \mathbf{e}_i \rangle < 1$, as in Figure 4.11 (a, bottom). The orthogonal MSD transitions to a diffusive regime only after reaching order L^2, as we verified via a finite-size investigation. These results originate from the transient organization of the flow pattern in large structures with a size comparable to that of the system, as in Figure 4.11 (b)-(d). These structures are not the turbulent-like vortices of other active matter systems [43], as their dimension is fixed by the system size rather than by motility and interaction parameters.

4.4.2 Jamming vs unjamming

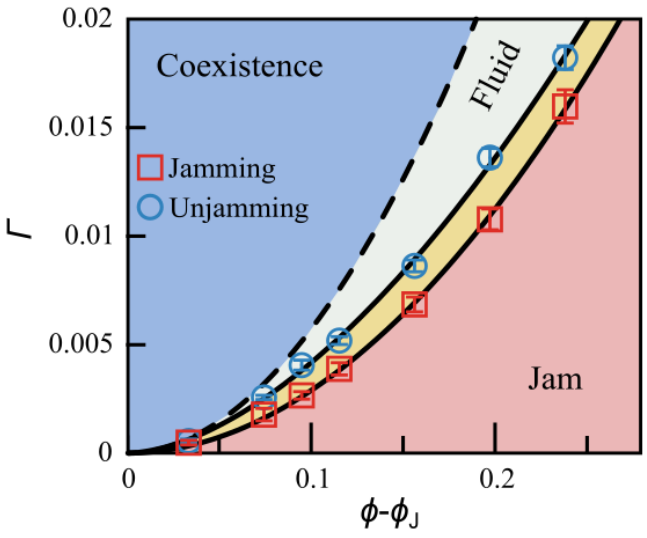

FIGURE 4.12: The phase plane of jamming transition of Figure 3.13, with stiffness exponent $n = 12$, after adding unjamming transition curve. Within the yellow area, the systems could behave as liquid or jammed state determined by different preparation protocols.

A liquid configuration jams as the magnitude of the active forces becomes smaller than a threshold. Similarly, a jammed configuration starts flowing if the magnitude of randomly oriented active forces overcomes an unjamming threshold. Surprisingly, the unjamming threshold is larger than the jamming one, as apparent in Figure 4.2.

The difference between these two thresholds decreases with the volume fraction and vanishes at the jamming point, where the jamming and unjamming lines meet, as illustrated in Figure 4.12. While this distinction between jamming and

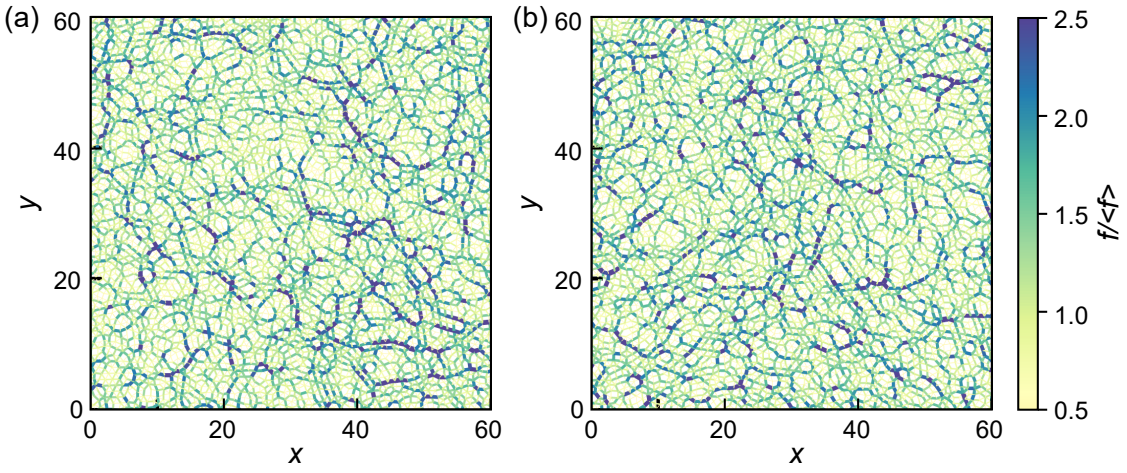

FIGURE 4.13: Force chain plots at jamming (panel (a)), and unjamming (panel (b)) transition points. The color bar is normalized strength of pair forces f by its averaged value.

unjamming resembles the inertia induced hysteresis occurring in sheared granular media [42], inertia in our system is negligible. Henceforth, the observed distinction implies differences in the configurations on the jamming and unjamming lines, which we unveil by investigating the features of their force network.

The visualization of the force network of configurations at the jamming and unjamming transition line does not exhibit obvious differences, as illustrated in Figure 4.13. Indeed, We find that configurations on the jamming and unjamming line have the same interparticle forces distribution, once the forces are scaled by their average magnitude, as we illustrate in Figure 4.14.

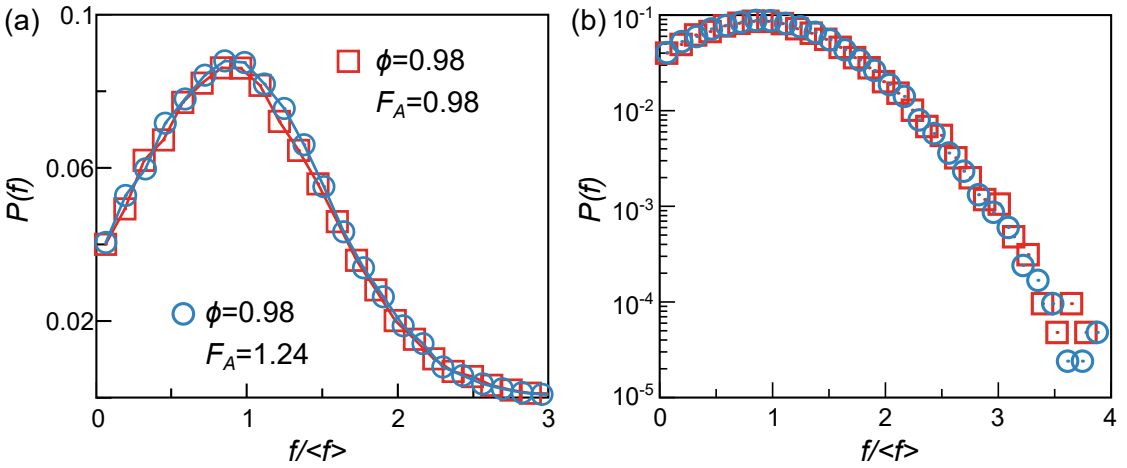

FIGURE 4.14: Probability distribution of the interparticle forces at the unjamming curve (blue circles: $\phi = 0.98, F_A = 1.24$) and on the jamming line (red squares: $\phi = 0.98, F_A = 0.98$). Panel b is a zoomed $P(f)$ in log-linear scale.

Active forces do not influence the force distribution as their value on the jamming/unjamming lines is a small fraction ($\simeq 1/10$) of the typical interparticle force.

We investigate correlations in the interparticle forces by considering that each force f act at the contact point $\mathbf{r}_c$ of our extended interacting particles. We then study the correlation function between interaction forces at a distance $r = |\mathbf{r}_c - \mathbf{r}'_c|$, given by the following equation,

$$C_f(r) = \langle |f(\mathbf{r}_c)|^q |f(\mathbf{r}'_c)|^q \cos(2\theta) \rangle, \tag{4.6}$$

where θ the angle between the two forces and q a parameter used to weight the contribution of forces of different magnitude to the correlation function. The factor of 2 in the cosine accounts for the fact that a contact force $f(\mathbf{r})$ is defined up to a sign, as it could act on one of the two interacting particles. For $q = 0$, $C_f(r)$ reduces to the two-dimensional nematic correlation function.

The panel (b) of Figure 4.15 reveals that $C_f(r)$ for $q = 1$ is the same on the jamming and unjamming lines. Analogous results occur at different q values, proving the absence of two-body correlations between the interaction forces.

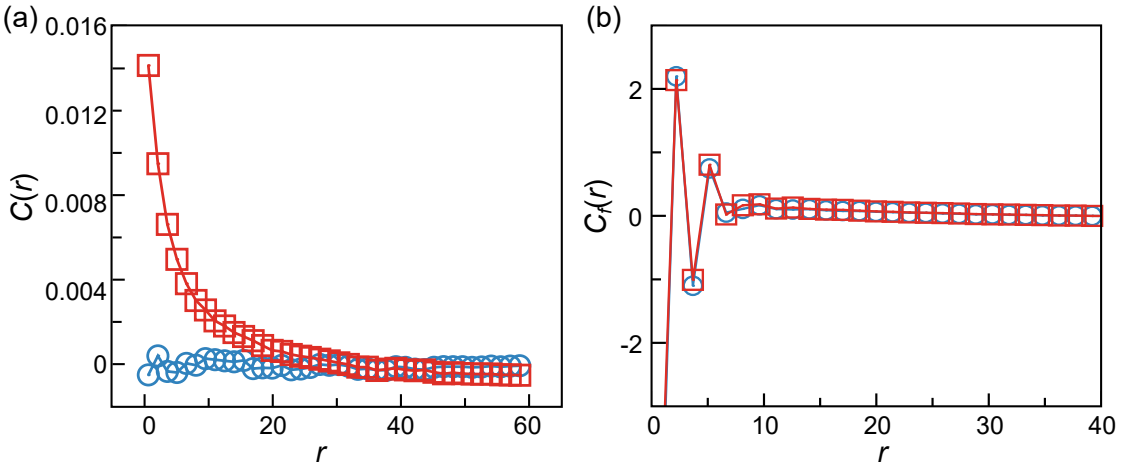

FIGURE 4.15: The correlation functions at the unjamming curve (blue circles: $\phi = 0.98, F_A = 1.24$) and on the jamming line (red squares: $\phi = 0.98, F_A = 0.98$). We illustrate (a) the correlation functions of active force and (b) the correlation function of the inter-particle forces.

We rationalize the difference between configurations on the jamming and unjamming lines considering that spatial correlations between the active forces build up in the liquid phase [28, 38]. If these correlations persist as the system jams, then

they induce correlations in the interparticle forces as in a jammed configuration,

$$\mathbf{F}_{A,i} = -\sum_j f_{ij}. \tag{4.7}$$

We check this possibility by investigating the correlation function of the active force direction,

$$C(r) = \langle \mathbf{e}_i(0) \cdot \mathbf{e}_j(r) \rangle. \tag{4.8}$$

The numerical results are in Figure 4.15.

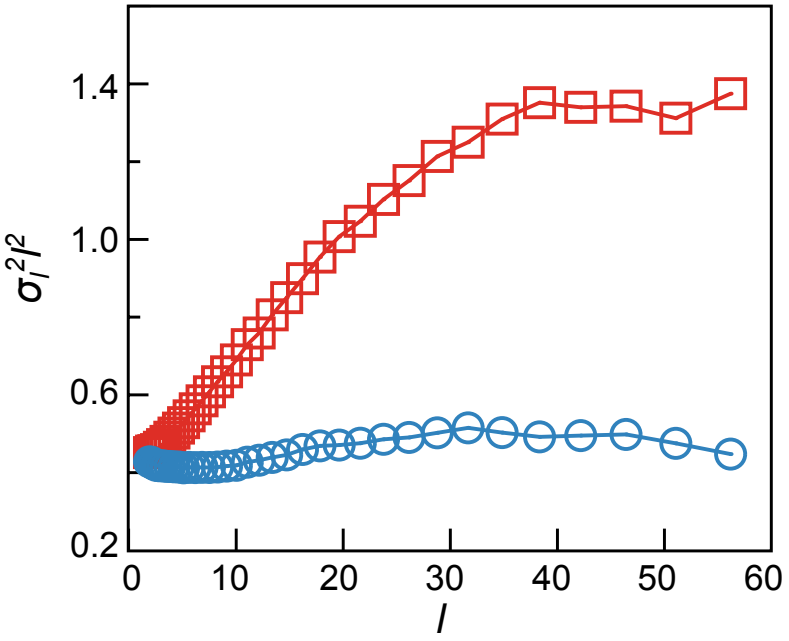

FIGURE 4.16: Panel (a) demonstrates the fluctuations after scaling $\sigma_l^2 l^2$ of the active force averaged over grid regions with a linear length l. Panel (b) illustrates the extracted correlation length, suggesting no clear variations of this range.

At the unjamming threshold, forces are uncorrelated, so that $C(r) = 0$. Conversely, on the jamming line $C(r)$ only approaches zero at large distances. As an alternative measure of correlations of the interparticle forces, we investigate the fluctuations σ_l^2 of $|\sum_{i \in l^2} \mathbf{F}_{A,i}|$, where the sum is over all particles located in square regions of linear size l. At the unjamming threshold, forces are uncorrelated, and in Figure 4.16, we find $\sigma_l^2 \propto l^2$ at all l, as dictated by the central limit theorem. Conversely, on the jamming line the above scaling signaling the absence of correlations only occurs for large l. The results of Figure 4.15 and Figure 4.16 consistently show the existence of many-body [44] correlations extending up to $r \simeq 30$ in the considered configuration. We have not observed clear variations of this correlation

length along the jamming line. Henceforth, while forces on the unjamming line are uncorrelated, those on the jamming line possess many-body correlations.

4.5 Conclusions

Our results demonstrate an interplay between jamming and motility induced phase separation in systems of persistent self-propelling particles. In the Γ-ϕ plane, with Γ a measure of the relative particle deformation induced by the active force, the MIPS and jamming lines meet in the $\Gamma \to 0$ limit (hard sphere or zero activity) at the jamming point.

This interplay induces surprising size effects in the dynamics of the liquid phase separating MIPS and jamming at finite Γ. Particle motion is collective on a length comparable to that of the system for a long transient also scaling with the system size. During this transient, particle displacements do not correlate with the directions of the self-propelling forces. In this liquid phase, active forces develop spatial correlations that persist as the system jam, inducing many-body correlations in the interparticle forces of jammed configurations. In the presence of a finite and large persistent time, at high density the system evolves through an intermittent avalanche dynamics [23]. The huge many-body correlations in the interparticle forces we have reported may explain why these avalanches are extensive.

References

[1] Tamás Vicsek, András Czirók, Eshel Ben-Jacob, Inon Cohen, and Ofer Shochet. Novel type of phase transition in a system of self-driven particles. *Physical Review Letters*, 75(6):1226, 1995.

[2] Yaouen Fily and M Cristina Marchetti. Athermal phase separation of self-propelled particles with no alignment. *Physical review letters*, 108(23):235702, 2012.

[3] M. C. Marchetti, J. F. Joanny, S. Ramaswamy, T. B. Liverpool, J. Prost, Madan Rao, and R. Aditi Simha. Hydrodynamics of soft active matter. *Rev.*

Mod. Phys., 85:1143–1189, Jul 2013. doi: 10.1103/RevModPhys.85.1143. URL https://link.aps.org/doi/10.1103/RevModPhys.85.1143.

[4] Clemens Bechinger, Roberto Di Leonardo, Hartmut Löwen, Charles Reichhardt, Giorgio Volpe, and Giovanni Volpe. Active particles in complex and crowded environments. *Rev. Mod. Phys.*, 88:045006, Nov 2016. doi: 10.1103/RevModPhys.88.045006. URL https://link.aps.org/doi/10.1103/RevModPhys.88.045006.

[5] Michael E Cates and Julien Tailleur. Motility-induced phase separation. *Annu. Rev. Condens. Matter Phys.*, 6(1):219–244, 2015.

[6] Jeremie Palacci, Stefano Sacanna, Asher Preska Steinberg, David J Pine, and Paul M Chaikin. Living crystals of light-activated colloidal surfers. *Science*, 339(6122):936–940, 2013.

[7] Julian Bialké, Thomas Speck, and Hartmut Löwen. Crystallization in a dense suspension of self-propelled particles. *Physical Review Letters*, 108(16):168301, 2012.

[8] Gabriel S Redner, Michael F Hagan, and Aparna Baskaran. Structure and dynamics of a phase-separating active colloidal fluid. *Physical Review Letters*, 110(5):055701, 2013.

[9] Pasquale Digregorio, Demian Levis, Antonio Suma, Leticia F Cugliandolo, Giuseppe Gonnella, and Ignacio Pagonabarraga. Full phase diagram of active brownian disks: From melting to motility-induced phase separation. *Physical review letters*, 121(9):098003, 2018.

[10] Ahmad K Omar, Katherine Klymko, Trevor GrandPre, and Phillip L Geissler. Phase diagram of active brownian spheres: Crystallization and the metastability of motility-induced phase separation. *Physical Review Letters*, 126(18): 188002, 2021.

[11] Silke Henkes, Yaouen Fily, and M. Cristina Marchetti. Active jamming: Self-propelled soft particles at high density. *Physical Review E*, 84(4):040301, oct 2011.

[12] Silke Henkes, Kaja Kostanjevec, J Martin Collinson, Rastko Sknepnek, and Eric Bertin. Dense active matter model of motion patterns in confluent cell

monolayers. *Nature Communications*, 11(1):1–9, 2020. doi: https://doi.org/10.1038/s41467-020-15164-5.

[13] Dapeng Bi, Xingbo Yang, M. Cristina Marchetti, and M. Lisa Manning. Motility-Driven Glass and Jamming Transitions in Biological Tissues. *Physical Review X*, 6:021011, 2016. doi: 10.1103/PhysRevX.6.021011.

[14] Simon Garcia, Edouard Hannezo, Jens Elgeti, Jean-François Joanny, Pascal Silberzan, and Nir S Gov. Physics of active jamming during collective cellular motion in a monolayer. *Proceedings of the National Academy of Sciences*, 112 (50):15314–15319, 2015.

[15] Fabio Giavazzi, Matteo Paoluzzi, Marta Macchi, Dapeng Bi, Giorgio Scita, M. Lisa Manning, Roberto Cerbino, and M. Cristina Marchetti. Flocking transitions in confluent tissues. *Soft Matter*, 14:3471, 2018. doi: 10.1039/c8sm00126j.

[16] Alessandro Mongera, Payam Rowghanian, Hannah J Gustafson, Elijah Shelton, David A Kealhofer, Emmet K Carn, Friedhelm Serwane, Adam A Lucio, James Giammona, and Otger Campàs. A fluid-to-solid jamming transition underlies vertebrate body axis elongation. *Nature*, 561(7723):401–405, 2018. doi: https://doi.org/10.1038/s41586-018-0479-2.

[17] Anshuman Pasupalak, Li Yan-Wei, Ran Ni, and Massimo Pica Ciamarra. Hexatic phase in a model of active biological tissues. *Soft Matter*, 16:3914, 2020. doi: 10.1039/D0SM00109K.

[18] Yan-Wei Li, Leon Loh Yeong Wei, Matteo Paoluzzi, and Massimo Pica Ciamarra. Softness, anomalous dynamics, and fractal-like energy landscape in model cell tissues. *Physical Review E*, 103(2):022607, feb 2021. doi: 10.1103/PhysRevE.103.022607.

[19] Elizabeth Lawson-Keister and M. Lisa Manning. Jamming and arrest of cell motion in biological tissues. *Current Opinion in Cell Biology*, 72:146–155, oct 2021. doi: 10.1016/j.ceb.2021.07.011.

[20] Bradley R Parry, Ivan V Surovtsev, Matthew T Cabeen, Corey S O'Hern, Eric R Dufresne, and Christine Jacobs-Wagner. The bacterial cytoplasm has glass-like properties and is fluidized by metabolic activity. *Cell*, 156(1-2): 183–194, 2014.

[21] Morgan Delarue, Jörn Hartung, Carl F Schreck, Pawel Gniewek, Lucy Hu, Stephan Herminghaus, and Oskar Hallatschek. Self-driven jamming in growing microbial populations. *Nature Physics*, 12(8):762–766, aug 2016. ISSN 1745-2473. doi: 10.1038/nphys3741.

[22] Junyi Yang, Paulo E Arratia, Alison E Patteson, and Arvind Gopinath. Quenching active swarms: effects of light exposure on collective motility in swarming serratia marcescens. *Journal of the Royal Society Interface*, 16(156): 20180960, 2019. doi: https://doi.org/10.1098/rsif.2018.0960.

[23] Rituparno Mandal, Pranab Jyoti Bhuyan, Pinaki Chaudhuri, Chandan Dasgupta, and Madan Rao. Extreme active matter at high densities. *Nature communications*, 11(1):1–8, 2020.

[24] Rituparno Mandal and Peter Sollich. Multiple types of aging in active glasses. *Physical Review Letters*, 125(21):218001, 2020.

[25] Matteo Paoluzzi, Demian Levis, and Ignacio Pagonabarraga. From motility-induced phase-separation to glassiness in dense active matter, 2021.

[26] Pin Nie, Joyjit Chattoraj, Antonio Piscitelli, Patrick Doyle, Ran Ni, and Massimo Pica Ciamarra. Stability phase diagram of active brownian particles. *Physical Review Research*, 2(2):023010, 2020.

[27] Yaouen Fily, Silke Henkes, and M Cristina Marchetti. Freezing and phase separation of self-propelled disks. *Soft Matter*, 10(13):2132–2140, 2014.

[28] Yann-Edwin Keta, Robert L Jack, and Ludovic Berthier. Disordered collective motion in dense assemblies of persistent particles. *arXiv preprint arXiv:2201.04902*, 2022.

[29] Carl Merrigan, Kabir Ramola, Rakesh Chatterjee, Nimrod Segall, Yair Shokef, and Bulbul Chakraborty. Arrested states in persistent active matter: Gelation without attraction. *Physical Review Research*, 2(1):013260, 2020. doi: https://doi.org/10.1103/PhysRevResearch.2.013260.

[30] Qinyi Liao and Ning Xu. Criticality of the zero-temperature jamming transition probed by self-propelled particles. *Soft Matter*, 14(5):853–860, 2018.

[31] Charles Reichhardt and Cynthia J Olson Reichhardt. Absorbing phase transitions and dynamic freezing in running active matter systems. *Soft Matter*, 10, 2014. doi: 10.1039/c4sm01273a.

[32] Ralf Brüning, Denis A St-Onge, Steve Patterson, and Walter Kob. Glass transitions in one-, two-, three-, and four-dimensional binary lennard-jones systems. *Journal of Physics: Condensed Matter*, 21(3):035117, 2008.

[33] P. Chaudhuri, Ludovic Berthier, and Srikanth Sastry. Jamming Transitions in Amorphous Packings of Frictionless Spheres Occur over a Continuous Range of Volume Fractions. *Physical Review Letters*, 104(16):165701, apr 2010. doi: 10.1103/PhysRevLett.104.165701.

[34] Massimo Pica Ciamarra, Antonio Coniglio, and Antonio De Candia. Disordered jammed packings of frictionless spheres. *Soft Matter*, 6(13):2975, 2010. doi: 10.1039/c001904f.

[35] Corey S. O'Hern, Stephen A Langer, Andrea J. Liu, and Sidney R. Nagel. Random Packings of Frictionless Particles. *Phys. Rev. Lett.*, 88(7):075507, 2002. doi: 10.1103/PhysRevLett.88.075507.

[36] Alexandre P Solon, Yaouen Fily, A. Baskaran, Michael E Cates, Y. Kafri, M. Kardar, and J. Tailleur. Pressure is not a state function for generic active fluids. *Nature Physics*, 11(8):673, 2015. doi: 10.1038/nphys3377.

[37] Thomas Speck, Julian Bialké, Andreas M Menzel, and Hartmut Löwen. Effective cahn-hilliard equation for the phase separation of active brownian particles. *Physical Review Letters*, 112(21):218304, 2014. doi: https://doi.org/10.1103/PhysRevLett.112.218304.

[38] Adam Wysocki, Roland G. Winkler, and Gerhard Gompper. Cooperative motion of active Brownian spheres in three-dimensional dense suspensions. *EPL (Europhysics Letters)*, 105(4):48004, feb 2014. ISSN 0295-5075. doi: 10.1209/0295-5075/105/48004.

[39] Julian Bialké, Jonathan T. Siebert, Hartmut Löwen, and Thomas Speck. Negative Interfacial Tension in Phase-Separated Active Brownian Particles. *Physical Review Letters*, 115(9):098301, aug 2015. ISSN 10797114. doi: 10.1103/PHYSREVLETT.115.098301/FIGURES/4/MEDIUM.

[40] Ludovic Berthier. Nonequilibrium Glassy Dynamics of Self-Propelled Hard Disks. *Physical Review Letters*, 112:220602, 2014. doi: 10.1103/PhysRevLett.112.220602.

[41] Peter K. Morse, Sudeshna Roy, Elisabeth Agoritsas, Ethan Stanifer, Eric I. Corwin, and M. Lisa Manning. A direct link between active matter and sheared granular systems. *Proceedings of the National Academy of Sciences of the United States of America*, 118(18):e2019909118, may 2021. doi: 10.1073/PNAS.2019909118/-/DCSUPPLEMENTAL.

[42] Massimo Pica Ciamarra and Antonio Coniglio. Jamming at zero temperature, zero friction, and finite applied shear stress. *Physical Review Letters*, 103(23): 235701, 2009.

[43] Ricard Alert, Jaume Casademunt, and Jean-François Joanny. Active Turbulence. *Annual Review of Condensed Matter Physics*, 13(1), 2022. doi: 10.1146/annurev-conmatphys-082321-035957.

[44] Yuanjian Zheng, Anshul D S Parmar, and Massimo Pica Ciamarra. Hidden Order Beyond Hyperuniformity in Critical Absorbing States. *Physical Review Letters*, 126:118003, 2021. doi: 10.1103/PhysRevLett.126.118003.

Chapter 5

Discussion and future works

This thesis addresses and clarifies emerging phenomena occurring in many-particles disordered systems. The primary objective of this thesis is to comprehend the fundamental principles governing the physics of a system, through an investigation of the dynamics. In confined systems, the dynamics are influenced by Mermin-Wagner long-wavelength fluctuations, leading to a crossover from a three-dimensional to a two-dimensional physical behavior. In the system of active particles, the presence of activity induces two non-equilibrium transitions. The first is a transition from a homogeneous state to a phase-separated state, which is observed as the active force increases. This phenomenon represents an out-of-equilibrium phase transition that is frequently observed in biological systems. The second is an active jamming transition, which we found it occurs with the non-equilibrium phase-separated transition, resulting in anomalous dynamics.

Through my research, I explored both active and non-active models and their complex dynamics, seeking to deepen our understanding of the underlying physics. In this concluding chapter, I summarize my investigations and suggest future research directions.

LWs fluctuations in confined liquids

Part of my research work addressed the long-standing question of how liquids confined in narrow gaps crossover from a two- to a three-dimensional behavior

as the confinement width increases. This is a question of fundamental theoretical interest related to biological and engineering problems wherein confined liquids are often present.

Upon observation, it has come to my attention that the behavior of two-dimensional systems is influenced by their long-wavelength fluctuations, whereas such fluctuations do not affect the behavior of three-dimensional systems. As such, investigating the influence of these fluctuations on the dynamics of confined system emerges as a novel strategy to unveil the dimensionality crossover. To pursue this approach, I first developed a novel Debye-like model to describe the density of vibrational modes of confined systems, and validated it via extensive numerical simulations in the solid phase. My novel model interpolates between the two- and the three-dimensional limit as the confinement width increases.

I investigated the dynamics of confined systems at different temperatures, changing both the confining width, the lateral length, and the confining mechanisms (periodic boundary conditions, flat walls, rough walls). These studies revealed a size-dependence of the relaxation dynamics that depends on the confining width, a result I was able to rationalise making use of the novel model for the density of vibrational states of confined systems.

Overall, this result represent a conceptual breakthrough in the current understanding of the physical behaviour of confined liquids, whose physical properties have challenged physicists and engineers for the past 30 years. Given the critical role of dimensionality, our findings may be relevant to rationalize the mechanical and transport properties of confined liquids, which play a prominent role in natural and engineering environments. Our results are relevant to a variety of applications involving micro and small-scale devices in which particles flow in confined geometries.

In the context of passive systems under confinement, further studies could concentrate on exploring the impact of different shapes of confinement geometries, e.g., systems confined in a ring shape geometry or other asymmetrical geometries. Furthermore, given that the current study has primarily focused on a de facto two-dimensional system with confinement, it would be worthwhile to explore how the density of states (DOS) behaves in a one-dimensional confined channel.

Future work could also investigate the dynamics of a 1D confined liquid, i.e., to understand how does a liquid flow in a narrow channel. Furthermore, previous results have demonstrated that confining may both speed up or slow down the liquid dynamics, depending on the interaction between the confined molecules and the confining boundaries. However, these work used as a measure of the relaxation dynamics the relaxation time extracted from the decay of the self-scattering function. It remains to be understood how these observations are affected by LWs. It is indeed possible that no such difference is observed when the dynamics is probed via cage-relative measures, or equivalently, focusing on the confinement dependence of the viscosity.

Out of equilibrium transitions in self-propelled particle systems

In this thesis, I further investigated the physics of self-propelling particles. Systems of self-propelling particles exhibit two out-of-equilibrium transitions, motility induced phase separation (MIPS) and active jamming. The scope of my research was to understand if and how these two transitions relate.

I have demonstrated that these transitions are related if each particle self propels in a fixed direction. When this is the case, these two transitions occur together in the limit of hard particles or small self-propelling forces.

I have further unveiled anomalous dynamical features that occur in systems of persistent self-propelling particles. The dynamics in fluid phase involves transient system spanning vortex-like structures. Correlations in the directions of the self-propelling particles that build up in the flowing phase make the jamming transition hysteretic.

The model considered in this work mimics specific biological systems with long persistence active force. It would be worthwhile to further investigate the system with a range of finite persistence and under more realistic conditions, such as taking into account the impact of friction on a system of long persistent active particles. In addition, it would be of great interest to rationalize how interplay between jamming and MIPS gradually evolves as the persistence time decreases.

Although my thesis primarily focuses on either confinement or activity in disordered systems, it would be intriguing to include both active forces and confinement in future research. Studying the dynamics of such systems would enable us to address issues such as crowd control.

Last but not the least, given the real-time dynamics, the integration of computer vision technology could be explored to predict and potentially prevent any potential stampede incidents.